CHALMERS
UNIVERSITY OF TECHNOLOGY

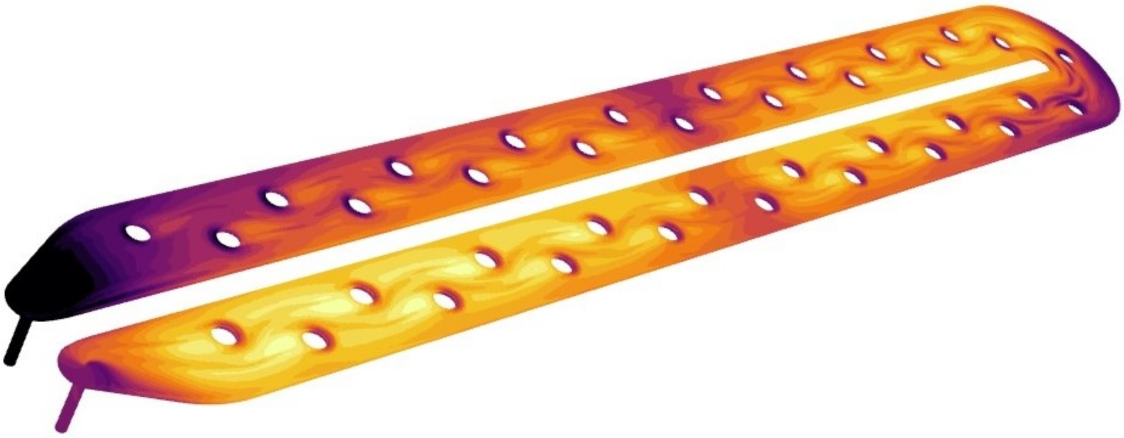

Optimisation of Battery Thermal Management System

A comparative CFD study on possible improvements of heat transfer within a vehicle battery

Master's thesis in Sustainable Energy Systems

NORA KRONVALL
SARA STRAND

Department of Mechanics and Maritime Sciences
CHALMERS UNIVERSITY OF TECHNOLOGY
Gothenburg, Sweden 2020

MASTER'S THESIS 2020:13

Optimisation of Battery Thermal Management System

A comparative CFD study on possible improvements of heat transfer within a vehicle battery

NORA KRONVALL
SARA STRAND

Department of Mechanics and Maritime Sciences
Division of Fluid Dynamics
CHALMERS UNIVERSITY OF TECHNOLOGY
Gothenburg, Sweden 2020

Optimisation of Battery Thermal Management System
A comparative CFD study on possible improvements of heat transfer within a vehicle battery
NORA KRONVALL
SARA STRAND

Supervisor: Daniel Buvarp and Jonathan Theorin, Cooling at CEVT
Examiner: Huadong Yao, Division of Fluid Dynamics at Department of Mechanics and Maritime Sciences at Chalmers University of Technology

Master's Thesis 2020:13
Department of Mechanics and Maritime Sciences
Division of Fluid Dynamics
Chalmers University of Technology
SE-412 96 Gothenburg
Telephone +46 31 772 1000

Cover: A contour plot over the temperature of the fluid for the new case combining a new flow pattern with a new thermal interface material. Using a different colour scale than later in similar figures, see Figure 4.7.

Optimisation of Battery Thermal Management System
A comparative CFD study on possible improvements of heat transfer within a vehicle battery
NORA KRONVALL
SARA STRAND
Department of Mechanics and Maritime Sciences
Chalmers University of Technology

Abstract

Electric driven vehicles with batteries are one way to enable lower emissions from transport sector. A key aspect to increase the battery performance, safety and lifetime is an efficient Battery Thermal Management System (BTMS). Therefore, this master thesis is performed in collaboration with the innovation center CEVT to answer the question: "How can the heat transfer in a branch standard BTMS solution be improved?". The branch standard solution, or base case, is a liquid BTMS with cooling plates and a thermal pad as thermal interface material (TIM).

The research question was answered through CFD simulations in a comparative study. The study aims to reduce the total heat transfer resistance from the battery module to the coolant as well as temperature variance in the battery module. Each case consisted of pre-study, mesh study and analysis. Firstly, the base case was evaluated. From analysis together with inspiration from literature, improvements were suggested. Thereafter the improved cases were simulated and analysed through a comparative study.

One identified problem was the thermal pad. So, a new TIM with higher conductivity and lower contact resistance was tested. The contact resistance was unsure, so two values were used to capture the range of improvement. This reduced the resistance with 15 - 63% and lowered the variance with 0,13 - 0,26K, compared to the base case. Another improvement was a fin in the battery module. This required additional assumptions, which made the results uncertain. But a risk of heat accumulation in the fin was recognised. A third improvement was to change the flow pattern to increase the mixture, which lowered the resistance with 5% and the variance with 0,69K. A combination case with the new TIM and flow pattern gave 20% reduced resistance and 0,98K reduced variance.

Based on the results, recommendations were to replace the existing thermal pad with a more efficient TIM. If fins are of interest, they may require cooling. A new flow pattern should be investigated and optimised by comparing different patterns. Lastly, it is suggested to combine a new TIM with an optimised flow pattern for a more efficient BTMS.

Keywords: Heat transfer, Battery pack, CFD, Sustainable Energy Systems, BTMS, TIM

Acknowledgements

It has been our honour to be involved in this master thesis project. We would like to start with the greatest of gratitude to our supervisors Daniel Buvarp and Jonathan Theorin at CEVT, who gave us the opportunity to perform this master thesis and strongly supported us throughout the entire process. We are especially thankful for how they introduced us to key persons at CEVT which learned us a lot and enabled the project.

We thank all the people at the cooling department for their support. Furthermore, we thank Patrik Sondell, Björn Jonsson and Chanin Lerdmaleewong at the CAE Engineer Energy department at CEVT for the input data and guidance in setting up the simulations.

We also send a thank you to Anna Kvarnström and Aleksey Gerasimov at ANSYS who gave us access and accounts at ANSYS learning hub. Together with their guidance and knowledge in the software, this gave the project a quick start which enabled the results to become as extended as they did.

A thank you is also sent to Åsa Persson at Henkel for the supplied material data and guidance in choosing a thermal interface material for our application.

We would also like to extend a warm thank you to our examiner Huadong Yao at Chalmers. He has not only guided us with his large knowledge in CFD, but also mentored and pushed us through occasional lows and given us confidence in our-self and the project. So, thank you Huadong Yao for you quick response full of hope at all hours of every day.

Last but not least, we send a warm-hearted thank to our family and friends for their support.

Nora Kronvall, Gothenburg, May 2020
Sara Strand, Gothenburg, May 2020

Contents

Nomenclature

GHG	Green House Gases
EV	Electric Vehicles
HEV	Hybrid Electric Vehicles
PHEV	Plug-in Hybrid Electric Vehicle
CEVT	China Euro Vehicle Technology
BTMS	Battery Thermal Management Systems
PCM	Phase Changing Material
CFD	Computational Fluid Dynamics
ANSYS Fluent	Software for CFD calculations
CAD	Computer Aided Design
Q_{irr}	Irreversible heat generation [W]
$R_i nt$	Internal resistance [Ω]
I	Working current [A]
C	Discharge capacity [1/h]
T	Temperature [K]
c_p	Specific heat capacity [J/kg K]
t	Time variable [s]
V	Velocity [m/s]
ρ	Density [kg/m^3]
k	Thermal conductivity [W/m K]
P	Pressure [Pa]
τ	Shear stress [N/m^2]
$R_m(C,T)$	Reaction rate at concentration C and temperature T
$Q" = q"$	Heat rate [W/m^2]
Nu	Nusselt number
h	Convective heat transfer coefficient [W/m^2K]
L	Characteristic length [m]
Pr	Prandtl number
ν	Kinematic viscosity [m^2/s]
α	Thermal diffusivity [m^2/s]
μ	Dynamic viscosity [$Pas = kg/ms$]
A	Area [m^2]
t_R	Resistance thickness [m]
R	Contact resistance [K/W]
$Q = q$	Total heat rate [W]
g	Gravity vector [m^2/s]

RTT	Reynolds Transport Theorem
FVM	Finite Volume Method
B_{sys}	Extensive Fluid Property
CV	Control volume
CS	Control surface
n	Normal vector
m	Mass [kg]
Re	Reynolds Number
D_h	Hydraulic diameter [m]
A_c	Cross flow Area [m^2]
P_w	Wetted perimeter [m]
y^+	Dimensionsless wall distance
TIM	Thermal Interface Material
$\dot{m}$	Mass flow [kg/s]
ECM	Equivalent Circuit Model
DNS	Direct number solution turbulence model
RANS	Reynolds Average Navier-Stokes turbulence model
SIMPLE	Semi-Implicit method for Pressure-Linked Equations
k-ω	A RANS two-equation Turbulence model
k-ϵ	A RANS two-equation Turbulence model

List of Figures

List of Tables

1

Introduction

Since the industrial revolution the global atmospheric concentrations of greenhouse gases (GHG) have rapidly increased. Among other effects, the accumulated emissions have led to climate changes. In order to reduce the emission rate alternatives to fossil energy sources are required. According to Our world in data the transport sector stands for approximately 20% of the global CO_2 emissions.[1] It has been shown that if a renewable electric power source is used, switching to EVs can reduce a country's GHG emissions up to 40% [2]. Therefore, the development of electric vehicles (EV) and hybrid electric vehicles (HEV) are of large interest for vehicles manufactures. HEVs have different levels of electrification, where a plug in HEV (PHEV) have a large enough battery to offer pure electric drive [3].

China Euro Vehicle Technology (CEVT) is an innovation and development centre within the area of smart mobility. They aim for modular development, virtual engineering, software system engineering and innovation.[4] One of their modular architectures is the PHEV 80. Which has a 15.2 kWh battery and can go up to 80 km on a single charge [5]. The development of EVs and HEVs have been rapid, and the main focus for battery development have been to maximise power and energy density. For these two parameters lithium-ion batteries show great prospect. However, lithium-ion batteries still have problems with high costs, limited calendar-life and safety. One way of improving lithium-ion batteries is by implementing efficient BTMS, as research have shown that BTMS largely impact performance as well as safety and lifetime. This has led to an increased interest and investigation of BTMS over the last years. [6]

The cooling system of PHEV have several tasks as it cools the cabin, the engine, the electrical motor, the battery and other heat generating components. Since a PHEV have more components than a pure EV or internal combustion engine vehicle, the space limitations can be tougher. Research of BTMS have ranged from system perspectives to detailed Computational Fluid Dynamics (CFD).[7] On a system level the drive cycle is often included to see how the BTMS can be optimised to the rest of the cooling system in different situations [8]. There are three main categories of BTMS, which are: air cooling, liquid cooling and phase changing material (PCM). Today, indirect liquid cooling, with coolant flow in a pipe or between cooling plates, is the most common BTMS for vehicle application. [6] Furthermore, different patterns of air cooling [9] and indirect liquid cooling have been investigated [10] [11]. PCM as a passive cooling system has become of increasing interest [12], although it is suggested to require complementing air or liquid cooling of the PCM to avoid heat accumulation [13]. The goal of any BTMS is to keep temperatures uniform and within optimal operation ranges[7].

To investigate how an BTMS can be improved, the research question of this study was: "How can the heat transfer in a branch standard BTMS solution be improved?". The branch standard solution, also referred to as the base case (BC), was an indirect liquid cooling system for a battery pack in a PHEV. The analysis focused on the heat transfer where a low heat transfer resistance and uniform temperature distribution was of importance. Analysis were done on the battery package isolated from the rest of the cooling system, using the CFD tool ANSYS Fluent. Based on the base case and inspired by literature and previous research, improvements of the design were suggested. The suggested improvements were evaluated in a comparative study with the branch standard solution as a base line.

1.1 Aim

The aim of this master thesis was to perform a comparative study by investigating an indirect liquid cooling system, which is a branch standard solution for cooling of a battery package, and suggest improvements. Improvements was to focus on increasing the heat transfer from the battery module to the coolant.

1.2 Assumptions and limitations

This project was limited to the spring of 2020 with the available computational power of two laptops. So, several limitations were implemented to restrict the required computation time. One of the first limitations was to not include the entire cooling system, but only the battery. As a consequence, properties for the incoming coolant as well as the battery were constant and did not depend on a drive-cycle. This enabled a comparative study of the efficiency of the heat transfer between the different cases at a reasonable level of computational power. Another limitation was to only focus on fluid and heat transfer properties while mechanical properties was not investigated, although they can be affected by choice of BTMS. Since the design changes were relatively small and applied in similar applications it was not vital to look at mechanical properties for the aim of the study. As the cost of the current solution was unavailable, this was not an investigated parameter. Since the temperature differences in the battery package is relatively small the radiation could be neglected.

The model of the battery package was based on a computer aided design (CAD) model. However, this model did not include the design inside of the battery modules. So, design of the battery cells and other components inside of the module was unavailable. As a result, several simplifications were required. Firstly, the heat generated in the battery had to be based on other models and was simplified as a constant heat flux, instead of space and time dependent. Secondly, the project could not investigate the temperature distribution within the module and how it could be reduced to avoid hotspots even if it was recognised that within a battery module the temperature distribution over and between the cells are not uniform. Lastly, the suggested design changes could not change the outer diameter of the battery module and only assume effects of design changes within the module. Nevertheless, since this was a comparative study, it was still possible to investigate and suggest improvements of the heat transfer.

Several simplifications of the CAD model were applied to speed up the simulations. Therefore, the thesis investigated a worst-case scenario where all heat generated in the battery module had to be removed through the coolant. Surrounding structures which was in contact with the battery and could transfer heat, was removed. To limit the domain size further, only two out of eight modules was included, which was enough to study the heat transfer. These two models had a separate flow compared to the remaining six which made it possible to isolate them and still have access to boundary conditions. This gave a stripped-down model which only included the cooling plates enclosing the coolant and the thermal interface material (TIM) between the battery modules and the cooling plate. The thermal pad was modelled with a constant thickness, even if this could have variations due to uneven applied pressure. Since this possible variation was not mapped and expected to be small, it was reasonable to assume a constant thickness. Furthermore, the thermal pad was compressed, so the simulated thickness of the pad was the compressed thickness. The contact resistance of a TIM is an uncertain parameter, so for the new TIM two values was used and tested to capture the range of possible outcome.

A constant heat flux was applied on the interface between the battery module and the thermal interface material. Even if heat generation inside a battery is not constant over space this was a reasonable assumption, since the enclosing battery module in metal should have a relatively even temperature distribution. On the bottom of the battery module there was an electric isolating tape. This tape was believed to have negative impact on the heat transfer due to its isolating properties, it increased the number of interfaces and thereby contact resistances. However, the specific properties of the tape were unknown and included in battery module, which was why it was left out from the simulations. In addition, the tape was same for all cases, so its impact on the comparative results was limited. The geometry was further simplified by adjusting the flow channels to avoid small angles which would have required a large number of cells to resolve. By doing so, the contact area between the upper and lower cooling plate was slightly increased and possible wakes in the gaps where not detected. In addition, structures on the outside of the cooling plates was smooth out and holes where filled. Since this was a comparative study and the simplifications were done similar for all cases, it would still be possible to see improvements of the heat transfer between cases.

Lastly, kept in mind throughout the project was that a model is only a reflection of the reality. And it was recognised by the authors that each simplification moved the simulation results further away from the reality. How simplifications and assumptions might have affected the result and caused overseen possibilities is considered in the discussion in Chapter 5.

2
Theory

In this chapter relevant theory for the project, including previous research, is shortly presented. First comes an overview of Lithium-ion batteries with focus on how they are affected by temperature which may cause swelling and what this imply. Second, comes a presentation of the three main categories of BTMS: air-cooling systems, liquid cooling systems and phase changing materials. Third, is a basic description of heat transfer presenting governing equations, the heat transfer modes conduction respectively convection, ending with a section about contact resistance which has major importance for this project. Fourth, comes a concentrated summary of fluid dynamics and how it is coupled to heat transfer. Fifth, is a section about thermal interface materials focusing on important factors when selecting material and what effect this have on the performance. Last is a short summary of the chapter in form of possible improvements of the heat transfer based on presented theory.

2.1 Lithium-ion battery

A lithium-ion battery works after the basic principle of electrochemistry. The battery cell consists of anode, cathode, separator, electrolyte, one positive current collector and one negative current collector. The electrolyte carries charged lithium ions between the anode and cathode where the lithium is stored. This movement leads to free electrons inducting a charge at the positive current collector. The electrical current flows from the current collector through the powered device to the negative current collector. While the separator blocks the flow of electrons inside of the battery cell. There are different types of lithium-ion batteries where the electrodes, cathodes, anodes and electrolyte can be different combinations of materials.[14] This report investigate a battery pack with Lithium-ion cells. A battery pack consists of modules and other components such as frames and cooling plates. The modules in turn have several parts where the main part is the cells which are connected by an electric board and separated by materials between the cells. Battery cells can be designed in different ways. Two typical designs in vehicle applications are prismatic and cylindrical cells, which have different advantages. Cylindrical cells have a higher manufacturing maturity which gives them lower production cost. While prismatic cells, which are investigated in this project, have higher space utilisation and increased flexibility compared to other cell designs. The prismatic cell can be described as a flat bag that have been rolled together and squeezed to a rectangular shape. Consequently, the prismatic cell has an anisotropic heat transfer, with higher thermal resistance on the flattened side. [6]

A major obstacle with lithium-ion batteries are that they lose capacity and power at high temperatures [6]. Generally the fade of capacity is due to lost lithium and active material within the battery [15]. While the loss of power is caused by elevated temperatures which increases the internal resistances in the cell [16]. The heat generation within the battery can be simplified as the irreversible losses within the battery, according to

$$Q_{irr} = R_{int} I^2 \tag{2.1}$$

where Q_{irr} is the irreversible heat generation, R_{int} is the internal resistance and I refers to the working current in the cell. The current in the cell depends on the driving cycle and increases as more power is withdrawn or put in, for example at strong accelerating respectively fast charging. Since the heat generation depend on the current in square, the effect of high power gives a multiplied effect on the heat generation. With an ineffective BTMS the increased power leads to a temperature increase of the battery. The temperature of the battery cell also depends on type and design of the cell, where different chemical reactions, phase changes and mixing effects heat the battery with different amounts. [17] At low-temperature conditions, the cell temperature is below the desirable range which causes the discharge capacity to drop. This leads to a reduced driving range of the car. In the contrary case at high temperatures, an irreversible chemical reaction occur in the battery, which causes thermal runaway and in worst case an explosion. [18]

2.1.1 Swelling lithium-ion batteries

A problem with lithium-ion batteries is the risk of swelling which has been investigated by several researchers [19] [20] [21] [22] [23]. The swelling is often caused by high power usage, for example vehicle batteries, which causes the carbonaceous particles within the cell to fracture. Which leads to a swelling and volumetric change, due to lithium intercalation and deintercalation. [20] Battery cells are stacked in a module and a compression is applied to reduce the swelling. The amount of applied pressure affects the battery performance. Too high compression reduces the separator thickness which leads to degradation and power reduction. While the right amount of compression prevents delamination and deterioration of electronic conductivity of the electrodes. [21] Another aspect is that the electrodes close to the separator are extracted and inserted at a higher rate which results in more stresses and structural degradation [22]. A prismatic cell primary expands perpendicular to the largest face due to the structure with gaps between the electrode and casing around the top and bottom. Between the cells there are often plastic spacers to provide a mean of compressing the cells. [23]

Mechanical applied pressure on a cell affects the performance in a non-linear way and depends on several factors. By applying pressure, the electrodes and separators are compressed which reduces the volume and thereby the resistance, which increase the electric contact within the cell. The compression depends on the number of cells where fewer layers results in higher compression for the same amount of applied pressure. Neither this relationship is linear but levels out at an increased number of layers. A property that is influenced by the pressure is the discharge capacity. Which has a non-linear dependency on the discharge rate. For low rates, below 0.8C, the discharge capacity is increased with increasing cell pressure. While the behaviour is reversed for higher rates. So, the choice of mechanical pressure is not a straightforward decision, but of high importance.[19]

2.2 Battery thermal management systems

As stated above the performance and life span of a battery strongly depend on its temperature. Due to the resent years increased interest in battery applications, research in BTMS has grown rapidly. Optimal temperature operation range for a lithium-ion battery cell is usually between 15°C and 35°C. When operating outside of this range, the risk of capacity loss is impending.[6] In order to stay within the recommended temperature range battery thermal management systems are used [18]. Today there are several types of BTMS in use, which are divided into three main categories based on the coolant and its phase. The first category is air cooled system, where the coolant is air and remains in gaseous phase. The second category is liquid coolant systems, with a coolant in liquid phase. Lastly, phase changing materials absorb heat latent as it changes phase. A BTMS can either be evaluated based on the maximum battery temperature, or the maximum temperature difference within the battery, which should be as low respectively even distributed as possible [24]. In the following section the three main categories are roughly described, and a selection of previous research is shortly presented.

2.2.1 Air-cooling systems

There are two categories of air-cooled systems: active and passive. Passive air-cooling systems use natural convection and heat dissipation through a passive heat spreader or heat sink. Since it is limited to only a few numbers of extra components the solutions have relatively low cost and weight. An active cooling system include at least one extra component, traditionally a fan or a blower [9], in order to increase the heat transfer. In such way active cooling achieve an increased flow rate which increases the convection rate and thereby heat removal [25]. Due to increased complexity and extra components an active air-cooling system is usually more expensive than a passive. Although, an active system usually has higher cooling rates. [25] Air-cooling structures can be of different types, the two most widely used are: serial cooling structure and parallel cooling structure [26]. Choice of structure and streamline of air-cooling BTMS are two important parameters, since they have effect on the heat dissipation performance, temperature distribution and energy consumption of the fan [27].

Different design solutions of air-cooling have been investigated, proposed and compared by researches. Several of these studies try to optimise the design of the flow channels. One common design of the channels is variants of a double U-type duct for cooling the battery from a bottom plate [28]. Furthermore, the ventilation channels can be designed either in series or in parallel. When compared, a parallel active air-cooled system achieved lower temperature and a more uniform temperature distribution than the design using series.[29] A third variant of the pattern of the flow channel, is to install a sub-module of the battery in a parallel structure. Which enable a more flexible design although it also risks to increase the size of the system. [30] Another improvement of the air-cooled BTMS is to use aluminium foam in the air channels to increase the heat transfer surface. By using aluminium foam in a forced air-cooled BTMS the required flow for a certain cooling effect was reduced. Therefore, is the stress on the BTMS reduced, which in turn can reduce the driving cost. On the other hand, the aluminium foam ads an additional material. So, there can be a trade of between lower running cost and increased investment cost. [31]

To sum up, the usage of air-cooled systems in electric vehicles is limited due to low effectively. However, they are favourable due to simple structure, relative low cost and easy maintenance [32]. Beside the main advantages of possible low weight and cost, air-cooled systems are also capable to work at low ambient temperature [33].

2.2.2 Liquid cooling systems

Since liquids has higher thermal conductivity than air, they are more attractive as coolants. Liquid cooling systems can be divided into direct and indirect liquid cooling. As the name suggest a direct cooling system have liquid circulating in direct contact with the battery which restrict the choice of coolant to avoid hazards. For an indirect system the choice of coolant is less restricted, as the fluid is separated from the battery. Since the coolant in indirect cooling is contained, it has additional thermal resistance compared to direct liquid cooling. Still, indirect cooling the more employed system in vehicle applications. [6]

Naturally, an important component for liquid cooling BTMS performance is the choice of coolant where typical liquids are water, glycol, oil, acetone and refrigerants [9]. Since freezing-point is a critical factor, choice of coolant depends on working environment. The fluid properties also have a major influence on turbulence and pressure drop. As describe in Section 2.3, increased turbulence can increase the efficiency of the liquid BTMS. Turbulence is affected both by viscosity, density and velocity, see Equation 2.14. The same factors affect the pressure drop over the system, so an increase in turbulence is often connected to increased pressure drop and thereby required pump work. [34] A possible enhancement of the coolant is to add nano-particles in order to enhance the cooling performance and get a more uniform battery temperature [35]. A conventional way of increasing the heat transfer is by increasing the heat exchange area by implementing fins, either on the fluid side or in contact to the cells [36].

Direct liquid cooling systems with the battery cells submerged in a coolant have the potential to provide a better heat transfer, due to less thermal resistance and increased contact surface compared to indirect cooling [37]. Direct liquid cooling can be similar in design to air-cooled systems. One such design was based on the structure of an air-cooled system but replaced air with silicon oil, which substantially improved the cooling efficiency. [38] Solutions using direct cooling have mostly been investigated for cylindrical cells and generally limited to use electric insulating coolants. Even so, the usage of liquid metals, so called super coolants, which are not electric insulators have been investigated. These showed great potential. However, further research of direct cooling is required before commercialisation. Three areas for further investigation are: viscosity of cooling media which have effect on the required pump power, stability of coolant for safety reasons, and sealing properties required of the system. [39] Concluded from several comparative studies for vehicle applications the liquid indirect cooling have been regarded as the better choice. Which is why the impractical direct cooling and the inefficient air-cooling are less studied. [6]

A common design of indirect liquid cooling systems includes a cooling plate either between cells, modules or battery packs. Naturally, the further into the battery structure the plate is located, the effectiveness and complexity of the system increases. A cooling plate is designed to maximise the contact surface, minimising pressure drop and retain a uniform temperature. The physical design of the cooling plate channels such as length, width or route, obviously influence the performance of the cooling plate. In addition, there are optimisation possibilities regarding material, mass flow rate, flow direction and entrance size which have been investigated. [39] Experiments using cooling plates with mini-channels between the cells have shown a significant decrease of the maximum temperature. In addition, the studies of mini-channels have shown that the temperature variance is reduced with increased coolant flow rate. However, there is an optimal flow rate after which the influence of further increased flow rates weakens. [40] Increased flow rate also increases the required energy of the pump dramatically. One study showed that for an increase from 1 l/min to 4 l/min the pump work increased nearly 47 times [41]. Due to the increased pump work, balance optimisation of the flow rate is required. A possible improvement of the mini-channel design is to embed flexible graphite between the channels and battery cells to obtain a more uniform cooling performance. This design reduced the temperature difference within the battery from 7K to 2K. [42] Another variant of mini-channels is to have tubes encircle the cells, which has been studied on prismatic cells [6].

Another approach of improving the indirect liquid cooling system is by optimising the pattern of the cooling plate. This can have impact on both mini-channels and regular flow channels. Optimisation of the pattern can achieve a more even temperature distribution, lower pressure drop and lower average temperature. [6] Analysis of mini channels have shown that the optimal flow direction is from the electrode side. More channels in the plate as well as an increased flow rate reduces the temperature rise. To keep in mind is the optimal flow rate as a trade of between cooling performance and pressure drop. [43] Investigations of the pattern of mini-channels have been done from several angels. One study examined an optimisation of the spread of the coolant by having one inlet which branched out to get an even temperature distribution over the cell. Another investigated different patterns, where a U-shaped mini channel noticeable enhanced the cooling effect.[35] For cylindrical cells, Tesla have developed a solution where aluminium tubes covered in a dielectric material are bend around the cells. This was implemented with a counter flow using a water-glycol mixture as coolant.[6] The shape of the cooling channel have significant impact on the overall pressure drop, where a narrow channel give a larger pressure drop. However, research has shown that the hydraulic diameter of the cooling channel has no influence on neither the maximum cell temperature nor the temperature uniformity. Which indicates that the hydraulic diameter should be adjusted to limit the pressure drop. Although, the diameter is also limited by size and weight of the system. [44]

According to several researches, liquid cooling systems are the current best solutions for cooling vehicle battery packs. But there are also several drawbacks, for instance: potential coolant leakage, weight, and high complexity [39] [6] [45]. Due to these flaws research in air-cooled systems for vehicle applications have increased in interest. [9] A problem with air-cooled systems is the low heat capacity. Nevertheless, small-scale research has shown that air-cooled systems can become as effective as liquid. But for larger instalments there are several challenges to overcome.[45] Today there is not a shared opinion on what BTMS system are best. Although, it can be established that liquid cooling systems is favoured as BTMS by several major car companies today [39].

2.2.3 Phase changing materials in BTMS

The use of phase changing materials is a passive cooling method. As the material change phase, either between liquid and gas or between solid and liquid, it absorbs or releases large amounts of energy over a small temperature range. Since the heat flux from a battery depend on the driving cycle, the cooling requirements are not constant. As a passive system, PCM has shown better performance than other BTMS for sudden temperature rises at high power usage. [12] PCM absorbs or release heat until the phase have completely changed, after which there is a risk of temperature run-off since the PCM no longer absorbs heat. Therefore, PCM require complementing cooling systems with air or liquid to cool the PCM and avoid heat accumulation.[13] By combining PCM with a complementing BTMS, the complementing system can work at constant low power. This give an opportunity to reduce weight, space and cost of the cooling system. The reduced need of large equipment together with fast feedback on sudden temperature rise is the two main advantages of PCM. [6]

PCM most often refer to the phase change between liquid and solid. However, the phase change between liquid and gas have also been studied, where one example is boiling fluid in micro channels.[46] Using a direct boiling system it has been shown that a battery package of prismatic cells can be maintained at a constant operation temperature of 35°C by. Even when the discharge rate was as high as 20C, the temperature was kept low and even, with a temperature variance over the cell of 4K. As the boiling temperature is constant and can be adjusted with pressure and working fluid the potential efficiency of a direct PCM is demonstrated through these low numbers.[47] [48] For boiling systems different working fluids and orientation designs have been tested. It has been discovered that the optimal performance of a boiling system depends on the heat generation of the battery. In addition, for an efficient heat transfer the contact surface is of absolute importance. This is why pipes generally are flattened instead of circular. Furthermore, thermal grease is often utilised as a thermal interface material to reduce the contact resistance. [6] Similar to liquid cooling systems a way of increasing the heat transfer efficiency in pipe applications is to insert nano-particles into the working fluid [49].

Some merits of the passive PCM system, is among others; simplicity, lightness, high efficiency and smaller components. All these factors are practical in a vehicle application. One of the biggest challenges with PCM is the poor thermal conductivity within the PCM, with high risk for thermal run-away once the phase change is complete. The poor conductivity can be enhanced by including conductive fillers, embedding PCM in porous material or metal meshes. These methods also reduce the risk of leakage, by binding the liquid PCM with capillary forces. However, they are not always electric isolated which is problematic.[6] The potential of PCM is debated, where some tests show as low performance as for air-cooling, but with higher cost and complexity [50]. So, it is possible that implementation of PCM not reduces but instead increases weight, space requirements and cost of the system due to its complexity and need for additional cooling. [6]

2.3 Heat transfer

In this chapter the basic principles of heat transfer are described. In the Energy Equation 2.2, all parts of energy generation and transfer is included. Heat can be transferred through three modes: conduction, convection and radiation, which are illustrated in Figure 2.1 and explained in this chapter. However, in this project the temperature differences are too low for radiation to have a significant contribution and is therefore left out from more detailed description. While the contact resistance, which has a large impact on the heat transfer, is described. Last in the chapter, possible improvements of the heat transfer based included parts are shortly elaborated. [34]

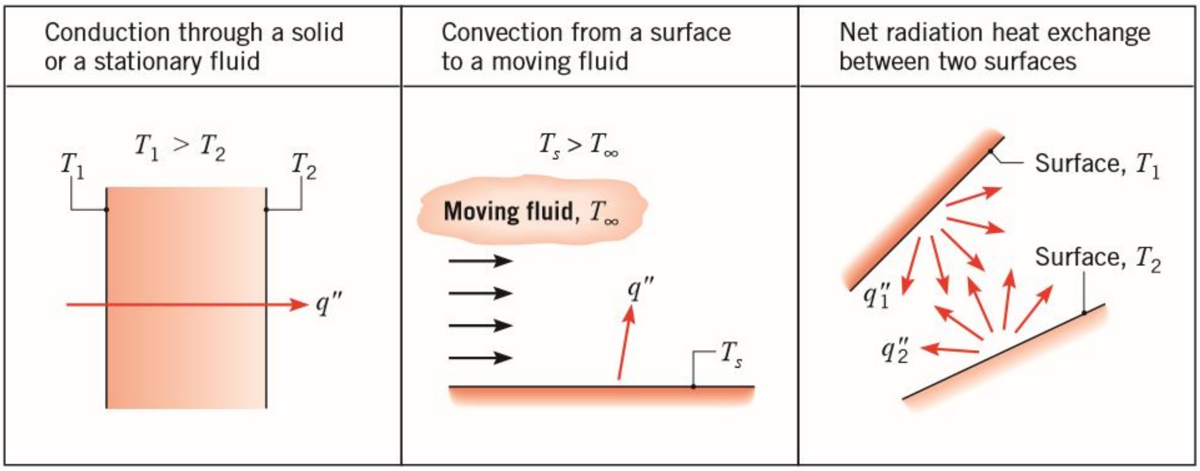

Figure 2.1: A simple illustration of the three heat transfer modes conduction, convection, and radiation. Short descriptions of the three modes are included. The temperature difference, the driving force, and the heat flux, q”, is marked in all three cases. [34]

2.3.1 The Energy Equation

Heat transfer is a complex phenomenon resulting from several factors. It is described in the Energy Equation as follows:

$$\frac{\partial(\rho c_p T)}{\partial t} = -V_j \frac{\partial(\rho c_p T)}{\partial x_j} + k \frac{\partial^2 T}{\partial x_j \partial x_j} - P \frac{\partial V_j}{\partial x_j} + \tau_{kj} \frac{\partial V_k}{\partial x_j} + \sum_m R_m(C,T)(-\Delta H_m) + S_T \quad (2.2)$$

where the term on the left side represents the accumulation of thermal energy over time. The terms on the right side in order from the left to right describes the convection, the conduction, the expansion, the dissipation, possible heat generations from chemical reactions and lastly an internal source term. All components are not present in all problems, for example there might not be generated heat from any chemical reaction. Heat transfer in a system is affected by all these components since they affect the temperatures and thereby the temperature difference which is the driving force behind all three modes of heat transfer. [51]

2.3.2 Conduction

When two objects with different temperatures are in contact with each other there is an exchange of heat between them, called conduction. This exchange is due to the physical mechanism of random atomic and molecular activity which causes collision between the particles. As the particles collide, they interchange energy and when the temperature increases the particles collide faster and more often. Thus, conduction is the transport of energy within a material. In Figure 2.1 conduction through a solid or stationary fluid is illustrated in the left cell. The conduction term is described in the Energy Equation 2.2 as the second term om the right side. And can be written in its three-dimensional form as

$$\mathbf{q}^{"} = -\Big(k\nabla\mathbf{T}\Big) \tag{2.3}$$

where k is the effective heat transfer coefficient and **T** is the temperature field. The negative sign implies that heat transfer rate, $q^{"}$, is in the negative temperature gradient, as heat is transferred from warm to cold. To sum up, heat flux resulting from conduction is a measure of how heat is transferred in each direction within an object or still standing fluid. [34]

2.3.3 Convection

As illustrated in the middle cell of Figure 2.1 convection is the exchange of heat between a fluid in motion and its bounding surface, between which two there are a temperature gradient. In Figure 2.1 the surface has a higher temperature than the fluid which result in a heat transfer from the surface to the fluid. If the fluid is hotter than the surface it is the other way around. In the convection mode energy transport is achieved both by bulk fluid motion, also known as advection, and the random motion of fluid of molecules, called conduction or diffusion. This makes convection more complex than conduction. To account for both advection and diffusion of convection a convective heat transfer coefficient, h, is introduced which can be computed from the dimensionless Nusselt number as follows:

$$Nu = \frac{hL}{k_f} \tag{2.4}$$

where L is the characteristic length, k_f is the thermal conductivity of the fluid. The Nusselt number (Nu) is a dimensionless parameter which either can be calculated from empirical relationships or computed numerically. Convection is strongly linked to fluid dynamic and how it is affected by fluid dynamic is captured by these relationships. Some important aspects of how fluid dynamics influence heat transfer is highlighted in Section 2.4. The Nusselt number is a measure of the convective heat transfer at the surface and is defined as the dimensionless temperature gradient at the surface according to

$$Nu = +\left.\frac{\partial T^*}{\partial y^*}\right|_{y^*=0} = f(x^*, Re, Pr).[34] \tag{2.5}$$

As is seen in Equation 2.5 the Nusselt number depends on the spatial variable x^*, the Reynolds number (Re), which is a fluid property see Equation 2.14, and the Prandtl number. The Prandtl number is a material property for the fluid defined as

$$Pr = \frac{\nu}{\alpha} = \frac{c_p\mu}{k} \tag{2.6}$$

where ν is the kinematic viscosity, α is the thermal diffusivity, c_p is the specific heat capacity and μ is the dynamic viscosity. So, the Prandtl number describes the ratio between the momentum diffusivity and the thermal diffusivity. For a system the average Nusselt number can be calculated according to

$$\overline{Nu} = \frac{\overline{h}L}{k_f} = f(Re, Pr).[34] \tag{2.7}$$

Similar to conduction, the heat transfer mode convection is driven by a temperature gradient. As is seen in Figure 2.1 the temperature of the moving fluid in the bulk flow is called T_∞. The bulk flow is the flow outside of the surface boundary layer, further explained in Section 2.4.2. So, the convective heat transfer can be calculated as:

$$Q = hA(T_s - T_\infty). \tag{2.8}$$

as a function of the convective heat transfer coefficient, the area of the surface and the temperature gradient between the bulk temperature and the surface temperature.[34]

2.3.4 Contact resistance

In some heat transfer applications there can be a significant temperature drop over an interface between two surfaces. This originates from the contact resistance between the materials which is illustrated in Figure 2.2 as an imperfect contact between surfaces due to surface roughness. The roughness causes voids in which air is present, which have a very low thermal conductivity. In addition, there is no convection present in the small voids since the air stands still. The result is an isolating layer of air bubbles at the interface. This resistance can be handled in simulations as anartificial wall according to

$$R = \frac{t_R}{kA} = \frac{\Delta T}{Q_x} \tag{2.9}$$

where R is the contact resistance, k is the thermal conductivity of the material and t_R is the thickness of the imaginary wall which correspond to the contact resistance. Contact resistance depend on several factors. A main factor is the surface roughness and its tolerance, another is the hardness of the material and a third is the applied pressure in a certain application. So, contact resistance is not a pure material property but is case dependent. It does not only depend on application but can also vary over time, for example as temperatures causes movement and materials age. [34]

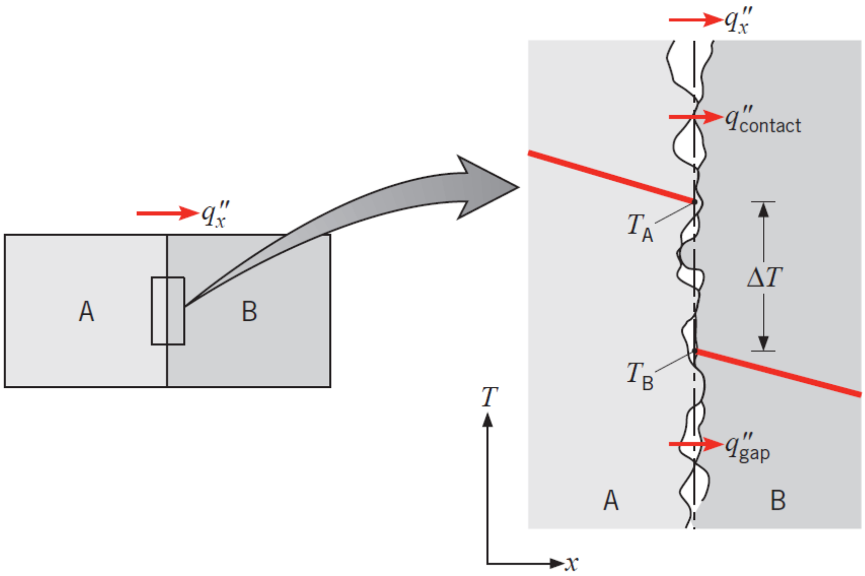

Figure 2.2: A zoom in to illustrate how surface roughness lead to imperfect contact and therefore air voids between two surfaces. The air have an isolating effect which lead to a temperature drop over the interface. So, the heat flux where there is contact, $q^{"}_{contact}$, is larger than where there are a gap, $q^{"}_{gap}$ and an average heat flux $q^{"}_{x}$ is reached. [34].

2.4 Fluid Dynamics

In this section some basic principles of fluid dynamics and its connection to heat transfer is presented. In addition, it is given how fluid dynamics is modelled using CFD, which is later picked up in the Chapter Method in Section 3.3. One of the governing equations of fluid dynamics is the Navier-Stokes equations which describes the flow of a Newtonian fluid. Navier-Stokes equations are in three dimensions and describe velocity, pressure, temperature and density of a moving fluid, according to

$$\rho \frac{d\mathbf{V}}{dt} = -\nabla P + \mu \nabla^2 \mathbf{V} + \rho \mathbf{g}, \tag{2.10}$$

where **V** is the velocity vector of the fluid, P is the pressure gradient of the fluid, μ is the fluid viscosity, **g** is the gravity constant and ρ is the density of the fluid. In order to solve the Navier-Stokes a numerical approach is applied. One approach is to use Reynolds Transport Theorem (RTT) together with the finite volume method (FVM) where the system is divided into small control volumes (CV), cells, within which all properties are conserved, but can be transported through the with control surfaces (CS). RTT can be described trough

$$\frac{d}{dt}(\mathbf{B}_{sys}) = \frac{d}{dt}\left(\int_{CV} \beta \rho \, dV \right) + \int_{CS} \beta \rho \, (\mathbf{V}_r \cdot \mathbf{n}) \, dA, \tag{2.11}$$

where $\mathbf{V}_r$ is the relative velocity vector, **n** is the normal vector, $\mathbf{B}_{sys}$ is an extensive fluid property representing either mass, energy, forces or momentum, and β represent the intensive fluid property given by the mass differential

$$\beta = \frac{d\mathbf{B}_{sys}}{dm}. \tag{2.12}$$

Another important differential equation describing fluid motion is the continuity equation. This describes the transportation within a domain and is defined as

$$\frac{\partial \rho}{\partial t} + \nabla \cdot (\rho \mathbf{V}) = 0 \tag{2.13}$$

where the first term is the changed density over time and the second term is the transportation of density with the velocity field. As described the FVM is applied on a domain by dividing the domain into a finite number of control volumes. The shape of the control volume can be of a variety of geometrical shapes. Different types of control volumes are tetra, hexa, and polyhedral cells. A subgroup of the polyhedral cells are prismatic cells. Prismatic cells are good at resolving curvature and give a smooth transition to domains with larger cell sizes. In each separate control volume, the Navier-Stokes equations are solved in order to obtain a numerical solution. First the boundary conditions of the domain are used to solve the boundary cells, which solution gives the boundary conditions to the neighbouring cells. In this manner the domain is solved from the given boundary conditions and information is transported in the domain until convergence is reached. [52]

2.4.1 Turbulence

Flows can be of different characters. It can be smooth and steady which is named laminar flow, or it can be fluctuating and agitated which is called turbulent flow. This division is a simplification of reality and between the two stages there are no clear line but an area of transition. In order to determine at what state a flow is, the dimensionless parameter Reynolds number (Re) is used, which is a ratio of the inertia and viscous forces. So, a low Reynolds number indicates viscous creeping motions with negligible inertia effects, while it is the opposite for high Reynolds numbers where inertia dominates. The Reynolds number is defined as

$$Re = \frac{\rho V L}{\mu} \tag{2.14}$$

where ρ is the density of the fluid, V the velocity, L the characteristic length scale and μ is the viscosity of the fluid. The characteristic length is defined depending on application. For internal flow, such as in a pipe or duct, the hydraulic diameter, D_h, is used as characteristic length. The hydraulic diameter is defined as

$$D_h = \frac{4A_c}{P_w} \tag{2.15}$$

where A_c is the crossflow area and P_w is the wetted perimeter. Since the division is a simplification of reality a laminar flow can have local turbulence and vice versa. But there are guidelines based upon the Reynolds number of the flow to determine whether a flow is laminar or turbulent. A general rule is that a high Reynolds number indicates turbulent flow, while a low Reynolds number is characteristic for a laminar flow. The following general guidelines for the transition between laminar and turbulent flow in ducts can be applied:

0 < Re < 1	Highly viscous laminar motion
1 < Re < 100	Laminar with strong Reynolds number dependence
100 < Re < 10^3	Laminar, boundary layer theory become useful
10^3 < Re < 10^4	Transition to turbulence
10^4 < Re < 10^6	Turbulent, moderate Reynolds number dependence
10^6 < Re < inf	Fully turbulent, slight Reynolds number dependence

where the Reynolds number dependence indicates how much the Reynolds number say about the statistic distribution between laminar and turbulent parts of the flow. However, the transition is case dependent, and is affected by surface roughness and possible fluctuations at the inlet. In addition, there is specific limits for internal flows for different hydraulic diameters. For flow in a circular or non-circular tube the transition region is between $2300 < Re < 10^4$, which is within the transition stage listed above. [52]

2.4.2 Boundary layer

Described in the previous Section 2.4.1 a flow can be described as laminar or turbulent with transitional region in between. The division is a simplification of reality where local turbulence can occur in a laminar flow. An example of laminar flow in an otherwise turbulent region is close to surfaces. As a fluid flows over a surface with a free flow velocity, u_∞, a boundary layer is developed due to friction between the surface and fluid, which is illustrated in Figure 2.3. The boundary layer is defined by having a velocity below 99% of u_∞. So, at the wall there is zero in velocity and then the velocity increase perpendicular to the wall. As is seen in Figure 2.3 it take time or the boundary layer to develop. Near the inlet the flow is laminar, then there is a transition region before the flow is fully turbulent. When the boundary layer has fully developed it is composed of different regions. The three regions of the boundary layer are marked in Figure 2.3 as the viscous sub-layer, the buffer layer and the turbulent region.

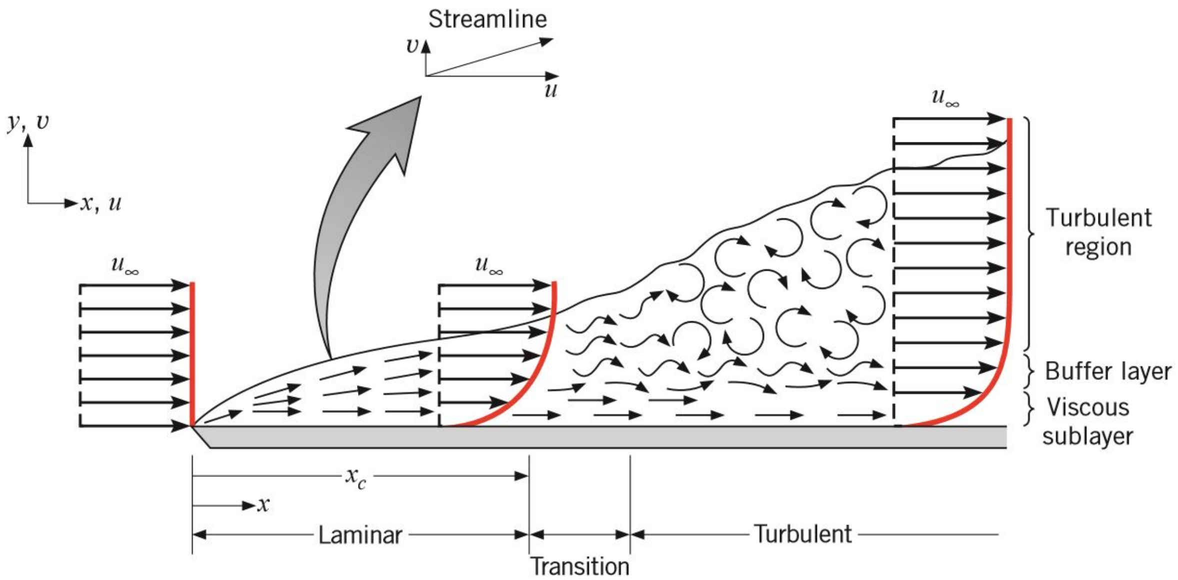

Figure 2.3: Development of velocity boundary layer on a flat plate. Including the three regions viscous sublayer, buffer layer and turbulent region of a fully developed flow. [34]

To determine which region the flow is at a certain distance from the wall, the dimensionless wall distance y^+ is used, which is defined as

$$y^+ = \frac{yu^*}{\nu} \tag{2.16}$$

where y is the distance to the surface, ν is the kinematic viscosity of the fluid and u^* depend on the shear stresses, τ and is defined by [52]

$$u^* = \sqrt{\frac{\tau_{wall}}{\rho}}. \tag{2.17}$$

The three layers are further described by Figure 2.4. Closest to the wall, $0 < y^+ < 5$, is the viscous sublayer where the flow is laminar and kinematic viscosity dominates. Outside of the viscous layer comes the buffer layer where the flow is impacted from both by kinematic and turbulent viscosity. Outermost is the turbulent region, also known as the log-layer, where the turbulent viscosity dominate. The turbulent layer has a lower limit of $30 < y^+$ with a higher limit between 300 and 1000, depending on flow and geometry.[52]

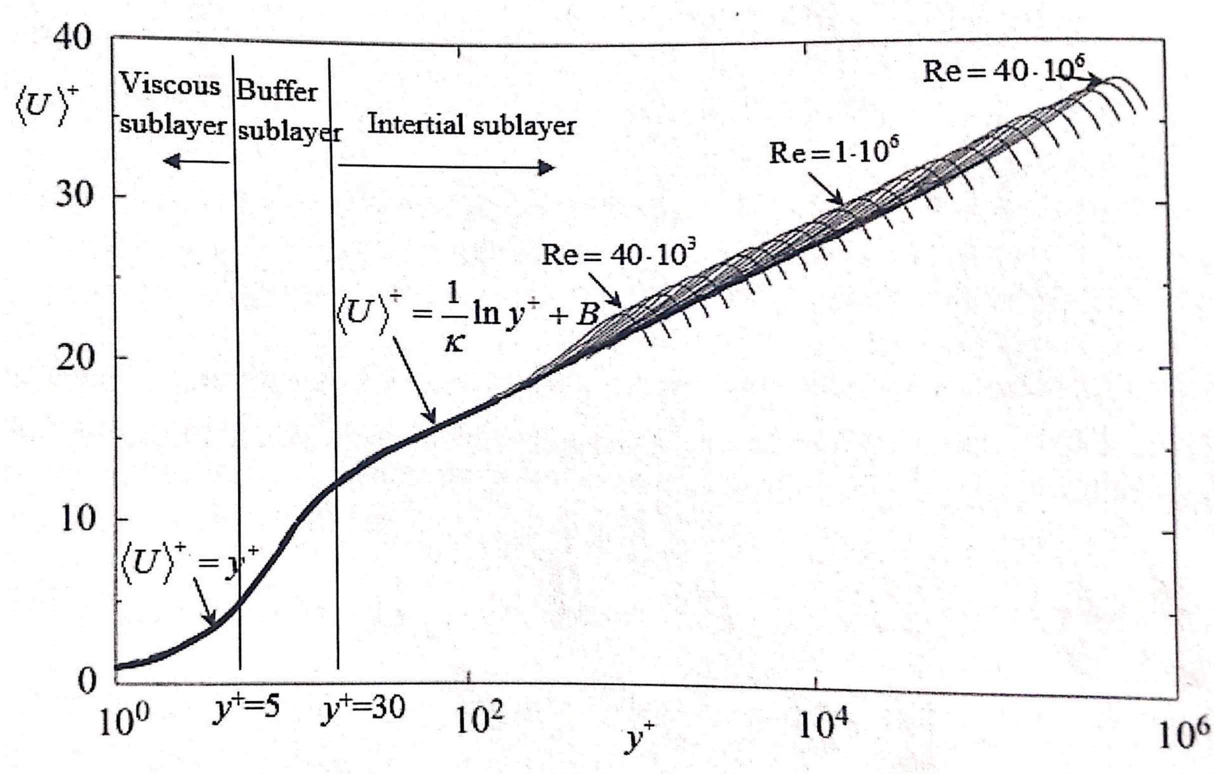

Figure 2.4: Graph of the boundary layer marking the viscous sublayer, buffer sublayer and the inertial sublayer with respective limiting value for y^+ [51]

Characteristics of the boundary layer of flow within a channel differ from flow over a plate. In Figure 2.5 the development of a boundary layer in a pipe flow application is illustrated and the effect this has on the development of the temperature boundary layer is also included. In the illustrated case the tube is heated with a constant temperature and constant inlet conditions. As the mean temperature is changing with x it is harder to determine a fully developed temperature boundary layer compared to the velocity boundary layer. So, to determine at what point the thermal boundary layer is fully developed a dimensionless temperature difference is introduced according to

$$dT^* = \frac{T_s - T}{T_s - T_m}. \tag{2.18}$$

where T_s is the surface temperature and T_m is the mean temperature of the fluid. As mentioned in Section 2.3.3 convection is strongly coupled to the fluid dynamics which gets clearer from this comparison in boundary layer development. The regions of the velocity boundary layer affect the heat transfer. So, close to the wall heat is transferred mostly by kinematic viscosity. While further out in the boundary layer the turbulent viscosity increases the mixture of the energy. [34]

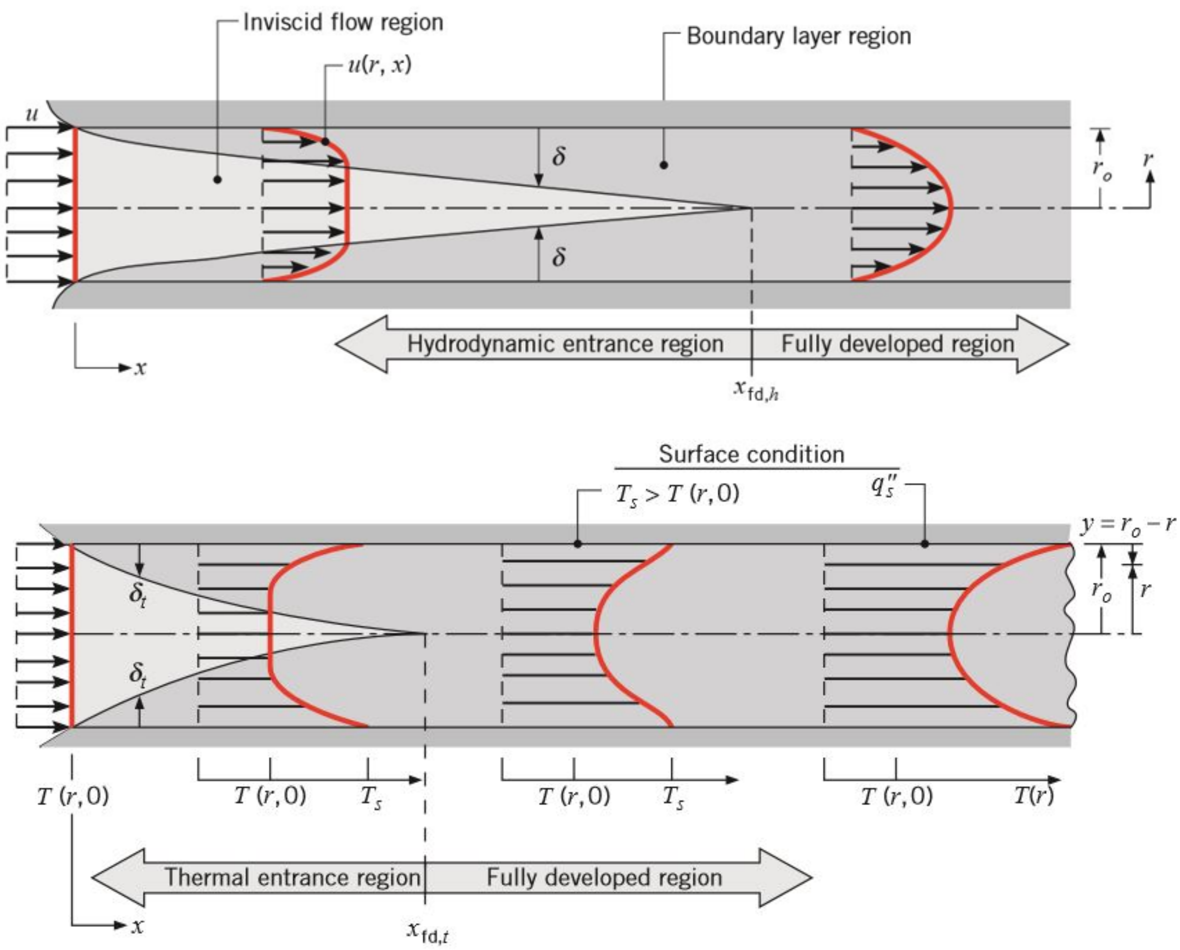

Figure 2.5: First illustration is of how a laminar velocity boundary layer develop in a circular tube. Below is the corresponding development of a thermal boundary in a similar heated circular tube.[34]

2.4.3 Turbulence modelling

In turbulent flow every pressure and velocity term are varying random as a function of time and space due to the fluctuations. The instantaneous and fluctuating variables would require immense computational capacity to handle, so instead models are used. [51] Therefore, the Navier-Stokes equations, see Equation 2.10, are transferred to an average called Reynold Average Navier-Stokes (RANS). RANS is a simplification of Navier-Stokes equation where the fluid properties are divided into one time-average term and one fluctuating term. RANS is like Navier-Stokes in three dimensions, written out for the x direction the RANS equation is

$$\rho\left(\frac{\partial \overline{u}}{\partial t}+\overline{u}\frac{\partial \overline{u}}{\partial x}+\overline{v}\frac{\partial \overline{u}}{\partial y}+\overline{w}\frac{\partial \overline{u}}{\partial z}\right) = -\frac{\partial \overline{P}}{\partial x}+\mu\left(\frac{\partial^2 \overline{u}}{\partial x^2}+\frac{\partial^2 \overline{u}}{\partial y^2}+\frac{\partial^2 \overline{u}}{\partial z^2}\right)-\rho\left(\frac{\overline{\partial(u'u')}}{\partial x}+\frac{\overline{\partial(u'v')}}{\partial y}+\frac{\overline{\partial(u'w')}}{\partial z}\right) \tag{2.19}$$

where the notion u' indicates a fluctuating term while $\overline{u}$ indicates a time average. In order to solve the fluctuating terms a turbulence model is applied. [52] There are several different turbulence models where choice of model to a large extend affect the computational time as well as accuracy of the model. In order to solve the steep gradients in the boundary layers at walls different approaches are applied depending on type of turbulence model. Some turbulence models can resolve the boundary layer using a fine resolution of the mesh to get the first grid point close to the wall at a certain y^+. While other turbulence models require wall functions since the turbulence model itself cannot resolve the dynamics of transition from laminar to turbulent which occurs within the boundary layer. Wall functions works by applying boundary conditions at a distance from the wall where the turbulence model is valid and are thereby not resolving the near-wall region. This is illustrated in Figure 2.6 where P represents the corresponding point W on the wall. This solution makes it possible to account for the rapid changes of flow variables in the near wall region with a coarser mesh. [51]

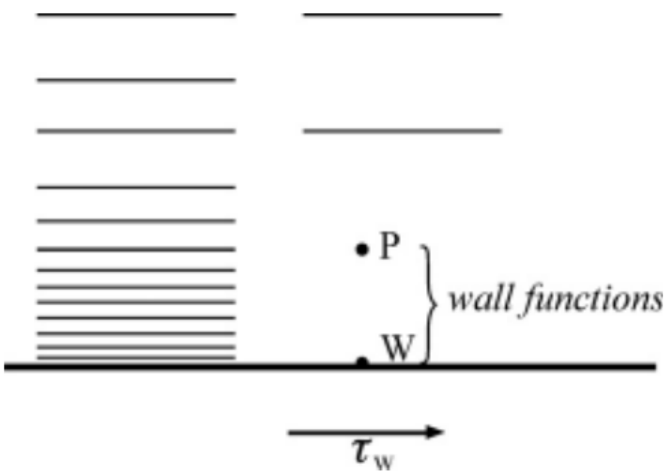

Figure 2.6: How wall functions is applied at a distance from the wall, where point P correspond to the position of W outside of the boundary layer [51]

2.5 Thermal Interface Materials

As described in Section 2.3.4, there is a contact resistance at material interfaces due to air voids between them. By including a thermal interface material (TIM), the voids can be filled and the contact resistance reduced. A TIM replace the original contact resistance with a new since the total thermal resistance of a TIM consists of both the bulk thermal resistance and two contact resistances. Bulk thermal resistance describes the conduction through the TIM, so it depends on the thermal conductivity and thickness of the TIM. While contact resistance depends on the surface characteristics respectively the ability of the TIM to scatter out and flow into surface features. So, selection of TIM for an interface between a heat source and sink is critical for a good heat transfer performance. [53]

Even if the contact resistance has a major impact on the heat transfer, evaluation of a TIM is often only based on thermal conductivity. Since a good surface contact is just as important, it needs to be taken into consideration. A reason why contact resistance often is neglected, is because it is not as simple as thermal resistance but case dependent. The contact resistance depends on several parameters. Although, a general and logical guideline is that a soft TIM usually adjusts better to surface roughness and provide a lower contact resistance.[54] However, the performance of a TIM is affected by several more properties than its thermal conductivity. The complexity in how the contact resistance of a TIM is assembled and how to evaluate and choose a TIM is illustrated in the fishbone diagram in Figure 2.7. [53] Some of the most important parameters to reach a low contact resistance is the ability to achieve required bond line thickness and possessing long term performance reliability. It should be noted from Figure 2.7 that performance of a TIM is degraded by non-optimised assembly, long term use at high temperatures and thermal expansion mismatches between materials. So, not only selection of material but also assembly and operation should be optimised to the selected TIM. [54]

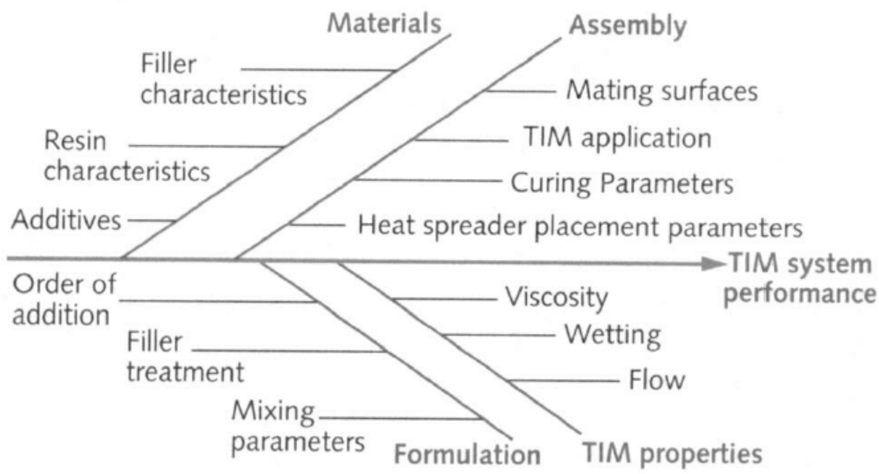

Figure 2.7: A fish-bone diagram over important material properties influencing the performance of a thermal interface material (TIM), to illustrate the complexity of choosing and evaluating a TIM. [53]

There are several materials that is suitable as TIM with different advantages and drawbacks. Most TIMs consists of a polymer matrix, such as epoxy or silicon resin, with fillers to increase the thermal conductivity. Some types of TIM are adhesive, greases, gels, gap fillers, phase changing materials, and pads. In short, thermal adhesives are particle-laden materials applied via stencil printing. Adhesives are cured to allow cross-linking and provides structural support. While thermal greases and gels risk of pump-out over time. The advantage of grease or gel is how they conform well to the surfaces, which reduces the contact resistance. [53] Gap fillers also conforms well to surfaces and are often cured in place to avoid leakage. Gap fillers are relatively new as TIM and are making advancement on the market. A main advantage of gap fillers is how they spread and conform to a surface. They can be adhesive and allow efficient use of material, as only the material required to fill voids are applied.[55] Gap fillers can also be used to fill up large cavities, for example a battery module. In this way the heat transfer inside of the battery module can be improved since it otherwise is isolated by air.[56] PCM also conforms well to surface roughness and do not require curing. In addition, PCM can absorb high heat content to avoid thermal run-away. Pads are usually silicon with fillers to increase their thermal conductivity, which is limited. They offer gap filling functionality but is often pre-cut which may increase the thickness, which is sensitive to applied pressure. [53]

Manufactures of TIM can usually provide thermal data and compression forces. However, since the difference in thermal expansion make the data unreliable, it is not advised to rely only on published data to predict the performance of an application. Instead specific physical test of an application is required.[54] If no delamination of the TIM and the main materials occur the properties such as the contact resistance remains stable. Although, repeated temperature cycles, for example battery use in a PHEV, tend to cause delamination which reduces the surface contact. However, with a lower hardness usually leads to increasing creep behaviour when removing compressing stresses. Therefore, TIMs needs to remain elastic at low temperatures and keep thermal stability at high temperatures. [57]

2.6 Possible improvements of the heat transfer based on the presented theory

Based on the presented BTMS, the three modes of heat transfer, the effect of fluid dynamics and the contact resistance between surfaces, some basic principles of improving the heat transfer can be concluded. All modes of heat transfer can be increased by increasing the temperature gradient. As this project excludes both the temperatures within the cells and how the coolant is cooled the possibilities to increase the temperature difference are restricted. Another classic approach to increase either of the heat transfer modes is to increasing the heat transfer area, either toward the heat source or sink. This have been done through fins either in the flow channels or the battery, see Section 2.2.

A main parameter for heat flux through conduction is the thermal conductivity, see Equation 2.3. By increasing the thermal conductivity of materials between the battery and the coolant, the resistance is reduced and the heat transfer increased. Another way to reduce the resistance is by reducing the total thickness between the heat source and sink. However, this is limited by structural restriction. The conduction can also be increased by reducing the thermal contact resistance described by Equation 2.9. As described in Section 2.5 there are several new TIMs on the market and the selection process is complex. But another TIM can have a lower contact resistance. If the tolerance for surface roughness is reduced the thickness of the TIM can be reduced. This require less TIM to fill all voids but the finer tolerance can lead to higher production cost. The thermal conductivity of a TIM can be increased with additives, which often are scarce and expensive materials. But, if the tolerance is increased the required thickness and amount of TIM is reduced. Which increases the heat transfer and since less material is used the cost might not rise to much.

According to Equation 2.8 heat transfer through convection can be increased by either increasing the temperature difference or heat transfer area as discussed above, or by increasing the convective heat transfer coefficient. The convective heat transfer coefficient can according to Equation 2.4 be increased by increasing the Nusselt number. According to Equation 2.7 the average Nusselt number for a surface depend on the Reynolds number and the Prandtl number. The Prandtl number is a material property while the Reynolds can be increased by introducing more turbulence into the flow. Which according to Equation 2.14 can be done by increasing the coolant velocity or changing the characteristic length. Higher levels of turbulence, or mixture of the flow, can also be accomplished by structures in the flow channels which causes swirl.

3
Method

In this chapter the methodology of the project is presented. This study evaluated the heat transfer for a branch standard BTMS through CFD simulations in the software ANSYS Fluent. The improvements composed cases which were benchmarked against the base case in a comparative study. An overview over the workflow of the project is illustrated in Figure 3.1. After an overview, more detailed descriptions of the base case, the new cases, choice of models and discretization scheme, mesh generation respectively analysis is given.

As illustrated in Figure 3.1 the first step was to collect data, perform a mesh study and analyse the base case. Second step was to generate improvements of the base case through a brainstorming. Thereafter, the new cases required pre-studies with data collection and mesh studies if the geometry was changed. After analysis of the new cases, an additional iteration was performed to generate further improvements. This led to a combined case of two previous tested improvements. In addition, it led to recommendations of future research which fell outside the limits of this project.

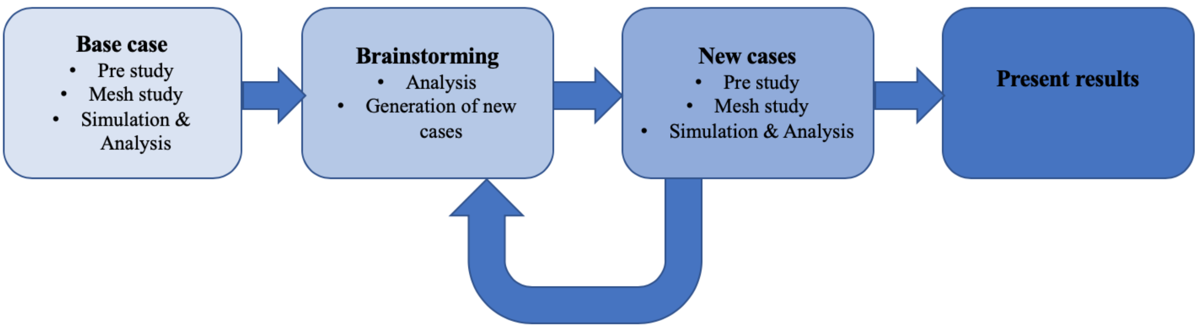

Figure 3.1: Flow sheet over the working process, including illustration of the iterative process.

Parallel with the workflow illustrated in Figure 3.1, a literature study was conducted. Focus of the literature study was twofold. First, in order to make the right assumptions, a common knowledge of best practice when simulating heat transfer problems in CFD was gathered. In addition, required data for the base case and the new cases was collected. Second focus was to map BTMS in terms of what previously has been developed, implemented and investigated. This also included some spot research, for example of different materials. The mapping of BTMS is presented in Section 2.2 and was used as inspiration during brainstorming.

3.1 Base case

First a pre-study was preformed to obtain boundary conditions and material properties for the CFD simulations. The model was based on a CAD model of the battery package and simplified in SpaceClaim. The first simplifying step was to remove redundant components from the model. Only two out of eight modules were included, which had a separate cooling flow for which boundary conditions was known. The empty battery modules and surrounding components was removed. So, the final stripped down model included cooling plates, inlet, outlet and thermal pads, see Figure 3.2. This constructed the worst-case scenario where all heat generated in the battery had to be removed by the coolant.

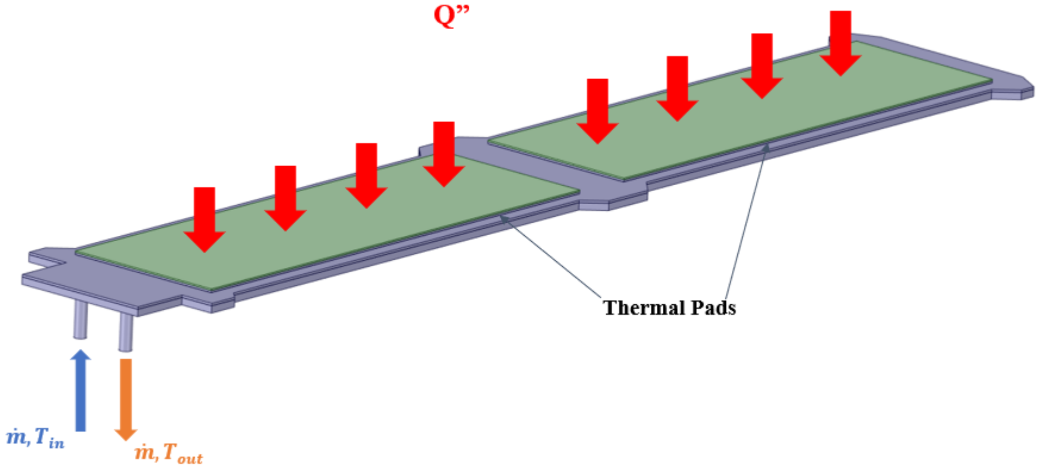

Figure 3.2: Overview of the simplified model for two out of eight battery modules removed from on top of the pads. Marking heat flux, $Q^{”}$, mass flow, $\dot{m}$, inlet temperatures, T_{in}, outlet temperature, T_{out} and location of pads.

Second part of simplifying the geometry was to reduce the complexity of investigated parts and the structure of the flow channel. An example of how this was done is shown in Figure 3.3 where it can be seen how both the geometry of solid parts and flow channels are simplified. The large structures were kept while small features, example rounding of edges and holes, was removed.

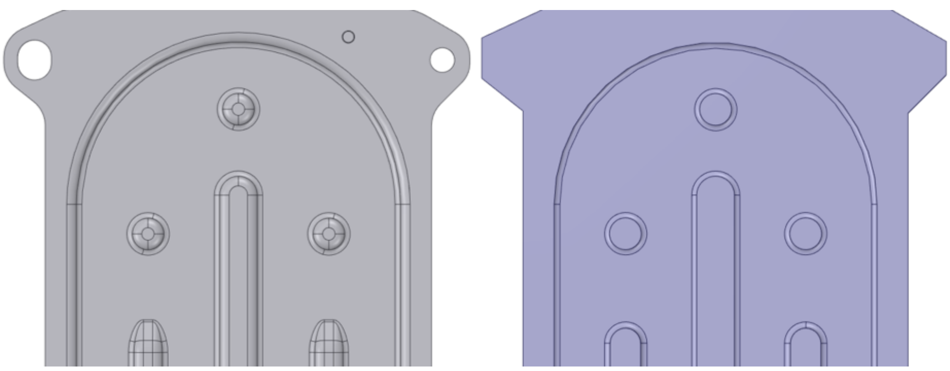

Figure 3.3: Example of how the cooling plate constructing the flow channels were simplified by removing small features. To the left is the original and to the right is the simplified geometry

3.1.1 Boundary conditions and Material Properties

As described in Section 2.1, the drive cycle of a battery change the amount of generated heat from the battery over time. With access to the design inside of the modules this could have been included in the model using ANSYS's battery model. As it was not available a constant, evenly distributed heat flux was applied at the interface between the thermal pad and the battery module, see Figure 3.2. The amount of generated heat was based on previous studies with an Equivalent Circuit Model (ECM) of the battery package, which showed that at a constant battery power of 36 kW all eight modules generated 1350 W of heat. By dividing this with the bottom area of all eight modules a heat flux of 4794 W/m^2 was calculated. This composed the worst-case scenario, which was why the outer walls were set as adiabatic.

Inlet boundary conditions came from the same ECM as the heat generation and is given in Table 3.1. The Reynolds number at the inlet was calculated according to Equation 2.14 to 3832, which indicate that the flow in the inlet channel was in the transition to turbulent region, see Section 2.4.1. Geometry of the pipes entering the flow channels was simplified and only included the closest geometry of straight pipes. Prior to the included geometry, the pipes had several bends which would induce turbulence, which was why a turbulent intensity was implemented at the inlet. The inlet was not long enough for the flow to develop. However, since the inlet was not a specific area of interest it was an acceptable simplification. The outlet was set to a pressure outlet. Pressure drop over the entire battery pack was known, which gave the backflow pressure.

Table 3.1: The main Boundary Conditions for the Base Case.

Mass flow	0,05275 kg/s
Inlet Temperature	283 K
Inlet absolute pressure	180 kPa
Hydraulic diameter	4,7 mm
Turbulent intensity inlet	5%
Outlet absolute pressure	16,21 kPa
Heat Flux	4794 W/m^2
Outer walls	Adiabatic

As described in Section 2.3.4 there is a contact resistance between interfaces. The original contact resistance in the base case was reduced by including a thermal pad as a TIM. The contact resistance for the TIM was included in the module as an imaginary wall with a thickness according to Equation 2.9. The contact resistance for the thermal pad was known from test data, which resulted in the wall thickness given in Table 3.2. In Table 3.2 material properties of the thermal pad are given. As the specific heat capacity of the thermal pad were missing it was assumed to be similar to a silicon material [58]. Other materials in the system was the cooling plates made of aluminium Al3003 and the coolant which was a mixture with 50% Ethylene-Glycol and 50% water.

Table 3.2: Material properties for the thermal pad in the base case

	Thermal pad
Thermal Conductivity, k	1,5 W/mK
Density, ρ	2500 kg/m^3
Heat capacity, c_p, @ 273 K	691 J/kgK
Heat capacity, c_p, @ 373 K	770 J/kgK
Thickness TIM	0,0013 m
Resistance thickness, t_R	0,0020 m

3.2 New Cases

The analysis of the Base case led to suggested improvements implemented in new cases, which were tested and evaluated. Three types of improvements were investigated in this study: a different TIM in order to reduce the thermal resistance, implementation of a fin in the battery module to increase the heat transfer area and a new design of the flow pattern to obtain a more even temperature distribution. After these cases were simulated and analysed a combination case were constructed where the new TIM and flow pattern were combined. Since all new cases were based on the base case a majority of the data and settings were the same. By using the same settings and assumptions the impact of model choices and other simulation settings was reduced.

3.2.1 New thermal interface material

Even before simulation, it was recognised that the thermal pad in the base case had a low thermal conductivity of 1,5 W/Km. As described in Section 2.3.4, there is also a contact resistance which usually is lower for softer materials. There are several types of TIM mentioned in Section 2.5, and it is clear that choice of TIM is a complex procedure. Therefore, material experts at Henkel were consulted when selecting a TIM to test [56]. The suggested material was a gap filler which was cured in placed and used in similar applications which made it a reasonable choice. As described in section 2.5 the total heat transfer resistance consist of a bulk resistance and a contact resistance. The chosen TIM had a thermal conductivity of 3 W/Km, which was two times higher than the original value. There are TIMs at the market with even higher thermal conductivity which can be used if electrical isolation is not required. [59]

Another important parameter for the thermal resistance is the thickness of the TIM. Required thickness most depend on the surface roughness of the materials in contact with the TIM. Since this was unknown and the original thickness fell within the manufactures recommended interval, the thickness was unchanged. [59]. The contact resistance of the new TIM for the application was unknown. However, as described in section 2.5 the contact resistance is lower for a TIM with higher wetness, so a gap filler was expected to have a lower contact resistance than a pad. Even if data had been available, the contact resistance is case dependent and given data from manufactures is just an indication. To capture the possible range of results a new TIM could have two values of contact resistance were tested. One case had the same contact resistance as the base case, which gave a worst case since literature strongly suggest that a gap filler have lower contact resistance than a thermal pad. The second case was an ideal case where the contact resistance was zero which is unrealistic but exposed the possible range of improvement.

Table 3.3: Material properties for the case with the new TIM material. One worst case with the same contact resistance as in the base case and one ideal case with zero contact resistance.

	Worst Case	Ideal Case
Thermal Conductivity, k	3 W/mK	3 W/mK
Density, ρ	3000 kg/m^3	3000 kg/m^3
Heat capacity, c_p	870 J/kgK	870 J/kgK
Thickness TIM	0,0013 m	0,0013 m
Resistance thickness, t_R	0,0041 m	0 m

3.2.2 Fins in the battery module

This project was limited to not change the outer dimensions of the battery module and did not have access to the design inside of the modules. Although, suggestions of modifications within the battery module were acceptable. One way to increase heat transfer is by increasing its area, see Section 2.3. According to research presented in Section 2.2, the usage of fins close to the cells improve the cooling efficiency. In addition, there was of interest for the company to investigate the effect of a fin within the battery module. Therefore, one of the new cases include a fin in the module. Similar to the base case, the heat flux was constant and calculated for heat flux on the fin as well. This gave a heat flux of 3016 W/m^2. Real heat flux is not constant over the fin, but as suggested in Section 2.1 higher near anode and cathode.

In Figure 3.4 it is illustrated how a fin was added on top of the base case model. To limit size and complexity only one fin was added. The fin was placed in the centre to allow an even heat distribution and the thickness was based on a visual evaluation. A more comprehensive analysis would be required to consider all effects of including a fin, for example swelling see Section 2.1.1. But the aim of this fin case was to determine if further investigation was of interest.

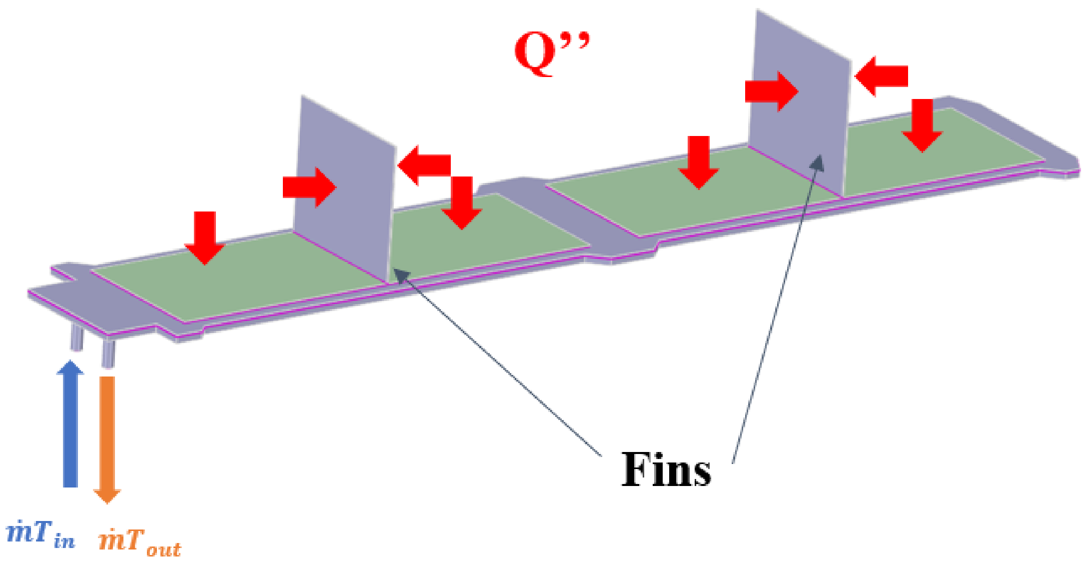

Figure 3.4: Layout of how the fins were placed in the model used in the simulations. Marking heat flux, Q^{J}, mass flow, $\dot{m}$, inlet temperature, T_{in} and outlet temperature, T_{out}.

3.2.3 New Flow Pattern

From analysis of the base case it was discovered that the mixture of the coolant was low, which led to an uneven temperature distribution. As described in Section 2.1 and further developed in Section 2.2 an even temperature is important for the performance, safety and life-span of a lithium-ion battery. Therefore, it was investigated if a different pattern would have an effect on the temperature variance.

The design of the new pattern was developed using initial simulations with the same mesh settings as for the base case. This was done to quickly see if the developed pattern had an effect on the mixture. A first attempt to increase the mixture, and thereby increase the turbulence intensity, was done by moving the already existing structures within the channels to increase the turbulence, see Pattern 1 in Figure 3.5. The aim was to try to change the structures as little as possible, since neither mechanical properties or manufacture restrictions were investigated. By comparing the result from the initial evaluation of Pattern 1 with the Base case it was deducted that the movement had a limited effect on the mixture, see comparing contours in Appendix D. Therefore, a second design was developed inspired by heat exchangers with banks of tubes. For design of tube banks a staggered tube arrangement, see Figure 3.6, have a higher mixture than an aligned arrangement. Which was why the structures in the flow channels of Pattern 2 were designed as they were, see Pattern 2 in Figure 3.5. An initial evaluation was performed in the same way as for Pattern 1. Since, this showed an improved mixture a mesh study and further analysis was conducted.

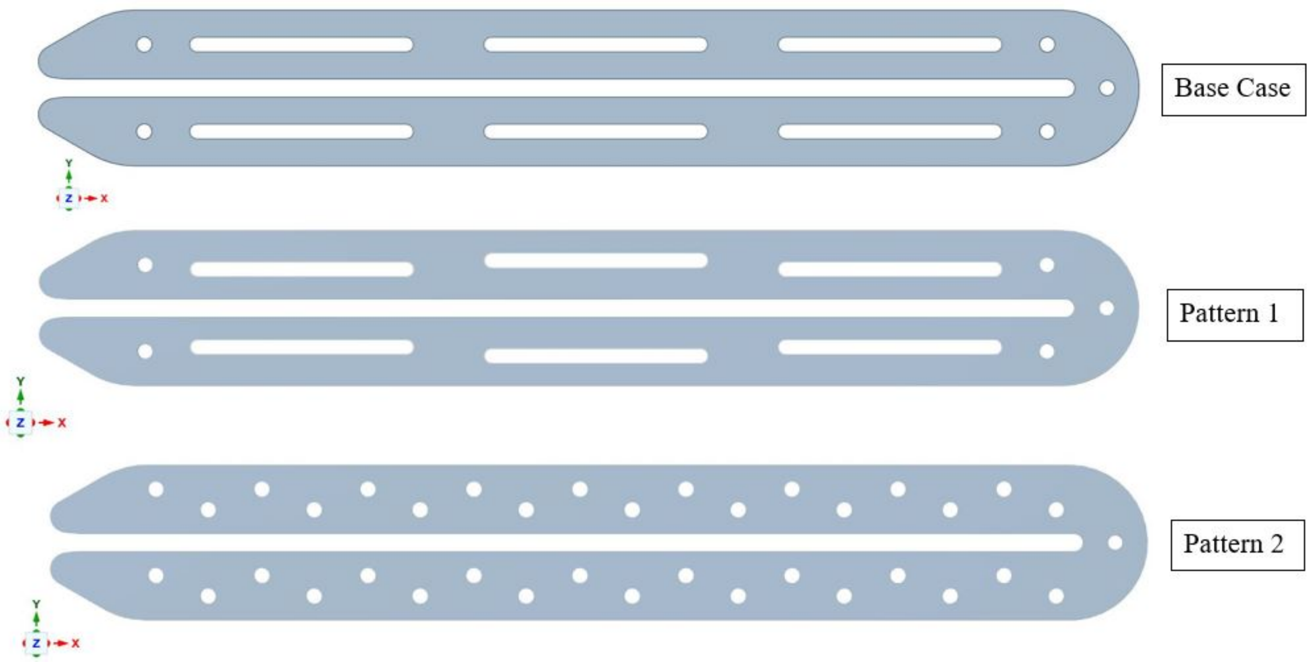

Figure 3.5: Comparison between the flow channels of the base case with the first new pattern where the same structures was used. In pattern 1 the flow channels were moved slightly so the structures were not places in a perfect row. The final second new pattern 2 was inspired by tube banks.

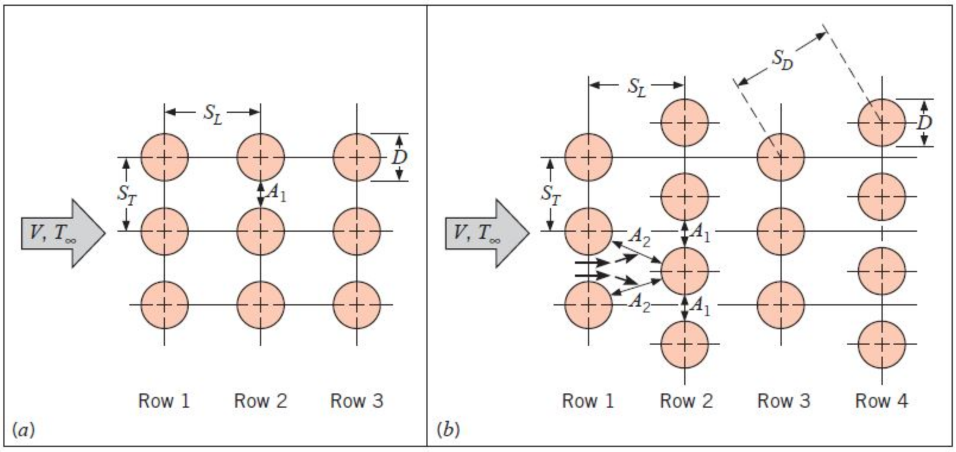

Figure 3.6: Tube arrangement in heat exchangers with tube banks. (a) Aligned. (b) Staggered [34]

3.3 Models and Discretization scheme

A model is always a simplification of the reality. In CFD there are several models available to solve the equations, where some were presented in Section 2.4 and Section 2.3. Choice of models both depend on type of problem and is a trade of between level of detail and computational power. However, there is no clear right or wrong model, but best of practice where some models are more validated and recommended for certain types of problems.

3.3.1 Turbulence modelling

As stated in Section 3.1.1 the flow in both the inlet and between the plates are turbulent. A turbulent flow can be resolved with different levels if detail. The highest level of resolution is the direct numeric solution (DNS) where all fluctuations is resolved, which require extreme high computational cost. So, it is only applicable for very small domains. For most problems a turbulence model is applied so either none or some parts of the flow is resolved. A common approach is to use one of the Reynolds Average Navier Stokes (RANS) two-equation models. In this project the RANS model k-ω was used. This model was preferred over the more validated k-ϵ model since it works better in low turbulence areas, such as near walls, and it avoids suppressing of swirl. Both k- ω and k-ϵ are complete models in the sense that velocity and length scales of turbulence are predicted together with transport equations. Furthermore, the k-ω is a robust and economical model in terms of computational requirements. [51]

There are two methods for modelling the near-wall region. Either to use wall functions to gain boundary conditions for the first grid point outside of the boundary layer, see Section 2.4.2. The other method is to use a turbulence model which can resolve the boundary layer. The k-ω model is such a model as it is able to predict the law of the wall for the viscous sub-layer. This is another advantage compared to the k-ϵ model which require wall functions. However, in order for the k-ω model to work correctly the first grid point near the walls needs to be in the viscous boundary layer, with a $y^+ < 5$, see Figure 2.4. This gives a very fine mesh near the walls and increase the number of cells, which is a disadvantage compared to the k-ϵ. [51]

3.3.2 Pressure coupling and Discretization schemes

Since a fluid problem has more unknown than available equations an iterative process is required to solve the velocity field. Therefore, a connection between pressure and velocity is applied, by using either a segregated or coupled algorithm. Neither of the approaches are generally better than the other with respect to robustness or efficiency. Although, since the segregated algorithms solves the pressure and momentum equations separately it can have a slower convergence than the coupled solver for some problems. [51] In this project both segregated and coupled solvers was tested. It was found that the segregated solver Semi-Implicit-Pressure-Coupling-Equations (SIMPLE) gave the most robust convergence and faster calculations than the coupled solver, which was why it was used. [51]

In order to solve the flow and energy equations disretization schemes are required. Discretization schemes decide how the calculation of the cell value depend upon its nearby cells. So, first order schemes only use values from the nearest cells while second order use the values from two cells away. In accordance with best practice, higher than second-order discretization was used in this project. Second order is less stable than first order since its unbound but include transportiveness and avoid overestimation of entities in flow direction, which is a risk with first order schemes. For higher schemes than second order the stability decrease. Higher order schemes were tested and showed that the solution was independent of method for second order schemes and up. Therefore, it was concluded that for this case second order schemes were enough. Relaxation factors was used to get a stable solution from the beginning. After the solution had stabilised these where increased to get a faster result. [51]

3.4 Mesh generation

For each case with a new geometry a mesh was generated through a mesh study in order to get valid results from the model. Aim of the mesh study was to obtain an independent mesh. Mesh independence is reached when a refined mesh gives the same result as a coarser mesh. Then the coarser mesh is independent. For all generated meshes the following quality criteria was checked:

- Maximum skewness < 0,95
- Average skewness < 0,33
- Maximum Aspect Ratio < 5, up to 10 inside boundary layer
- Minimum Orthogonal quality > 0,1.

which all are criteria for how well suitable the shape of the cell is. Where a perfect cell has zero skewness and one in aspect ratio respectively orthogonal quality. [51]

All mesh studies followed the same steps which were the following. Firstly, the boundary layer was adapted. An initial coarse mesh gave the total height of the boundary layer and how high the first layer thickness had to be to get an average y^+ for the first boundary layer of 1 and the maximum below 5. For the cases with identical flow region the same values as in the the base case could be used. Nevertheless, the y^+ was controlled to be acceptable for all cases.

Secondly, the mesh was refined globally by reducing the maximum cell size in steps of 10% of the original value to investigate mesh independence. To ensure that each mesh converged several parameters beside the standard residual was monitored. Convergence was reached when the residual had levelled of and all monitored parameters varied with less than 0,01% over 1000 iterations. The parameters was the mixed cup outlet temperature, the total heat transfer rate and the surface Nusselt number. In addition, velocity, pressure and temperature in a probe was monitored to ensure a fully developed flow. The probe was placed after initial simulation in a wake after the stirring U-turn. In Figure 3.7 the probe was placed in the middle of the outlet channel in y-direction at intersection between the cross section in x-direction below the U-turn and the cross section in z-direction in the middle of the flow.

Finally, the meshes with different levels of refinement was compared to see if mesh independence was reached or further refinement was required. Convergence criteria for the mesh independence was based on best practice, the time limitation of the project and the fact that flow features was not studied. So, a convergence criterion of less than 0,01% variation of parameters between two cases was used to determine mesh independence. The parameters was total heat rate, surface Nusselt number and temperature difference between outlet and inlet. Result of mesh study for the base case is presented in Section 4.1.1.

3.5 Simulation and Analysis

After the simulations were completed a simple sanity check of the system domain was performed to ensure conservation of mass and energy. Thereafter, analysis of the simulations was done by comparing the efficiency of the BTMS from different angles. In order to compare the total thermal resistance between the different cases an overall heat transfer resistance from the top of the thermal pads to the fluid was calculated. This was done by taking the difference between the average temperature of the pads surfaces and the volumetric average of the fluids temperature and divide it on the total heat transfer rate, according to Equation 2.9. This gave an average heat transfer resistance. Furthermore, contours of temperature in cross sections and surface plots was compared. In Figure 3.7 cross sections in two directional dimensions are illustrated. First is the cross sections in x-direction where one was placed below the U-turn and another at the middle of a fin. The second part is the cross section in z-axis which is placed in the middle of the flow channel. The results was later discussed and effect of different simplifications were weighted in. These are the cross sections which were used in the presented result. However, more cross sections were investigated but did not contribute any additional input to the conclusions.

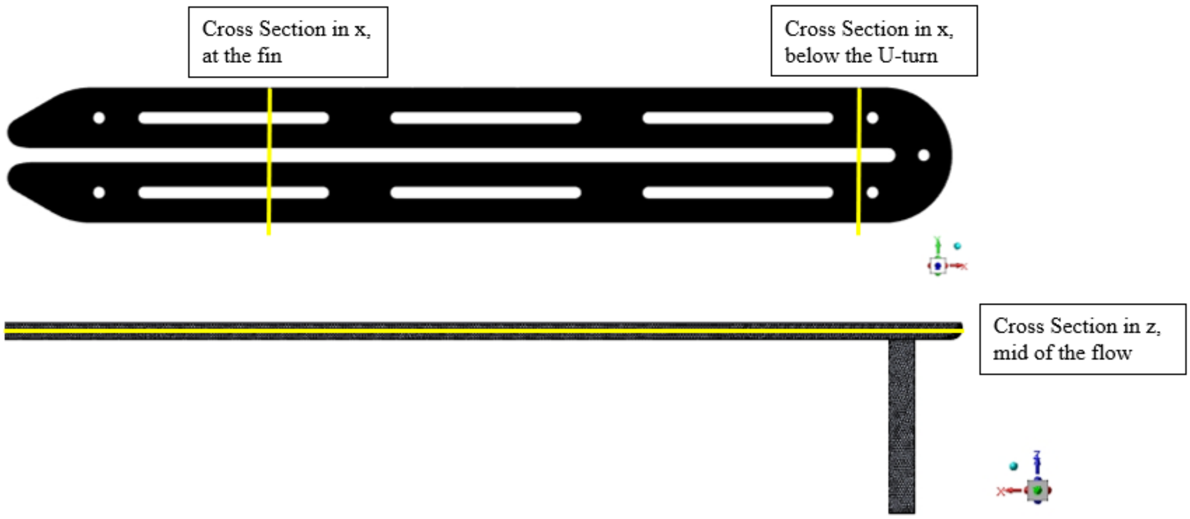

Figure 3.7: Cross sections in the two of the three directional dimensions which where used to present the result of the analysis of the cases. First is two planes in x and then one i z.

To notice is that the Nusselt number given from ANSYS Fluent is based on the reference values in the set-up. As is seen in Figure 3.5 the characteristic length vary along the z-direction. For the simulations a general characteristic length of 5,64mm was applied based on Equation 2.15. The Nusselt number as well as other parameters is dependent on the reference values which was the material properties of the coolant at 273,15K. Since this is a comparative study the reference values were set to the same for all cases which reduced the impact on the results. However, the confidence in the presented values should be questioned and not put out of perspective by separating them from this comparative study.

4

Results

In this chapter results of the project are presented. First are results of the base case presented, including its mesh study. After which, the results of new cases are presented. The three types of new cases were as follow: replace the TIM, use a fin and change the pattern of the flow channels. For the new cases validation of the meshes were performed after the same procedure as for the base case, and are not presented here but in Appendix B for the fin respectively Appendix C for the changed flow pattern.

4.1 Base Case

In this section the results of the Base Case is presented. First is the result of the mesh study for the base case, followed by the results of the simulation. During the analysis, several plots and contours was investigated, but only those contributing to conclusions are presented. The result was both used to see possible improvements and as a baseline in the comparative study of the improvements.

4.1.1 Result of mesh study

The mesh study of the base case was performed according to the procedure presented in Section 3.4. All generated meshes had approved mesh quality criteria. Complementing figures to this mesh study can be found in Appendix A.

First step of the mesh study was to generate a good mesh boundary layer that captured the entire velocity boundary layer and had the first grid point at $y^+ < 5$. From initial simulations it was concluded that the boundary layer had a total thickness of approximately 0,25 mm. It was controlled that the final mesh captured the entire velocity boundary layer, which can be seen in Figure A.1. The number of layers was limited to five, since an increase to seven drastically increased the number of cells. In accordance with the limits of y^+, a first layer thickness of 0,15mm gave an average y^+ for the first grid point around 1, see Figure A.2. Most cells had an $y^+ < 5$, but a few cells near the inlet respectively outlet had $5 < y^+ < 7{,}89$, see Figure A.3. This was acceptable since it was not any area of interest.

Second step was to globally refine the mesh until mesh independence was reached. This was done by reducing the maximum cell size in steps of 10% according to Table 4.1, which increased the total number of cells. It was confirmed by Figure A.5 and Figure A.4, that the increase in number of cells took place in areas of interest, which was desirable. Each mesh was run until the convergence parameters presented in Section 3.4, was stable. In addition the trends of the different plots were studied, so the simulations run until they had flattened out. In Table 4.2 the total heat transfer rate and temperature difference between outlet and inlet are presented for the three investigated meshes of the base case. In addition, the parameters surface Nusselt number, standard residuals respectively temperature, pressure and velocity in a probe was controlled but showed the same trends as the two presented parameters, and are therefore not presented. Further refinements were not required and it was decided to use the second level of refinements which was independent from further refinements, see Table 4.2.

Table 4.1: How the mesh was globally refined in three steps with 10% reduction of maximum cell size per step. Also presented the total number of cells this resulted in.

	Maximum Cell Size	Maximum Fluid Face Size	Total Number of Cells
Refinement 1	3 mm	0,75 mm	5153641
Refinement 2	2,7 mm	0,675 mm	5426729
Refinement 3	2,43 mm	0,6075 mm	5815155

Table 4.2: Result of the mesh study. The parameters total heat transfer rate and temperature difference between outlet and inlet are presented. Deviation refer to the one from from preceding coarser mesh.

	Total Heat Transfer Rate	Deviation	$dT = T_{out} - T_{in}$	Deviation
Refinement 1	337,74 W	-	1,91 K	-
Refinement 2	337,77 W	7,49e-5	1,91 K	9,21e-5
Refinement 3	337,77 W	3,21e-5	1,91 K	6,27e-5

4.1.2 Evaluation of heat transfer

In this section the performance of the heat transfer for the base case is presented. Results of the base case were both used to see possible improvements of the system and to use as a baseline for the comparative study.

As explained in Section 3.1 a worst-case scenario was studied, so all heat had to be removed through the coolant. The amount of removed heat should be the same as the applied heat flux since all parameters were constant. Calculated either from the increased heat value of the fluid or the total heat transfer rate through the flow channels walls, the amount of removed heat was 337,77 W. Which was the same amount applied heat for the two modules. So, the energy balance added up and so did the mass balance as the same amount of fluid was removed as inserted. Figure 4.1 show a contour of the temperature distribution at a cross section in x-direction below the U-turn. Left side of the contour is the side of the inlet and is cooler than the right side. On the right side the fluid has increased in temperature. While the temperature at the interface toward the battery module is higher on the inlet side. The average heat transfer resistance from the bottom of the battery module to the coolant was calculated according to Equation 2.9 to 0,041 K/W.

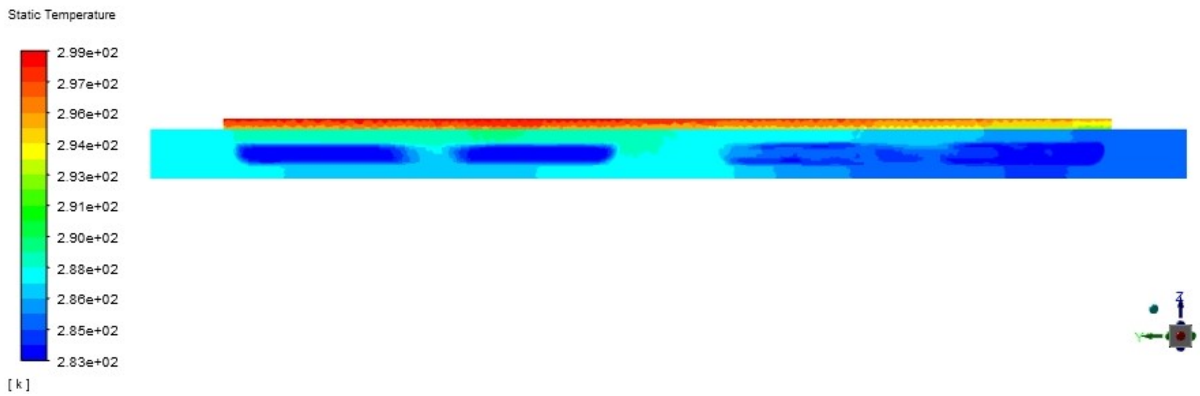

Figure 4.1: A contour of the temperature distribution through a cross section just below the U-turn. It can be seen that the highest temperature of the thermal pad surface occur where the heat flux was applied.

As was seen in Figure 4.1 the highest temperature occurred at the interface between the thermal pad and the battery module. The highest temperature at the interface was 299,60 K. Figure 4.2 shows the temperature distribution over the interface which has an temperature variation of 5,71K.

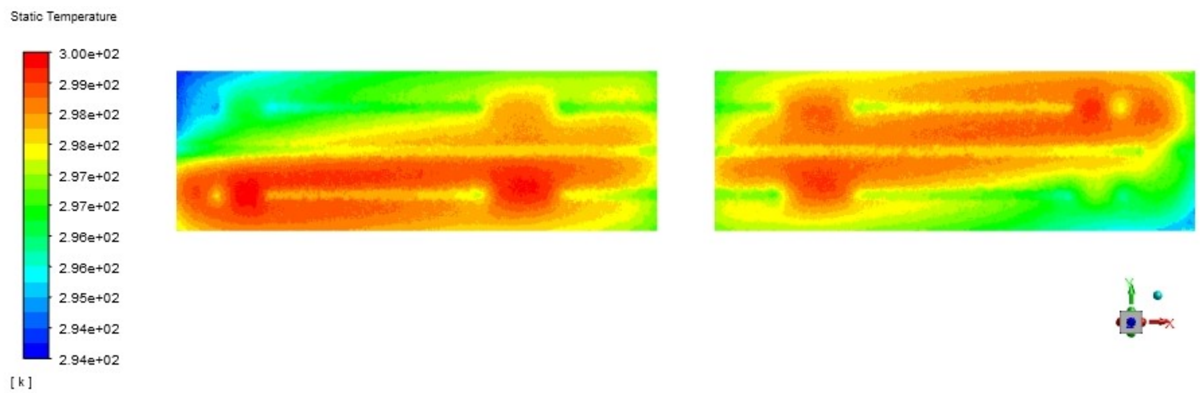

Figure 4.2: A contour of the temperature distribution at the interface between the two thermal pads and the battery module.

The temperature of the coolant is illustrated in Figure 4.3 and it is seen that the temperature is not well mixed. By comparing Figure 4.2 with Figure 4.3 it can be concluded that the increased turbulence and mixture at the U-turn increases the cooling noticeable. This is further seen from Figure 4.4 where the total surface heat flux is plotted in a contour for the interface between the thermal pad and the cooling plate. The fluid dynamic of the coolant flow affects the cooling rate which is why the heat flux varies over the interface. The highest rates are at the stagnation points at the structures in the flow channels and at the walls of the mirrored flow channels.

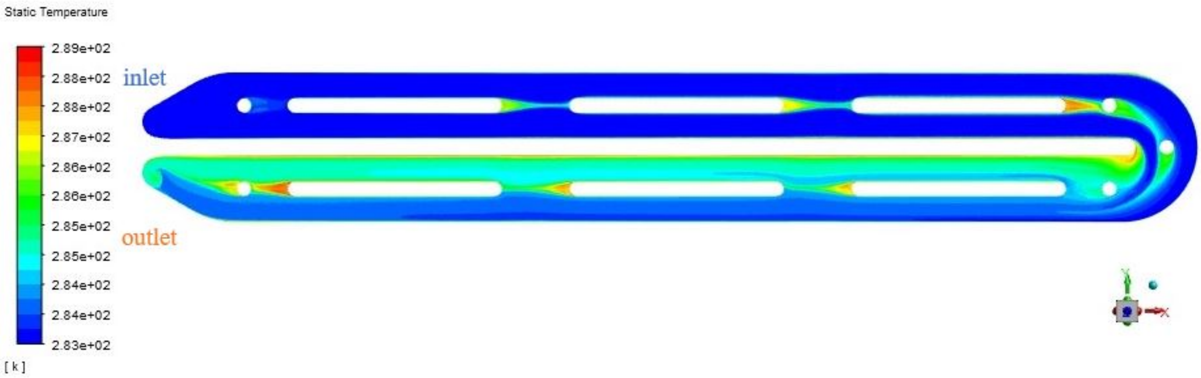

Figure 4.3: A contour of the temperature of the fluid in z-direction, in the plane at the middle of the flow. Side of inlet respectively outlet is marked.

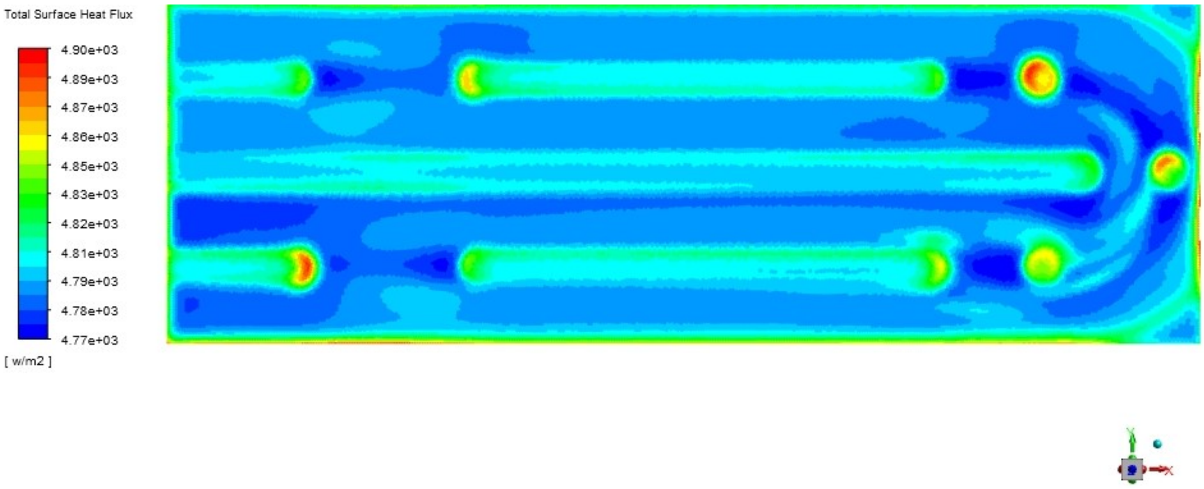

Figure 4.4: A contour of the total surface heat flux at the interface between one of the thermal pads and the cooling plate.

4.2 New Cases

In this section the results of the new cases are presented. All results, except the case with a fin, are presented in parallel to each other and the base case to simplify comparison. Since result of the case with a fin diverted drastically from the remaining cases, comparative contours with common scales was unsuitable. Instead the result from the fin case is presented separately. In accordance with the way of evaluating efficiency of a BTMS, presented in Section 2.2, the result is divided into the two parts heat transfer resistance and temperature distribution.

4.2.1 Heat Transfer Resistance

Similar to the base case the overall energy balance respectively mass balance added up. In Table 4.3 the calculated average heat transfer resistance, according to Equation 2.9, for all cases is presented. All new cases, except the one with a fin, showed improvement compared to the base case. This is further illustrated in Figure 4.5 over the temperature distribution in x-direction. As the top temperature is lower and the temperature distribution is more even, less heat is accumulated due to the reduced resistance. The combination of the new TIM and flow pattern show the lowest resistance after the ideal case with a new TIM. Since, the combined case almost have the same improvement as the product of the two separate improvements, the gain from increased mixture respectively higher thermal conductivity are almost independent of each other.

Table 4.3: Average heat transfer resistance for all cases calculated according to Equation 2.9.

	Average Heat Transfer Resistance	Compared to base case
Base Case	0,041 K/W	1
New TIM, worst case	0,035 K/W	0,85
New TIM, ideal case	0,015 K/W	0,37
One Fin	0,678 K/W	16,54
New Flow Pattern	0,039 K/W	0,95
New Flow Pattern and TIM	0,033 K/W	0,80

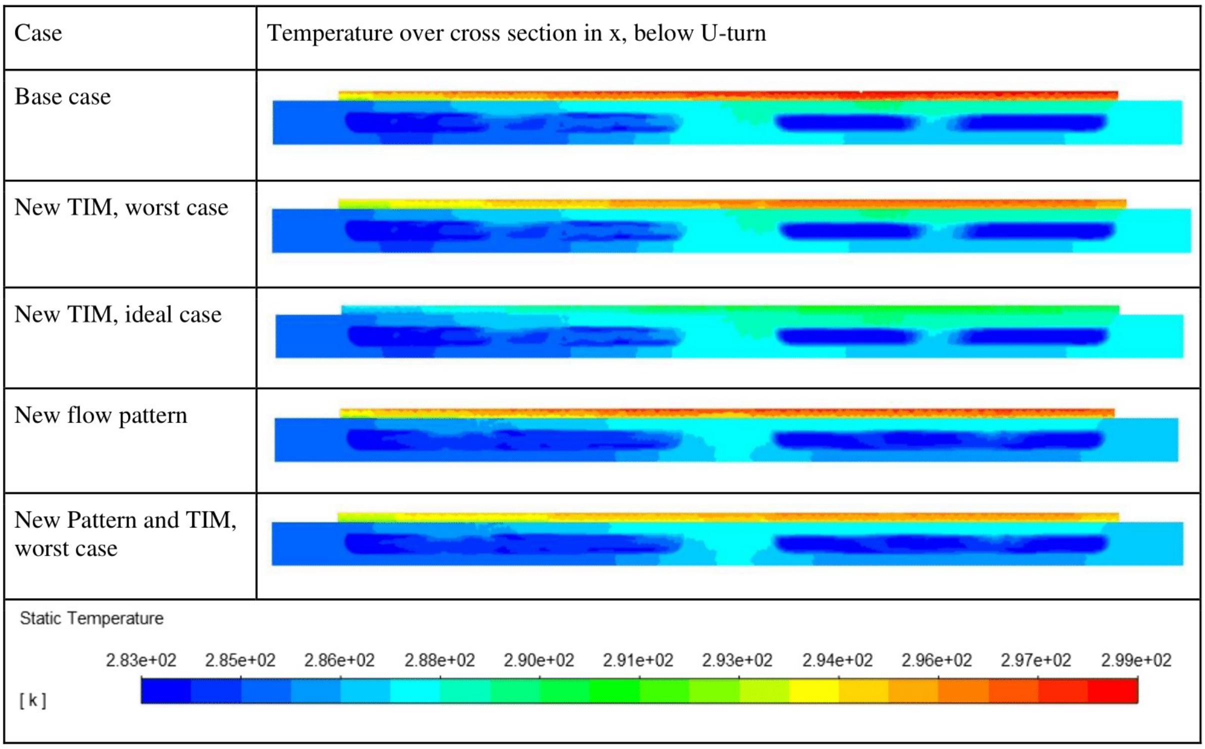

Figure 4.5: Comparative contours for all cases except the fin case, over the temperature distribution taken at a plane in x-direction below the U-turn. With a common scale to enable comparison.

4.2.2 Temperature distribution

Table 4.4 present the maximum temperature respectively the temperature difference (ΔT) at the interface between the battery module and the TIM for all cases. The case with a fin stands out with its large values. Except the fin case, all new cases have lower values than the base case. This is illustrated in Figure 4.6 of the bottom temperature of the battery module, where both reduced maximum temperature and variance is clear. The increased mixing from the new pattern have effect on the temperature facing the battery, which is more even than the original pattern. The combination case had the best performance. The product of the improvement of new flow pattern and the new TIM with worst case resistance was 0,836, which is lower than the combination case improvement. So, the two design changes reinforce each other.

Table 4.4: Maximum temperature and the temperature difference at the interface between the TIM and the battery module for all cases.

	$T_{max,interface}$	ΔT	ΔT compared to base case
Base Case	299,60 K	5,71 K	1
New TIM, worst case	297,74 K	5,45 K	0,95
New TIM, ideal case	291,30 K	5,58 K	0,98
One Fin	1654,79 K	1371,08 K	240
New Flow Pattern	298,83 K	5,02 K	0,88
New Flow Pattern and TIM	296,96 K	4,73 K	0,82

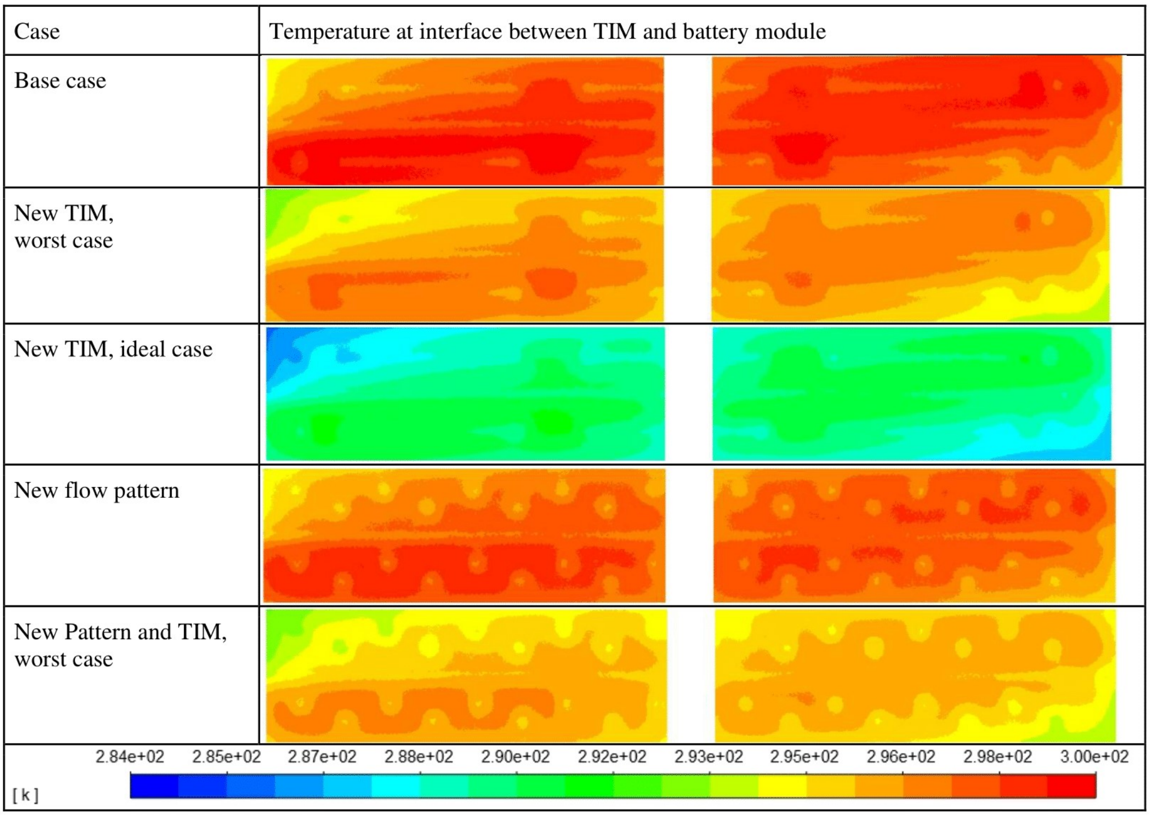

Figure 4.6: Comparative contours for all cases, except the one with a fin, over the temperature distribution over the interface between the TIM and the battery module. With a common scale to enable comparison.

How the new pattern increase the mixture can be seen in Figure 4.7, which shows the temperature of the in a cross section in z-direction for the cases. It is recognised that contours are similar for the cases using the old pattern. So, even if the resistance have been lowered with the new TIM, concluded from Table 4.3, the coolant temperature is barely affected. What stands out is the new pattern which has more mixture and even distribution than the old pattern. As was seen in Table 4.3, the increased mixing had a positive effect on the heat transfer resistance. Effects of increased mixture is also reflected at the surface heat flux in Figure 4.8. The new pattern shows a more even distribution of heat flux. The heat transfer is most effective for the ideal case of the new TIM, respectively the combination case. Similar to the base case, the highest rates of heat flux are at the stagnation points of the structures and the edges of the new designed flow channels.

Case	Temperature of fluid in cross section in z at the middle of the flow
Base case	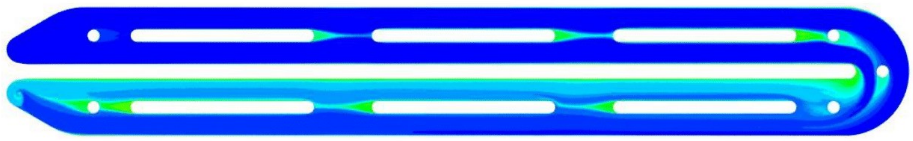
New TIM, worst case	
New TIM, ideal case	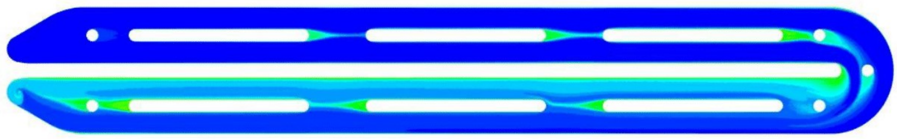
New flow pattern	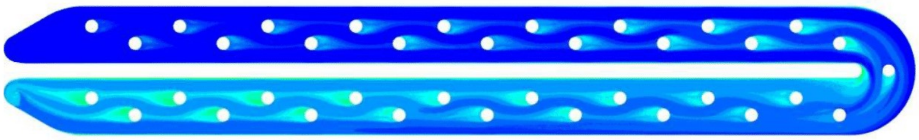
New Pattern and TIM, worst case	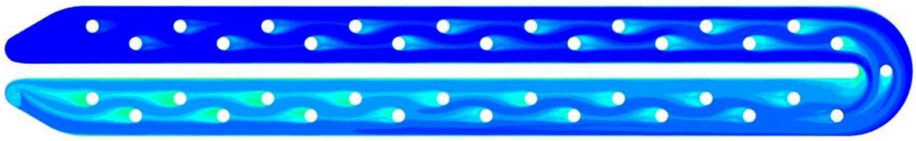

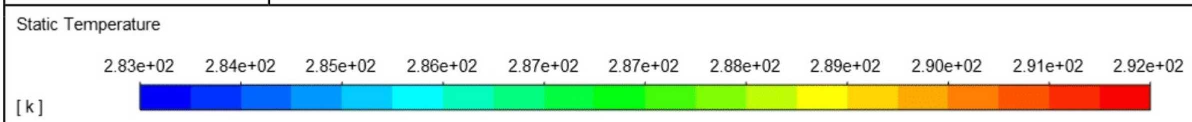

Figure 4.7: Comparative contours for all cases except the one with a fin, over the temperature distribution in the fluid, taken at a the z plane in the middle of the flow channels. With a common scale to enable comparison.

Case	Total surface heat flux at interface between TIM and cooling plate
Base case	
New TIM, worst case	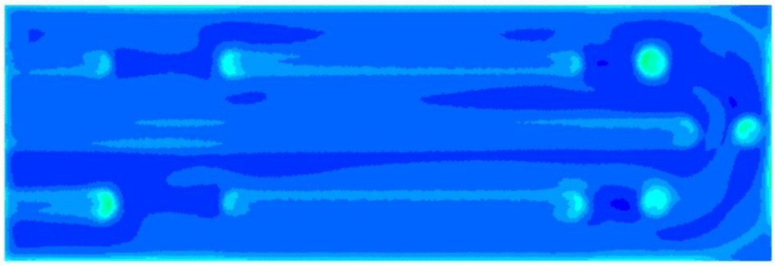
New TIM, ideal case	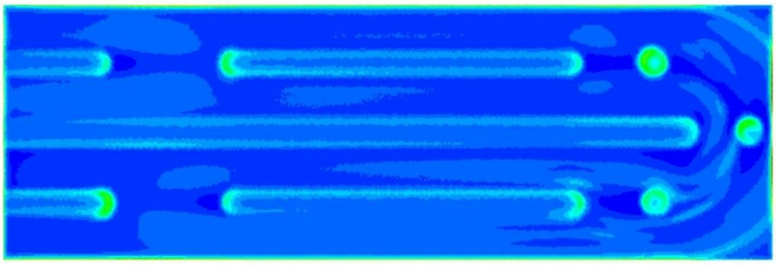
New flow pattern	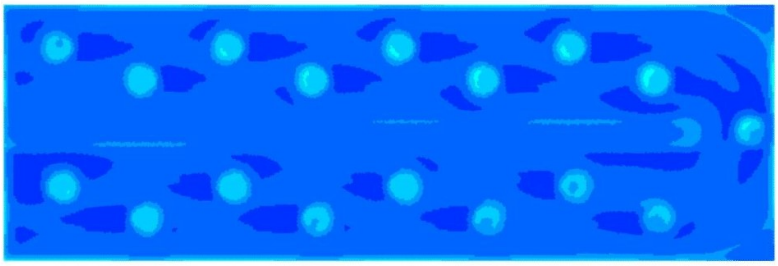
New flow pattern and TIM, worst case	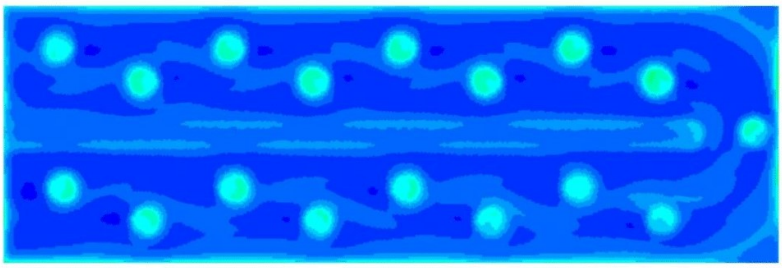

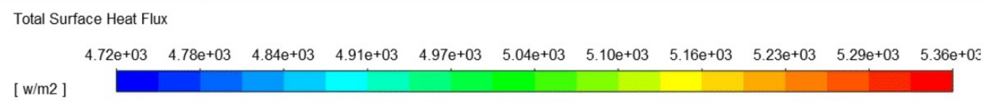

Figure 4.8: Comparative contours for all cases, except the one with a fin, over the heat transfer rate at the interface between the TIM and the cooling plate. With a common scale to enable comparison.

4.2.3 Effect of a fin

There are substantial differences in scale for the results of the case with a fin compared to remaining cases. So, the contours from the fin case are presented separately in this section. Same contours presented for remaining cases and more over was investigated, but only the contours relevant for the result are presented. Figure 4.9 shows a contour over the temperature distribution at a cross section in x-direction at the fin. From this it is seen how the heat accumulates in the fin which results in the extremely high temperature of 1654 K at the top of the fin. This results in an uneven temperature distribution, as presented in Table 4.4 and a high heat transfer resistance, presented in Table 4.3, due to the high temperature difference, see Equation 2.9. The uneven temperature distribution illustrate that the heat transfer rate was uneven, so contour over total heat transfer rate was redundant. However, the effect on the coolants temperature was small. This can be seen by comparing Figure 4.10 with Figure 4.7, which looks very similar. So, the high temperatures in the fin, see Table 4.4, did have a limited effect on the fluid temperature. Which gave the high temperature difference in Table 4.4.

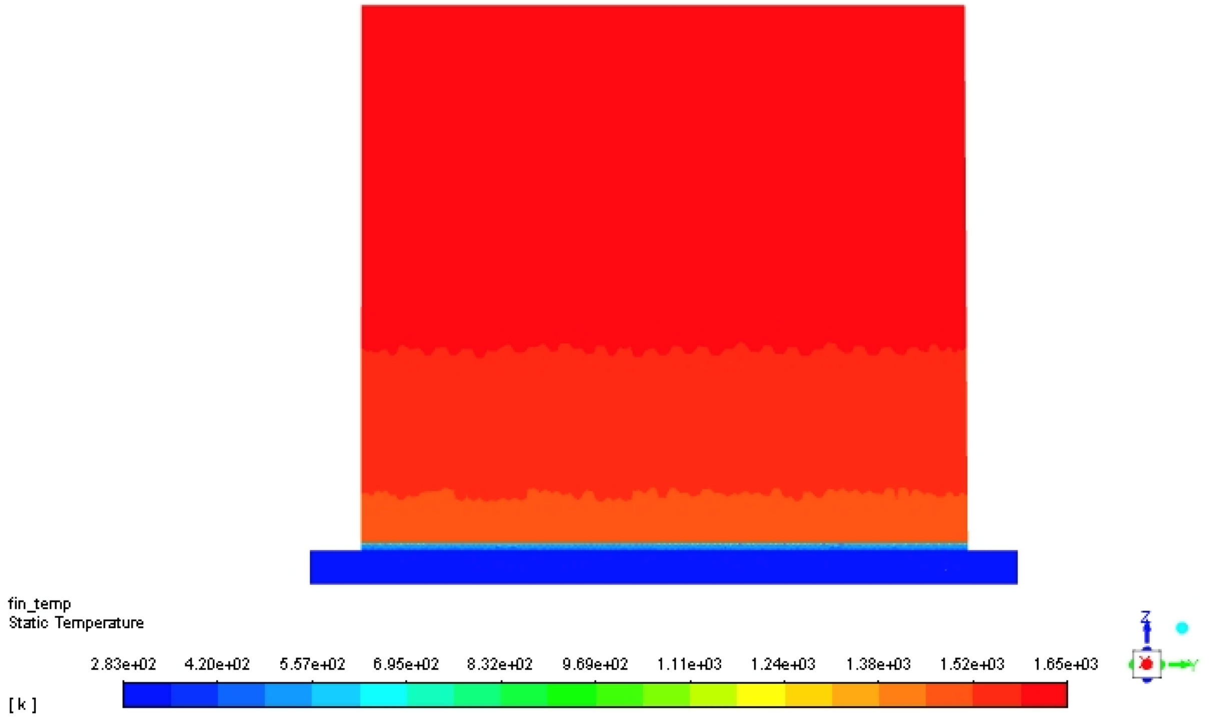

Figure 4.9: Contours of the fin case showing the temperature distribution over the fin in x-direction.

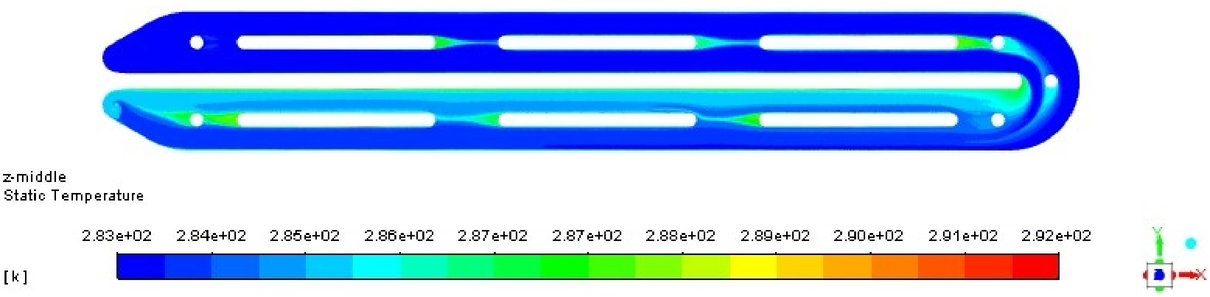

Figure 4.10: Contours of the fin case showing the temperature distribution in the fluid in z-direction.

5 Discussion

In this chapter the results of the project are discussed. First come the analysis and discussion of the base case, followed by a comparison between the new cases and the base case. After is a discussion on how simplifications and assumption throughout the project may have impacted the result. Last is the possible future research on the subject shortly discussed.

5.1 Analysis of Base Case and development of new cases

To summarise, from the analysis of the base case three possible design improvements were identified. Those where: reduce the thermal resistance by replacing the thermal pad, increase the heat transfer area by including fins in the module, and change the flow pattern to achieve a more even temperature distribution.

From Figure 4.1 it can be seen that the temperature is at its highest at the top toward the thermal pad. As described in Section 2.5 and 2.3.4 the heat transfer resistance is affected both by the bulk conductivity and the contact resistance. In order to reduce the heat transfer resistance from the battery module, the TIM could be replaced. As described in Section 2.5 the choice of TIM is not straightforward but depends on several factors. As this thesis overlooked mechanical properties, several parameters where not investigated. By reducing the thickness of the TIM, the resistance would be reduced. However, to ensure complete filling of voids the required thickness of a TIM depends on the tolerances of the surface roughness. Since this was unknown, the thickness of the base case was kept. Overall, by replacing the thermal pad with a gap filler a potential large improvement is enabled with relatively small design changes.

Since the heat is accumulated at the interfaces and not evenly distributed, see Figure 4.1, it is concluded that the base case is unoptimised. Several researchers presented in Section 2.2.2 suggest that fins can improve the heat transfer efficiency. In particular fins close to the cells are suggested to have a positive effect by increasing the heat transfer area. In addition, the company had an interest of investigate the possible effects of fins. However, as design inside the modules where missing a conceptual design based on several assumptions was developed. It had the purpose to investigate how a larger area to absorb heat from the battery affected the heat transfer resistance.

Figure 4.3 shows the temperature in a cross section in the z-direction, and from this it is clear that the flow is unmixed. Compared with a boiling BTMS presented in Section 2.2 which had 4K temperature variance within the cells, the base case had 5,71K in the interface. There are cold streamlines along the borders, and the largest temperature increases occur in the wakes behind structures. Figure 4.4 strengthens that the heat transfer rate is the highest in the wakes and edges of the flow. In Figure 4.2 the effects of an unmixed flow on the temperature distribution of the interface towards the bottom of the battery module are seen. So, it is deduced that the temperature distribution is uneven. At the U-turn the mixing and thereby the cooling effect are increased due to increased turbulence. As described in Section 2.6, this increases the heat transfer coefficient, h, and convective heat transfer rate. Since the heat transfer rate was higher in the wakes and favoured by increased turbulence the pattern of the cooling placed was redesigned. In order not to change the outer design the solid structures within the channels where changed. In Section 2.2 the impact of pattern is discussed both for liquid and air-cooled BTMS. The pattern does not only increase the turbulence but also pressure drop, which was not investigated in this master thesis. Another important factor from changed design is the mechanical integrity, which was not controlled. But the size the structures was similar as to the base case to make the new case as realistic as possible.

5.2 Comparison of the cases

In this section the results of the new cases is compared with the base case as well as to each other. The discussion is divided like the result where heat transfer resistance and even temperature distribution is discussed separately even though there are some overlaps. Since the new case with a fin diverted drastically from the remaining it is discussed in a separate section. So, when referred to as "all cases", the case with a fin is not generally included.

5.2.1 Heat transfer resistance

The purpose of this report was to investigate the heat transfer from the bottom of the battery module to the coolant and suggest possible improvements. In Figure 4.5 over the temperature gradient in x-direction, it can be seen how the heat is accumulated at the top due to the contact resistance of the TIM. Unsurprisingly, the case with ideal contact resistance showed the most even temperature distribution in the x-direction. But the ideal case is unrealistic since it completely neglects the contact resistance. However, all new cases showed an improved heat transfer with less accumulated heat and thereby lower temperatures at the interface towards the battery module compared to the base case. The lower temperatures at the interface for the new cases compared to the base case is clear from Figure 4.6. This does not say anything about the temperature within the cells, which should be between 288-308K. However, a lower temperature at the interface toward the battery module increases the driving force, and thereby enable a more efficient BTMS.

In Table 4.3 the average heat transfer resistance for all cases included the Base case are presented. Since these values were calculated from average temperatures, they are only indications of the actual resistance of the system, which is different for each point. As is seen in Table 4.3 the resistances was reduced for all cases compared to the base case. The ideal case showed he highest reduction with 63% of the original resistance. The worst case new TIM also showed a noticeable reduction with 15% of the resistance. It was expected that the cases with a new TIM would show a reduced resistance. But it was less sure how the new pattern would affect the resistance. From Section 2.3.3 it is described that the heat transfer rate through convection is increased by increased turbulence. However, it was not certain that the new pattern would increase the turbulence enough to affect the heat transfer. The pattern was designed to increase the favourable structures of the flow through increasing number of wakes and turbulence. From Figure 4.8 it can be seen that the new pattern succeeded at this. By changing the pattern, the heat transfer resistance was reduced with 5% of the base case resistance, which is a noticeable reduction.

From the base case together with theory it was deducted that the total heat transfer resistance could be reduced by replacing the TIM. A new TIM with higher thermal conductivity and lower contact resistance was tested. However, the insecurity of the contact resistance led to a sensitivity study of the parameter. From Table 4.3 it is seen that both cases with a new TIM have a reduced resistance. In the worst case TIM the same contact resistance as in the base case was used, so all reduced resistance was because of increased thermal conductivity. The thermal conductivity of the new TIM was twice of the base case thermal pad. So, it was not surprising that the heat transfer was improved even without reduced contact resistance. However, the impact of contact resistance is clear, as the resistance of the worst case is 2,3 times higher than the ideal case, see Table 4.3. It is reasonable to say that the true contact resistance will land between the two tested cases. But as described in Section 2.5 the performance of a TIM depend on the application as well as the assemblage. So, it is hard to establish a true value as the contact resistance possible differs between cases as well as over time as the material age. From this reasoning it is reassuring that even if it is hard to establish the improvement from reduced contact resistance, the reduction in bulk resistance from increased thermal conductivity show a clear improvement by itself.

An iteration was performed where the new flow pattern was combined with the new TIM, using the worst case contact resistance to avoid overestimation. This combination case gave the largest reduction of contact resistance after the ideal case. The combined case almost had the same improvement as the product of the two separate improvements. Therefore, the combination showed that the two types of improvements was largely independent of each other. This imply that it is relevant to implement both changes to gain a larger reduction of heat transfer resistance. The independence of the improvements could have been expected since the new pattern reduced thermal resistance for heat transfer through convection. While increased thermal conductivity reduced the resistance for heat transfer through conduction. Since both of the design changes reduced the temperature deviation, see Table 4.4, the driving force for heat transfer was slightly reduced. As the heat transfer resistance increased from a smaller temperature difference, the improvement of the combined case is not as large as the product of the two individual cases. Since a high value of contact resistance was used, it can be expected that the actual improvement from the combination is larger than presented here.

5.2.2 Even temperature distribution

The temperature of a battery should be within the interval of 288-308K and evenly distributed, given in Section 2.1. Both these parameters are optimised for a BTMS to maximise the lifetime, performance and safety of a battery. Since the temperature within the cells themselves was unavailable for investigation, the contact temperature was studied. By reducing the contact resistance the driving force for heat from the battery would increased, see Section 2.3. In Table

4.4 the maximum temperature for all cases are presented. All cases show a reduced maximum temperature compared to the base case. Which implies that the heat transfer from the battery cell to the bottom should be increased. The lowest maximum temperature is achieved by the ideal case after which the more realistic combined case follows. This strengthen the reduced resistance discussed in previous section. The maximum temperatures are all below the maximum limit of 308K. However, as this is only the contact temperature it does not really say what happens inside of the cells. So, the only conclusion is that a lower temperature offers a higher driving force and thereby a more efficient heat transfer.

An even temperature distribution is also an important quality for an efficient BTMS. From the base case the low mixing of the coolant was identified as an obstacle of achieving even cooling performance. From comparing the contours in Figure 4.6 together with the temperature variance presented in Table 4.4 it is clear that the changed pattern gives a more even temperature distribution. All the new cases show a lower ΔT and lower maximum temperatures. The maximum temperature is as discussed before more advantageous for the new TIM, but the temperature distribution is clearly best for the new pattern. This can be seen in Figure 4.6 where the temperature towards the battery module is more even for the case with the new flow pattern compared to the other new cases which trends looks like the base case but with lower maximum and minimum temperature. This was somewhat expected since the new pattern already in its initial comparison with another new pattern showed increased mixture, see Appendix C. Also in Figure 4.7 the more even temperature distribution of the fluid is shown. This effect then pass down to the more effective heat transfer shown in Figure 4.8 due to increased convection and driving force. Which in turn have effects on the temperature on the bottom of the battery module, see Figure 4.6.

To use as a reference point the usage of mini-channels with aluminium foam achieved a temperature uniformity of the cells with 2K, see Section 2.2.2. None of the cases in this study achieved such a low variance in the interface. However, as this study only looked at the interface it is hard to compare. In addition, the mini-channel solution with aluminium foam have a higher complexity than the cases investigated in this study, which probably lead to higher costs. But from this comparison there is a hint of possible further improvement of the uniformity. Still, the combined case had almost 1K reduced variance which is a remarkable improvement of the branch standard solution.

The combination case showed the lowest temperature variation in the interface. Except from the ideal case, which is expected to be overestimated, the combination case also had the lowest maximum temperature. As the improvement of temperature distribution for the combined case was higher than the product of the two separate cases, see Table 4.4, the two design changes had reinforcing effects. Since heat transfer is a complex phenomenon, the reinforcement was probably a combination of several factors. One reason can have been that the increased mixture was reinforced by higher thermal conductivity of the TIM. So, the heat transfer in z-direction and y-direction was eased by higher thermal conductivity. Another synergy is how the increased heat transfer increased the surface temperature of the walls surrounding the coolant. By doing so the driving force for convection was improved. Also, since the heat spread out more evenly thanks to the thermal conductivity, the active surface increased. To sum up, there is clear advantage in implementing both design changes.

5.2.3 Effect of a fin

The case with a fin had results that drastically diverted from remaining cases. The deviation was so large, so no common comparison of contours was applicable. For example, the maximum temperature of the fin, see Table 4.4, was 1354K above the other cases. A reason for the extreme values could be the assumption of an evenly distributed heat flux over all area in contact with the battery module, see Figure 3.4. This resulted in a several times larger area of the fin exposed to the heat source compared to the area toward the heat sink. Since this induced an inertia for the heat flux, heat accumulated in the fin. As described in Section 2.1 a prismatic battery cell is anisotropic in its thermal conductivity, so the heat on the surface of the fin would probably be lower than toward the bottom. Furthermore, since the design inside the module was unknown the design of the fin might be unrealistic. Another factor explained in Section 2.1.1 is how the pressure applied on a cell have impact on its performance. So, there is a possibility that even if the fin had a positive effect on the cooling, it changed the cell pressure which reduced the cell performance. The result of this case with a fin have been affected by the assumptions and limitations to draw comparative conclusions from them in relation to the other cases.

Even if the validly of the results are questioned it is deducted that a risk with fins is the accumulation of heat within the fin. So, if fins are not properly cooled, they can just as well be an obstacle of effective heat transfer. Nevertheless, the result with the extreme temperatures in this study is probably a result of oversimplification rather than a reflection of the reality. As described in Section 2.1 the heat generation in batteries is usually highest at the top of the battery module close to the collectors, anode and cathode. So, if the cooling plate is at the opposite side of the hottest areas the cooling of the fins is of even higher importance.

5.3 Impacts of simplifications on results

All models are simplifications of the reality and from analysing only a general picture can be reached. Throughout this project several simplifications were made, and most of them for all cases. As this was a comparative study it was recognised that simplifications done for all cases had a limited impact on the result. In this section the possible impact of simplifications on the results and eventually overseen opportunities are discussed.

One of the first limitations was to only examine the battery and neglect the surrounding cooling system of the vehicle. This limited the possibility to optimise the coupled components in the cooling system in respect to each other. That type of optimisation would have to involve the drive cycle in a transient simulation. Therefore, possible optimisation opportunities on a system level have been overseen. Furthermore, the cooling of the coolant was left out from this study. Instead the inlet properties were kept constant and not evaluated. If these had been included mass flow and temperature could have been optimised, as suggested in Section 2.2.2 The geometry had several simplifications where the first step was to only look at two out of eight modules. This limited the investigated impact of a changed flow pattern, where the effect of the pattern on the entire battery's performance was left unknown. So, the system limits might have led to missed improvement possibilities of a new pattern. However, it can still be deducted that a redesign of the flow channels can have a positive effect on the cooling effect. Another factor which is affected by a redesigned flow pattern is the pressure drop. However, as only a part of the cooling system was investigated it was not relevant to look at the pressure drop. Also, the mechanical properties were neglected which may affect the realisation of the new cases. However, since the result of this study is to make comparison of the heat transfer to make suggestions, the result is not directly affected.

Second limitation of the geometry was by the unavailable design inside of the battery modules. This limited what was possible to investigate rather than the results. As described throughout the report the temperature within the battery cell be low and uniform. So instead of investigating temperatures within the cells, the temperature at the interface toward the module was aimed to be as low and uniform as possible to give an even cooling performance. The temperature within the cells vary, so an even distribution at the cooling plate do not really say anything about temperature distribution and possible hot spots within the cells. Nevertheless, by reducing the heat transfer resistance, which was the aim of the project, it still could be concluded that the cooling performance was improved. Without the design inside the modules a realistic heat generation was unavailable. Instead a constant heat flux was applied which enabled a comparative study and evaluation of the heat transfer. So, effect of the assumption of constant heat flux is not on the result, but rather on what was not investigated. The lack of design inside the modules led to the design of a fin based on visual estimation. The heat flux on the fin was constant, like in the other cases. However, heat generation have different intensities and are not evenly distributed and heat transfer in a cell is anisotropic. So, heat should easier be transferred to the bottom of the module than to the side of the fin. These extra simplifications for the case with a fin made it hard to put it in perspective to remaining cases. The implementation of fins close to battery cells have been investigated by several researches, especially in combination with micro-channels, see Section 2.2.2. To keep in mind is that the pressure applied on a cell have a complex impact on the cell performance and life-time, as explained in Section 2.1.1. So, implementation of a fin is not certain until further investigated. However, in this comparative study the fin case was only used to see if the heat transfer resistance could be reduced from an increased heat transfer area.

A third way the geometry was simplified was by looking at a worst-case scenario excluding surrounding structures. If surrounding structures had been included, they might have shown that heat was either further removed or added from them. Added since there are other heat sources in the engine room. This might have led to overseeing possible improvements or problems, but as it was done for all cases it was acceptable. A fourth simplification in terms of geometry was to simplify the CAD model itself by removing round edges and holes from the components. This was done for all cases so the impact on the results was limited. Nevertheless, by increasing the contact area the resulting heat transfer resistance may have been too low. Also, the thickness of the thermal pad in the base case was simplified to have a constant thickness, while it in reality can vary. But as the variations in thickness was unmapped and assumed small, the impact on the result is deemed to be negligible. Mentioned in the limitations and assumption, is that an electric isolating tape on the bottom of the battery module was not included. If this had been included the contact resistance would have increased since it adds contact resistance and had isolating properties. So, the values of heat transfer resistance would have been higher if the tape was included. But as it was excluded for all cases its effect on the relative caparison is negligible. However, if it would be possible to remove the tape, it is recognised that the designed could be improved.

Almost all input data for the coolant properties, generated heat, and material properties was based on previous studies. When properties could not be found they were based on literature. Since most of the data was used for all cases effects on the comparison was negligible. A property of large impact was the contact resistance which is unique for each application and therefore not possible to get for the use of a new material. Therefore, a sensitivity study of the parameter was performed from ideal to worst case, which was the same as in the base case. The comparison showed a heat transfer resistance 2,3 times larger for the worst case compared to the base case. The maximum temperature diverted with more than 6 K between the cases, which showed the large impact on the effectively of the BTMS. As suggested in Section 2.5 it is misleading to compare the performance of a TIM seldom on the thermal conductivity. So, these results strengthen the already known, that contact resistance is a parameter of great importance in the aim to improve the heat transfer.

In conclusion, several simplifications and assumptions were made throughout the study. However, since it was a comparative study the results were not as affected if the same simplifications were done for all cases. Instead it rather affected the investigated improvements which strongly was limited by available data and time. Therefore, the study might have left out improvements even if they were investigated in the literature study for the sake of limited possibility with the resources available.

5.4 Future Research

As highlighted at the beginning of the report, optimisation of BTMS have large impact on the battery performance, lifetime and cost. Since research of BTMS for a long time was overlooked in favour for maximising energy and power density there is large potentials for improvement, which this project together with previous research have shown. However, due to limitation in time, previous knowledge and available data not all possible improvements have been investigated in this project. Therefore, some suggestions of future research based on findings as well as literature is presented in this section.

With access to the complete battery module several interesting aspects could be investigated. The heat generated from the battery would not have to be constant. This would enable investigation of hot spots which could be reduced with fins between the battery cells. It would also give more realistic test of fins. To avoid heat accumulation the possibility of mini-channels in the fins, as investigated by several researches in Section 2.2.2, could be tested. If fins are of interest the pattern inside the fin, the thickness and distribution of fins should be investigated. It could also be tested if different length of fins have different impacts. Another subject to investigate with access to the cell design is to use PCM as TIM. As suggested in Section 2.2, PCM should be combined with additional cooling to avoid heat accumulation after phase change. If simulations including cells identify a problem with hot-spots within the cells, it could be of interest to use PCM in direct contact with the cells. With a real heat distribution inside of the module the possible impact of including an additional cooling plate on top of the module could also be investigated. This could both increase the cooling efficiency but also cost, weight and size of the battery package. So, all factors should be included when testing this.

From the base case it was deducted that the flow pattern was not optimal. In this study only one new flow pattern was thoroughly investigated to establish that there is possible to improve the heat transfer through a changed flow pattern. In Section 2.2.2 it is established that there is several possibilities to optimise a flow pattern. The flow rate impact both the cooling effect and pressure drop. But the impact on cooling effect is lessening, so one topic of investigation should be to find this point in order to optimise the flow rate. The flow rate could also be optimised in respect to the remaining cooling systems. Another finding in Section 2.2.2 was that the hydraulic diameter have a lower effect on cooling than on pressure drop. So, it could be tested how the hydraulic diameter can be optimised for a low pressure drop. However, it have to be kept in mind that a larger diameter increase weight and size of the system. Another topic of future investigation suggested in Section 2.2.2 is to look at several inlets and outlets to achieve a more uniform temperature. This is limited by size, but there is smart connections at the market to enable this design. In addition, by using connections which are less beds, the pressure drop and thereby the required pump work can be reduced.

Another aspect for further investigation is the contact resistance. One aspect is to test more different TIM and with respect to mechanical properties. It is also worth to evaluate if the TIM has to be electrical isolating. If not, a material with substantial higher thermal conductivity and cheaper additives can be used. As mentioned in Section 2.3.4 the contact resistance depend on the application. So, the assembly process could also be studied and standardised to guarantee a good contact resistance. Physical tests to establish the specific value of contact resistance is however required to get more specific result than this study. Another possible improvement presented in Section 2.5 is to insert a gap filler in all voids within the battery module. This would fill up the isolating air void between the cells and other components. However, this should be done with respect to the effects of pressure on cells presented in Section 2.1.1. Since the air voids between the components in the module isolate the cells this is expected to have a positive effect. Although, it would make the dissemble more difficult, which is disadvantageous from an environmental perspective. Since it reduces the easiness to service, reuse the parts in another application, and to separate and recycle the materials.

To sum up, further research with less limitations and assumptions would provide a better insight in how the battery would benefit from design changes. Since this study show great improvement potential of the current solution, this subject is worth to investigate further. As previous stated, an improved, more efficient BTMS would not only be good for the environment from increased lifetime. But also give possible performance improvements, increased safety and possible savings from reduced wear. A less worn-down battery would also have a larger aftermarket where it could be a possible energy storage with less restrictions on energy and power density than a vehicle.

6
Conclusion

One of the global challenges of our time is to limit the atmospheric concentrations of greenhouse gases. To reduce emissions changes are required and technical solutions are lusted for to avoid sacrifice of comfort. One technical solution is to electrified vehicles and use a battery as energy storage. To meet the space and weight limitations of vehicles, batteries have been optimised to have high energy and power density. However, the battery performance, safety and lifetime is strongly coupled to its working temperature and requires an efficient Battery Thermal Management System (BTMS). Therefore, this master thesis is performed in collaboration with the development centre CEVT to answer the research question “How can the heat transfer in a branch standard BTMS solution be improved?”. Where the branch standard solution, also referred to as the base case, is a liquid BTMS with cooling plates and a pad as thermal interface material (TIM).

The heat transfer was evaluated through CFD simulations in the software ANSYS Fluent. First was the base case simulated and evaluated, which together with inspiration from literature lead to three main areas of improvement. Those were: reduce the thermal resistance by replacing the thermal pad, increase the heat transfer area by including fins in the module, and change the flow pattern to achieve a more even temperature distribution. The aim of each improvement was to reduce the total heat transfer resistance from battery module to coolant and temperature variance toward the battery module. The improved cases were analysed through a comparative study with the branch standard as a base line.

By replacing the thermal pad with a gap filler as TIM the total resistance could be reduced with 15-63%. The range of improvement depend on the contact resistance of the new TIM which is an application dependent parameter. So, a sensitivity study using a worst case value and an ideal value to capture the range of possible improvement was used to get the values for the new TIM case. The new TIM also made the temperature toward the battery module more uniform as it reduced the variance with 0,13-0,26K. The maximum temperature toward the battery was also reduced with the new TIM which is an expected effect of lower heat transfer resistance. It was investigated how a fin in the battery module affected the heat transfer. But this case required several additional assumptions compared to remaining cases which made the results unsure. However, a risk of heat accumulation in the fin was identified. So, if fins are of interest, they could gain from being cooled by micro-channels. As the base case indicated low mixture of the coolant a new pattern was designed to increase the mixture and thereby offer a more uniform temperature. The new pattern achieved a reduced variance of 0,69K and lowered the resistance with 5%. A combined case with the new TIM and flow pattern gave a 20% reduced resistance and 0,98K reduced variance. As the improvement for the combination case was larger than the product of the two cases, the suggested improvements have a reinforcing effect on each other.

In conclusion, based on the findings our first recommendation is to further investigate the possibility to replace the thermal pad with a more efficient TIM. Physical tests to establish the contact resistance for the new TIM are required. It should also be investigated if the TIM needs to be electric isolating. The second recommendation is to optimise the flow pattern for the entire battery package. To achieve a low and uniform temperature, the combination of the two design changes is the third recommendation. As the results shows that there are large potential for improvement of the branch standard, it is worth to invest more time on further investigation.

Bibliography

[1] Max Ritchie Hanna; Roser. *CO and Greenhouse Gas Emissions*. 2017. URL: https://ourworldindata.org/co2-and-other-greenhouse-gas-emissions#citation.

[2] Poul H. Andersen, John A. Mathews, and Morten Rask. "Integrating private transport into renewable energy policy: The strategy of creating intelligent recharging grids for electric vehicles". In: *Energy Policy* 37.7 (2009), pp. 2481–2486. ISSN: 03014215. DOI: 10.1016/j.enpol.2009.03.032.

[3] EMMA ARFA GRUNDITZ. *Design and Assessment of Battery Electric Vehicle Powertrain, with Respect to Performance, Energy Consumption and Electric Motor Thermal Capability*. Vol. 59. 2016, pp. 3780–3788. ISBN: 9789175974125. DOI: 10.1109/TIE.2011.2178212. URL: http://www.chalmers.se/SiteCollectionDocuments/Energi%20och%20milj%C3%B6/Elteknik/EmmaGrunditz_PhDthesis_lowrez.pdf%0Ahttp://publications.lib.chalmers.se/records/fulltext/236616/236616.pdf%0Ahttp://ethos.bl.uk/OrderDetails.do?uin=uk.bl.ethos.320328.

[4] CEVT. *What we do - CEVT*. 2020. URL: https://www.cevt.se/what-we-do/.

[5] Geely Auto. *Xing Yue : Geely Global*. 2020. URL: http://global.geely.com/car/xing-yue/.

[6] Huaqiang Liu, Zhongbao Wei, Weidong He, et al. "Thermal issues about Li-ion batteries and recent progress in battery thermal management systems: A review". In: *Energy Conversion and Management* 150 (Oct. 2017), pp. 304–330. ISSN: 0196-8904. DOI: 10.1016/J.ENCONMAN.2017.08.016. URL: https://www.sciencedirect.com/science/article/pii/S0196890417307288.

[7] A Pesaran, A Vlahinos, and T Stuart. "Cooling and preheating of batteries in hybrid electric vehicles". In: *6th ASME-JSME Thermal Engineering Joint Conference* January (2003), pp. 1–7. URL: http://ci.nii.ac.jp/naid/110002495519/%5Cnhttp://www.nrel.gov/vehiclesandfuels/energystorage/pdfs/jte_2003-633_sw_ap.pdf%5Cnhttp://www.nrel.gov/vehiclesandfuels/energystorage/pdfs/jte_2003-633_sw_ap.pdf.

[8] Ming Shen and Qing Gao. "System simulation on refrigerant-based battery thermal management technology for electric vehicles". In: *Energy Conversion and Management* 203 (Jan. 2020). ISSN: 01968904. DOI: 10.1016/j.enconman.2019.112176.

[9] Heesung Park. "A design of air flow configuration for cooling lithium ion battery in hybrid electric vehicles". In: *Journal of Power Sources* 239 (2013), pp. 30–36. ISSN: 03787753. DOI: 10.1016/j.jpowsour.2013.03.102.

[10] Anthony Jarrett and Il Yong Kim. "Design optimization of electric vehicle battery cooling plates for thermal performance". In: *Journal of Power Sources* 196.23 (Dec. 2011), pp. 10359–10368. ISSN: 03787753. DOI: 10.1016/j.jpowsour.2011.06.090.
[11] Rajib Mahamud and Chanwoo Park. "Reciprocating air flow for Li-ion battery thermal management to improve temperature uniformity". In: *Journal of Power Sources* 196.13 (July 2011), pp. 5685–5696. ISSN: 03787753. DOI: 10.1016/j.jpowsour.2011.02.076.
[12] Amine Lazrak, Jean François Fourmigué, and Jean François Robin. "An innovative practical battery thermal management system based on phase change materials: Numerical and experimental investigations". In: *Applied Thermal Engineering* 128 (2018), pp. 20–32. ISSN: 13594311. DOI: 10.1016/j.applthermaleng.2017.08.172. URL: https://doi.org/10.1016/j.applthermaleng.2017.08.172.
[13] Ziye Ling, Fangxian Wang, Xiaoming Fang, et al. "A hybrid thermal management system for lithium ion batteries combining phase change materials with forced-air cooling". In: *Applied Energy* 148 (June 2015), pp. 403–409. ISSN: 0306-2619. DOI: 10.1016/J.APENERGY.2015.03.080. URL: https://www.sciencedirect.com/science/article/pii/S0306261915003827.
[14] Office of Energy Efficiency & Renewable Energy. *How Does a Lithium-ion Battery Work?* 2017. URL: https://www.energy.gov/eere/articles/how-does-lithium-ion-battery-work.
[15] Gang Ning, Bala Haran, and Branko N. Popov. "Capacity fade study of lithium-ion batteries cycled at high discharge rates". In: *Journal of Power Sources* 117.1-2 (May 2003), pp. 160–169. ISSN: 0378-7753. DOI: 10.1016/S0378-7753(03)00029-6. URL: https://www.sciencedirect.com/science/article/pii/S0378775303000296?via%3Dihub.
[16] Jeffrey R. Belt, Chinh D. Ho, Chester G. Motloch, et al. "A capacity and power fade study of Li-ion cells during life cycle testing". In: *Journal of Power Sources* 123.2 (Sept. 2003), pp. 241–246. ISSN: 0378-7753. DOI: 10.1016/S0378-7753(03)00537-8. URL: https://www.sciencedirect.com/science/article/pii/S0378775303005378?via%3Dihub.
[17] "J. Electrochem. Soc.-1985-Bernardi-5-12". In: ().
[18] Bizhong Xia, Yifan Liu, Rui Huang, et al. "Thermal analysis and improvements of the power battery pack with liquid cooling for electric vehicles". In: *Energies* 12.16 (2019), pp. 1–18. ISSN: 19961073. DOI: 10.3390/en12163045.
[19] Verena Müller, Rares George Scurtu, Michaela Memm, et al. "Study of the influence of mechanical pressure on the performance and aging of Lithium-ion battery cells". In: *Journal of Power Sources* 440 (Nov. 2019). ISSN: 03787753. DOI: 10.1016/j.jpowsour.2019.227148.
[20] John Christensen and John Newman. "Stress generation and fracture in lithium insertion materials". In: *Journal of Solid State Electrochemistry* 10.5 (May 2006), pp. 293–319. ISSN: 14328488. DOI: 10.1007/s10008-006-0095-1.
[21] Christina Peabody and Craig B. Arnold. "The role of mechanically induced separator creep in lithium-ion battery capacity fade". In: *Journal of Power Sources* 196.19 (Oct. 2011), pp. 8147–8153. ISSN: 03787753. DOI: 10.1016/j.jpowsour.2011.05.023.

[22] Robert Kostecki and Frank McLarnon. “Microprobe study of the effect of Li intercalation on the structure of graphite”. In: *Journal of Power Sources*. Vol. 119-121. June 2003, pp. 550–554. DOI: 10.1016/S0378-7753(03)00287-8.

[23] Shankar Mohan, Youngki Kim, Jason B. Siegel, et al. “A Phenomenological Model of Bulk Force in a Li-Ion Battery Pack and Its Application to State of Charge Estimation”. In: *Journal of The Electrochemical Society* 161.14 (2014), A2222–A2231. ISSN: 0013-4651. DOI: 10.1149/2.0841414jes.

[24] Hussam Jouhara, Navid Khordehgah, Nicolas Serey, et al. “Applications and thermal management of rechargeable batteries for industrial applications”. In: *Energy* 170 (2019), pp. 849–861. ISSN: 03605442. DOI: 10.1016/j.energy.2018.12.218. URL: https://doi.org/10.1016/j.energy.2018.12.218.

[25] Andreea Zaharia. *Passive Cooling vs. Active Cooling – What’s the Difference?* 2019. URL: https://www.simscale.com/blog/2017/01/active-and-passive-cooling/.

[26] Ahmad A. Pesaran. “Battery thermal models for hybrid vehicle simulations”. In: *Journal of Power Sources* 110.2 (Aug. 2002), pp. 377–382. ISSN: 0378-7753. DOI: 10.1016/S0378-7753(02)00200-8. URL: https://www.sciencedirect.com/science/article/pii/S0378775302002008.

[27] Z. Lu, X. Z. Meng, L. C. Wei, et al. “Thermal management of densely-packed EV battery with forced air cooling strategies”. In: *Energy Procedia*. Vol. 88. Elsevier Ltd, June 2016, pp. 682–688. DOI: 10.1016/j.egypro.2016.06.098.

[28] X.M. Xu and R. He. “Research on the heat dissipation performance of battery pack based on forced air cooling”. In: *Journal of Power Sources* 240 (Oct. 2013), pp. 33–41. ISSN: 0378-7753. DOI: 10.1016/J.JPOWSOUR.2013.03.004. URL: https://www.sciencedirect.com/science/article/pii/S0378775313003674.

[29] Ahmad A. Pesaran. “Battery thermal models for hybrid vehicle simulations”. In: *Journal of Power Sources* 110.2 (Aug. 2002), pp. 377–382. ISSN: 0378-7753. DOI: 10.1016/S0378-7753(02)00200-8. URL: https://www.sciencedirect.com/science/article/pii/S0378775302002008.

[30] Zhongming Liu, Yuxin Wang, Jun Zhang, et al. “Shortcut computation for the thermal management of a large air-cooled battery pack”. In: *Applied Thermal Engineering* 66.1-2 (May 2014), pp. 445–452. ISSN: 1359-4311. DOI: 10.1016/J.APPLTHERMALENG.2014.02.040. URL: https://www.sciencedirect.com/science/article/pii/S135943111400132X.

[31] Kai Chen, Weixiong Wu, Fang Yuan, et al. “Cooling efficiency improvement of air-cooled battery thermal management system through designing the flow pattern”. In: *Energy* 167 (Jan. 2019), pp. 781–790. ISSN: 0360-5442. DOI: 10.1016/J.ENERGY.2018.11.011. URL: https://www.sciencedirect.com/science/article/pii/S0360544218322151#bib16.

[32] Matthew Zolot Kenneth J. Kelly Mark Mihalie. *Battery Usage and Thermal Performance of the Toyota Prius and Honda Insight during Chassis Dynamometer Testing*. 2002. URL: https://ieeexplore.ieee.org/stamp/stamp.jsp?arnumber=986408.

[33] Rui Liu, Jixin Chen, Jingzhi Xun, et al. “Numerical investigation of thermal behaviors in lithium-ion battery stack discharge”. In: *Applied Energy* 132 (Nov. 2014), pp. 288–297. ISSN: 0306-2619. DOI: 10.1016/J.APENERGY.2014.07.024. URL:

https://www.sciencedirect.com/science/article/pii/S0306261914007053.

[34] Theodore L. Bergman, Adrienne S. Lavine, Frank P. Incropera, et al. *Incropera's Principles of Heat and Mass Transfer*. Global Edition. New York, United States: John Wiley & Sons Inc, 2017. ISBN: 1119382912.

[35] Zhen Qian, Yimin Li, and Zhonghao Rao. "Thermal performance of lithium-ion battery thermal management system by using mini-channel cooling". In: *Energy Conversion and Management* (2016). ISSN: 01968904. DOI: 10.1016/j.enconman.2016.08.063.

[36] Suman Basu, Krishnan S. Hariharan, Subramanya Mayya Kolake, et al. "Coupled electrochemical thermal modelling of a novel Li-ion battery pack thermal management system". In: *Applied Energy* 181 (Nov. 2016), pp. 1–13. ISSN: 03062619. DOI: 10.1016/j.apenergy.2016.08.049.

[37] Chengtao Lin, Can Cui, and Xiaotian Xu. *Lithium-ion Battery Electro-thermal Model and Its Application in the Numerical Simulation of Short Circuit Experiment*. Tech. rep.

[38] G. Karimi and A. R. Dehghan. "Thermal Management Analysis of a Lithium-Ion Battery Pack using Flow Network Approach". In: *International Journal of Mechanical Engineering and Mechatronics* (2012). DOI: 10.11159/ijmem.2012.011.

[39] Shuting Yang, Chen Ling, Yuqian Fan, et al. *A review of lithium-ion battery thermal management system strategies and the evaluate criteria*. 2019. DOI: 10.20964/2019.07.06.

[40] Wenzheng Li, Xiaoru Zhuang, and Xinhai Xu. "Numerical study of a novel battery thermal management system for a prismatic Li-ion battery module". In: *Energy Procedia*. 2019. DOI: 10.1016/j.egypro.2019.01.771.

[41] Ziyuan Wang, Xinxi Li, Guoqing Zhang, et al. "Thermal management investigation for lithium-ion battery module with different phase change materials". In: *RSC Advances* 7.68 (2017), pp. 42909–42918. ISSN: 20462069. DOI: 10.1039/c7ra08181b.

[42] Tianshi Zhang, Qing Gao, Guohua Wang, et al. "Investigation on the promotion of temperature uniformity for the designed battery pack with liquid flow in cooling process". In: *Applied Thermal Engineering* 116 (2017), pp. 655–662. ISSN: 13594311. DOI: 10.1016/j.applthermaleng.2017.01.069.

[43] Yutao Huo, Zhonghao Rao, Xinjian Liu, et al. "Investigation of power battery thermal management by using mini-channel cold plate". In: *Energy Conversion and Management* (2015). ISSN: 01968904. DOI: 10.1016/j.enconman.2014.10.015.

[44] Gautam Pulugundla, Prahit Dubey, and A. Srouji. "Time-accurate CFD analysis of liquid cold plates for efficient thermal performance of electric vehicle Li-ion battery modules". In: *SAE Technical Papers* 2019-April.April (2019), pp. 1–8. ISSN: 01487191. DOI: 10.4271/2019-01-0500.

[45] Taeyoung Han, Bahram Khalighi, and Shailendra Kaushik. "Li-ion Battery Thermal Management – Air vs. Liquid Cooling". In: Begell House, Apr. 2018, pp. 1309–1322. DOI: 10.1615/tfec2017.fna.017297.

[46] Todd M. Bandhauer and Srinivas Garimella. "Passive, internal thermal management system for batteries using microscale liquid-vapor phase change". In: *Applied Thermal Engineering* (2013). ISSN: 13594311. DOI: 10.1016/j.applthermaleng.2013.08.004.

[47] Hirano Hirokazu, Tajima Takamitsu, Hasegawa Takeru, et al. “Boiling Liquid Battery Cooling for Electric Vehicle”. In: *2014 IEEE Conference and Expo Transportation Electrification Asia-Pacific (ITEC Asia-Pacific)*. Beijing, China: IEEE, 2014.

[48] Zhoujian An, Li Jia, Xuejiao Li, et al. “Experimental investigation on lithium-ion battery thermal management based on flow boiling in mini-channel”. In: *Applied Thermal Engineering* (2017). ISSN: 13594311. DOI: 10.1016/j.applthermaleng.2017.02.053.

[49] Xiaoqin Xu, Tianli Xiao, Shumei Chen, et al. “Exploring the heat transfer performance of nanofluid as a coolant for power battery pack”. In: *Heat Transfer - Asian Research* 48.7 (Nov. 2019), pp. 2974–2988. ISSN: 15231496. DOI: 10.1002/htj.21526.

[50] Rami Sabbah, R. Kizilel, J. R. Selman, et al. “Active (air-cooled) vs. passive (phase change material) thermal management of high power lithium-ion packs: Limitation of temperature rise and uniformity of temperature distribution”. In: *Journal of Power Sources* 182.2 (Aug. 2008), pp. 630–638. ISSN: 03787753. DOI: 10.1016/j.jpowsour.2008.03.082.

[51] Bengt Andersson. *Computational fluid dynamics for engineers*. Cambridge University Press, 2011. ISBN: 9781139093590.

[52] Frank. M White. *Fluid Mechanics*. 7th. New York, United States: McGraw-Hill, 2008. ISBN: 978-0.07-128645-9.

[53] Arun Gowda, Sandeep Tonapi, Brad Reitz, et al. “Choosing the Right Thermal Interface Material”. In: *Advanced Packaging* March (2005), pp. 14–18.

[54] *Thermal and Thermomechanical Phenomena in Electronic Systems (ITherm), 2010 12th IEEE Intersociety Conference on : date, 2-5 June 2010*. IEEE, 2010. ISBN: 9781424453436.

[55] *Selection Guide Thermal Interface Materials*. Tech. rep.

[56] Henkel AB. *Thermal Materials - Thermal Materials by Henkel*. 2020. URL: https://thermal.henkel-adhesives.com/en/na/thermal-materials-products/thermal-materials.html.

[57] John D. Ferry. *Viscoelastic Properties of Polymers*. 3 ed. New York: John Wiley & Sons, 1980. ISBN: 0471048941.

[58] H R SHANxs, P D Maxcocx, P H SrnrEs, et al. *Thermal Conductivity of Silicon from 300 to 1400’K˜*. Tech. rep. 1963.

[59] Henkel AB. *Bergquist Gap Filler TGF 3010APS - Henkel Adhesives*. 2020. URL: https://www.henkel-adhesives.com/de/de/produkt/thermal-gap-fillers/bergquist_gap_fillertgf3010aps.html?fbclid=IwAR2sOO1cnajZ-4eUYlS2I-k2HJWc11-tpPdFLABds4050pz8jw_auY8gJmY.

A

Mesh Study Base Case

In this Appendix the complementing Figures to the mesh study of the Base case are presented.

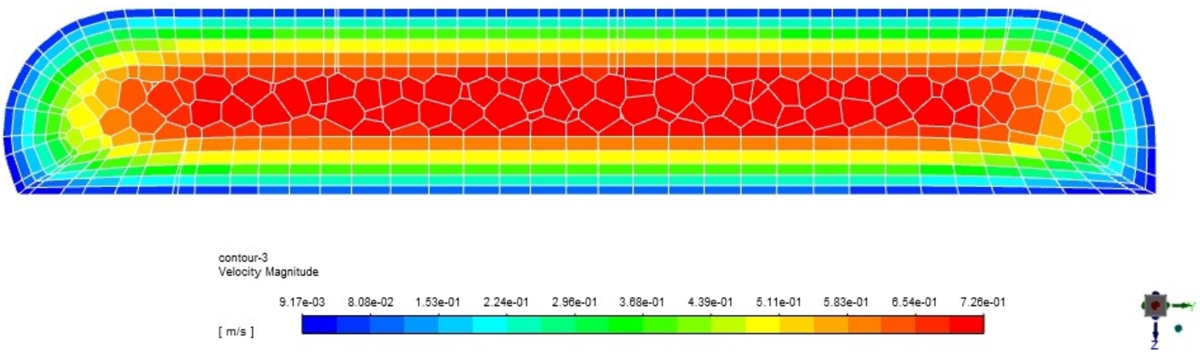

Figure A.1: Contour of the velocity field in a cross section in x direction including the mesh. Confirms that the total height of the mesh boundary layer capture the velocity field height of the boundary layer.

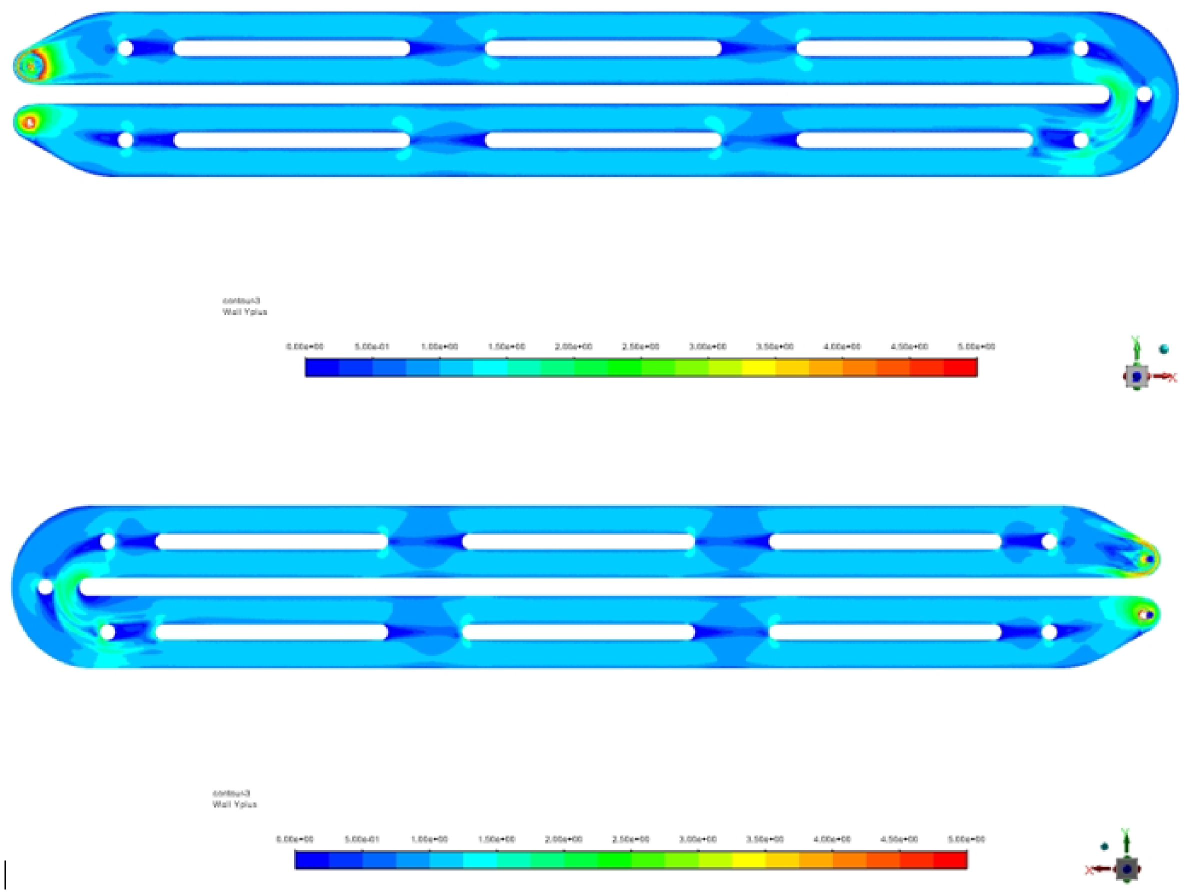

Figure A.2: Wall y^+ from above and from below for the Base Case, with a scale from zero to five

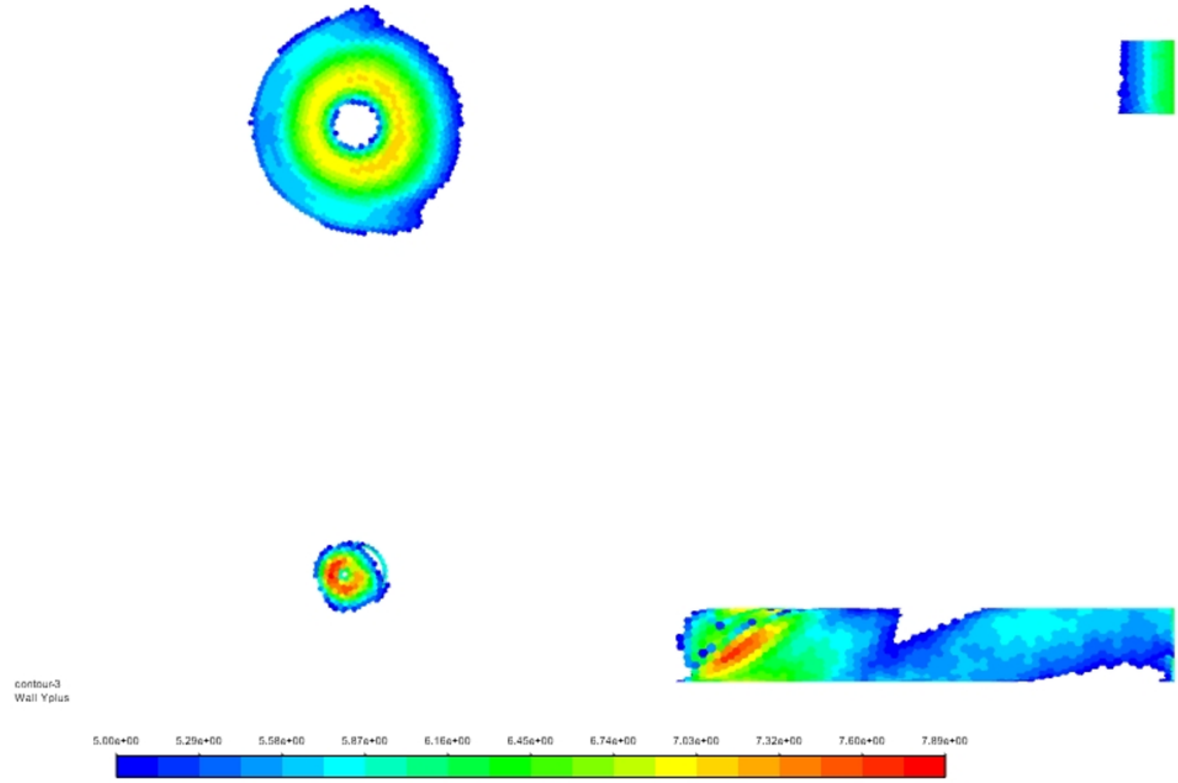

Figure A.3: y^+ above five which is outside the given limit. To the right from the side, and to the left from above

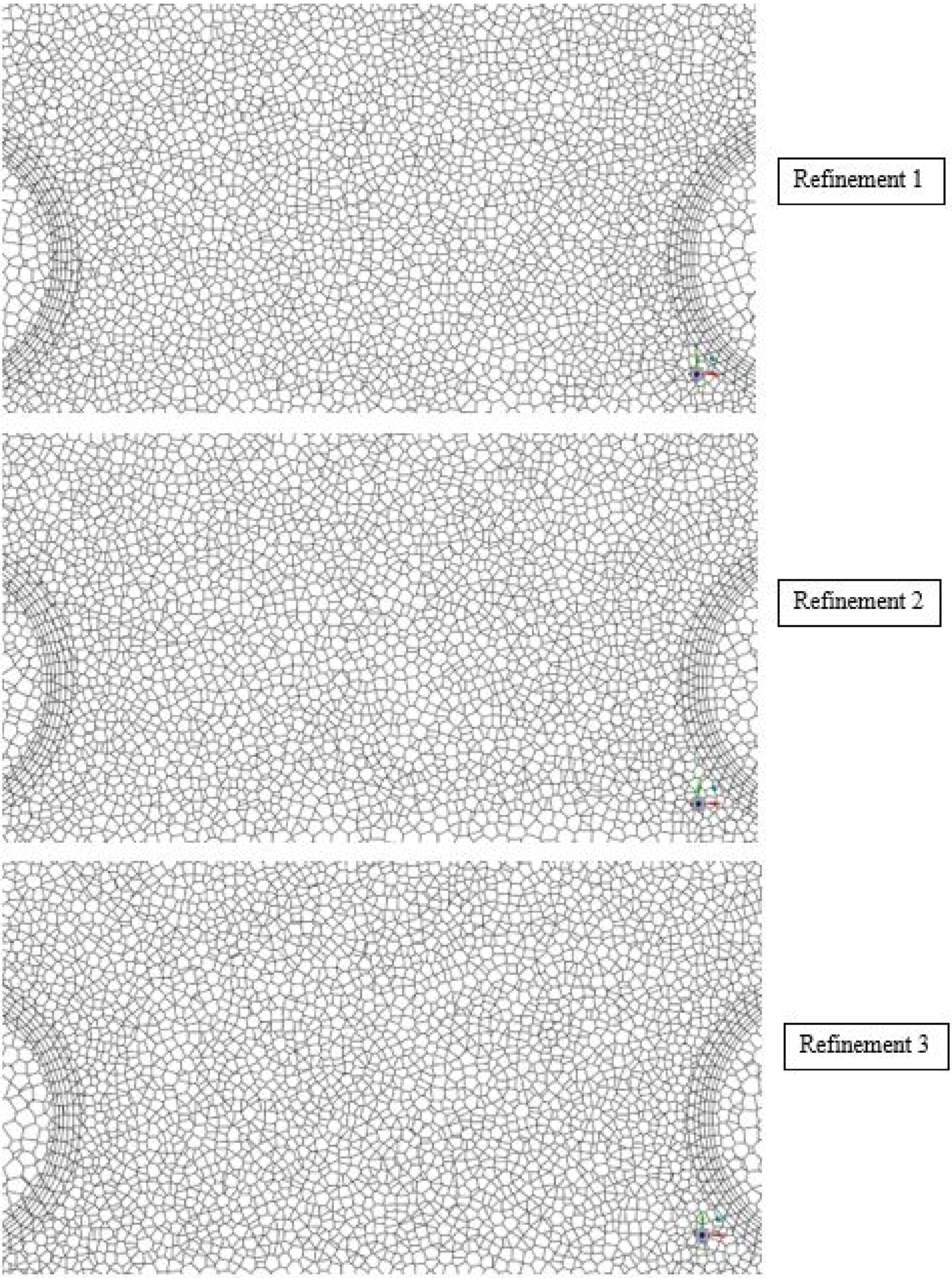

Figure A.4: Three steps of refinement of the Base Case. The picture is taken in the middle of the flow in z-led and just after the U-turn which was assigned an area of interest.

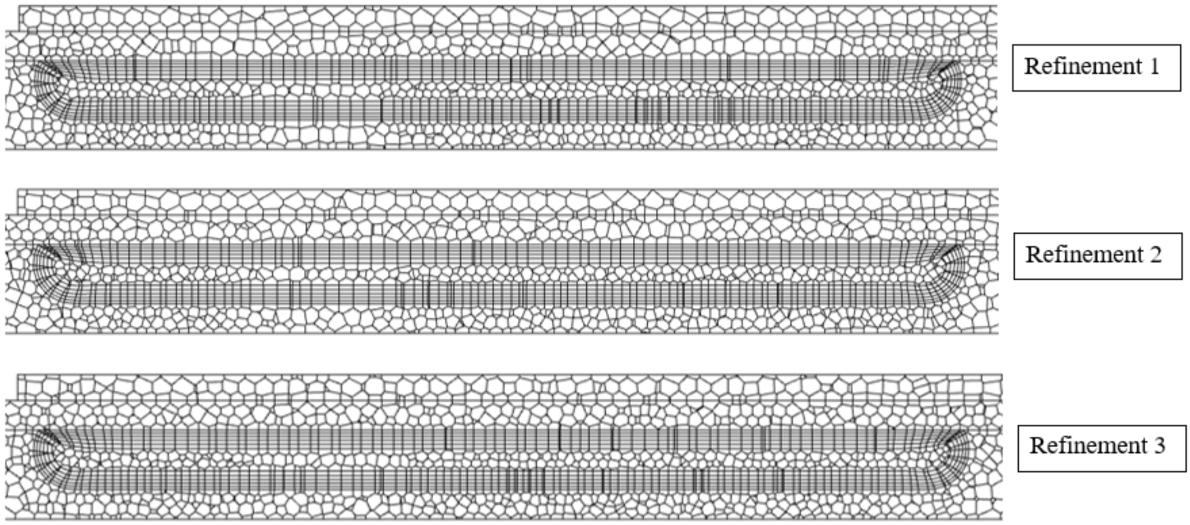

Figure A.5: Three steps of refinement of the Base Case. Picture taken in a cross section just after the U-turn which was assigned an area of interest.

B
Mesh Study Fin Case

In this section the mesh study of the Fin case is presented. The mesh study was performed the same way as for the base case. First the value of y^+ was confirmed to be within the acceptable range. In Figure B.1 the velocity boundary layer can be seen. This figure confirms the boundary layer capture the velocity field.

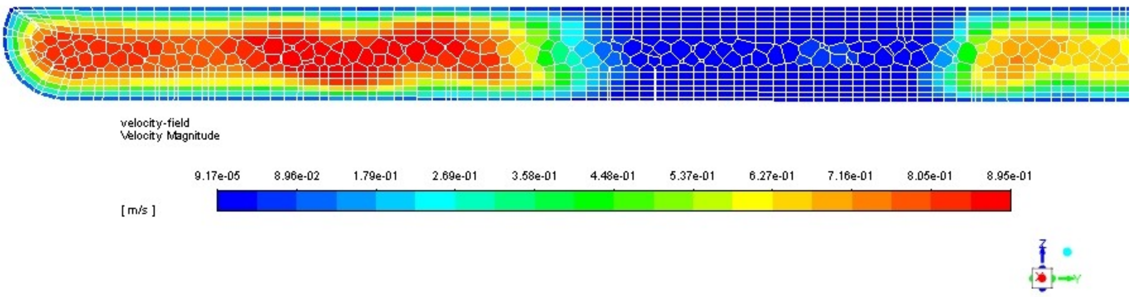

Figure B.1: Contour of the velocity field in a cross section in x direction including the mesh. Confirms that the total height of the mesh boundary layer capture the velocity field height of the boundary layer for the fin case.

After this the y^+ was controlled and in Figure B.2 for y^+ in the inteval $0 < y^+ < 5$ can be seen.

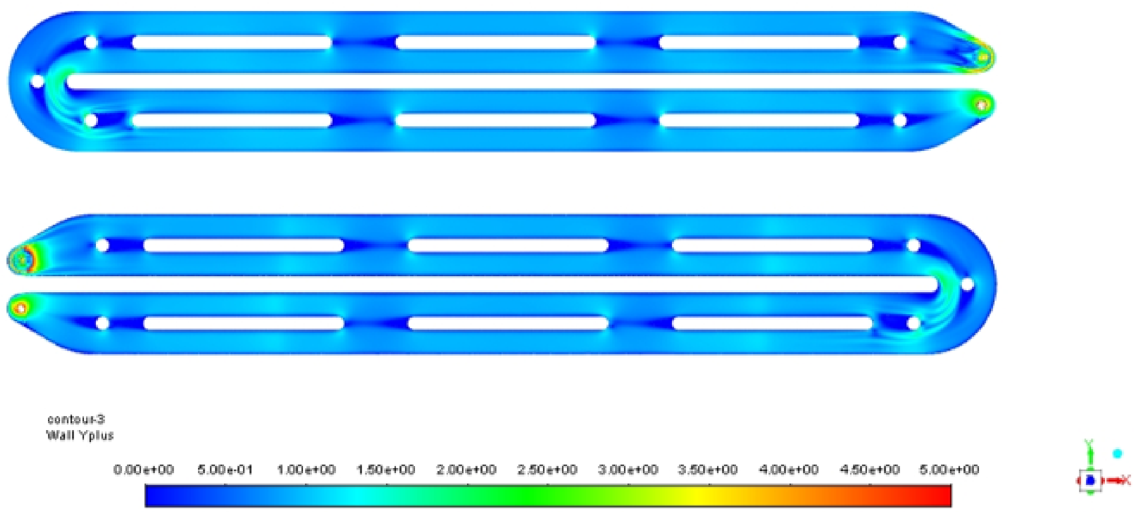

Figure B.2: Wall $y^+$from above and from below for the fin case, with a scale from zero to five

Regarding the y^+ outside the acceptable range (above five) can be seen i Figure B.3.

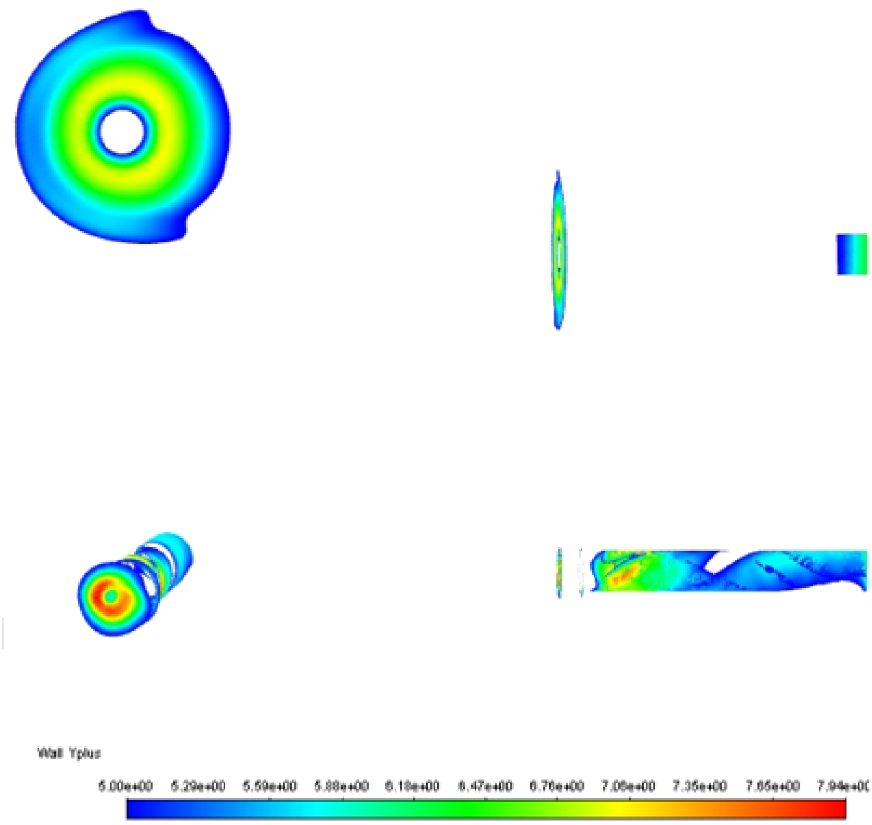

Figure B.3: y^+ above five which is outside of the given limit. To the right from the side and to the left from above.

Similar to the base case three levels of refinements were done. Each step with a global refinement of 10 %. In table B.1 each refinement step is described.

Table B.1: How the mesh was globally refined in three steps with 10% refinement per step for the new case with a fin.

	Maximum Cell Size	Maximum Fluid Face Size	Total Number of Cells
Refinement 1	3 mm	0,75 mm	5026015
Refinement 2	2,7 mm	0,675 mm	5304619
Refinement 3	2,43 mm	0,6075 mm	6171214

In Figure B.4 and Figure B.5 it is illustrated how the mesh was refined in areas of interests for the three steps.

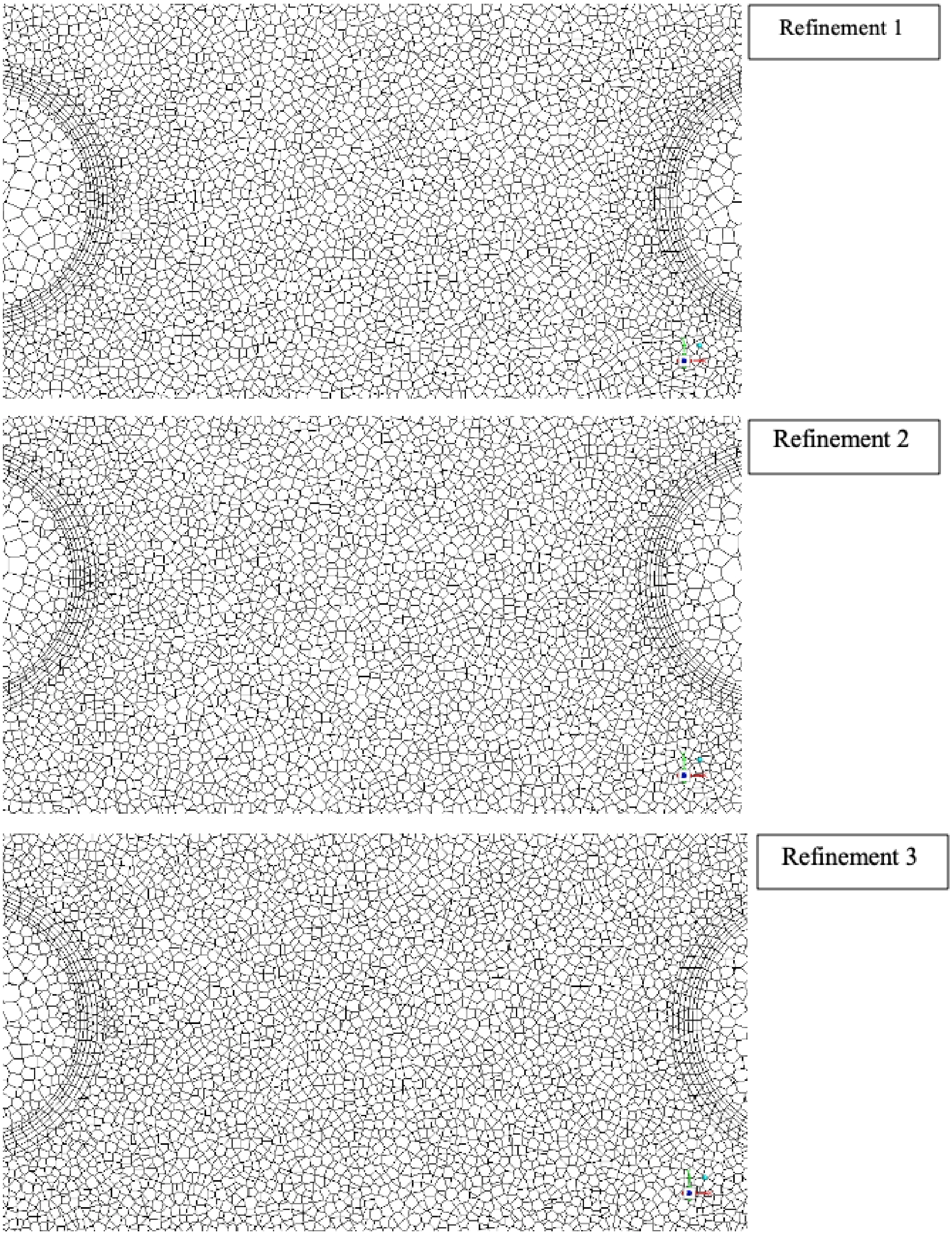

Figure B.4: Three steps of refinement of the fin case. The picture is taken in the middle of the flow in z-led and just after the U-turn which was assigned an area of interest.

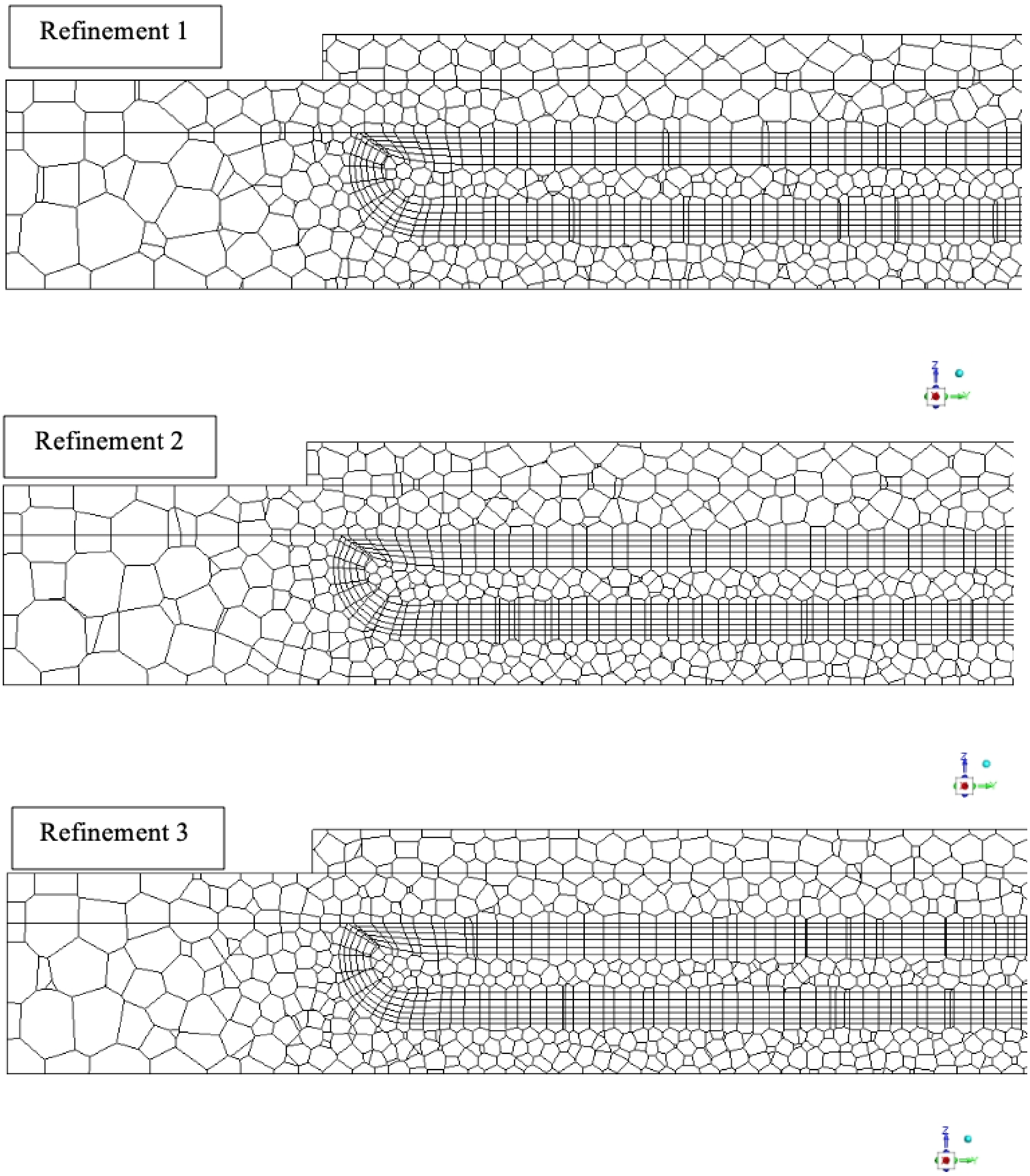

Figure B.5: A figure showing the three steps of refinement of the fin case. Taken in a cross section just after the U-turn which was assigned an area of interest.

Result of the mesh study for the case with the fin is presented in Table B.2.From here it was established that the mesh were independent and the second mesh was used.

Table B.2: Result of the mesh study of the the case with a fin . Deviation from previous mesh.

	Total Heat Transfer Rate	Deviation	$dT = T_{out} - T_{in}$	Deviation
Refinement 1	337,46 W	-	1,91 K	-
Refinement 2	337,46 W	2,03 e-05	1,91 K	1,57e-05
Refinement 3	337.45 W	2,14e-05	1,91 K	7,86e-05

C

Mesh Study Pattern

Here follow the mesh study for the changed pattern of the flow channels. It was preformed in the same way as the base case. First it was confirmed to have a y^+ within the limits. As can be seen in Figure C.1 the velocity boundary layer is captured.

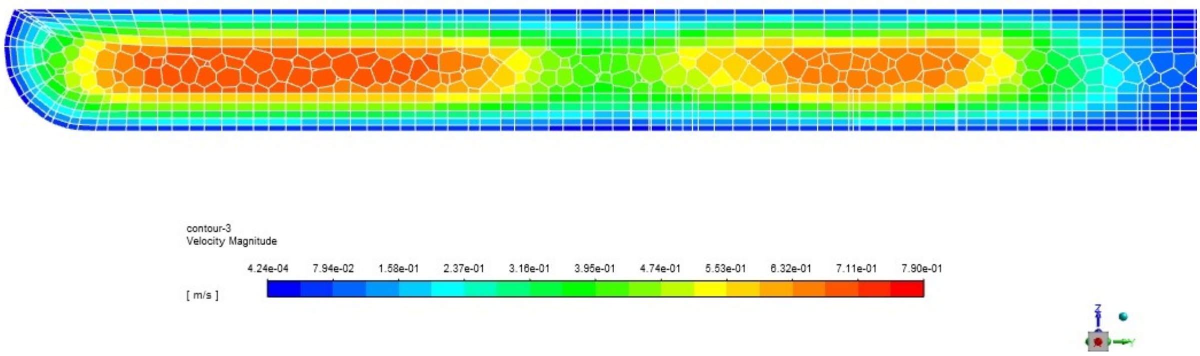

Figure C.1: Contour of the velocity field in a cross section in x direction including the mesh. Confirms that the total height of the mesh boundary layer capture the velocity field height of the boundary layer for the new pattern.

Secondly, the y^+ was controlled. Similar to the base case most cells were within the limit, as is seen in Figure C.2. Although, some cells near the entrance were still above the limit, see Figure C.3.

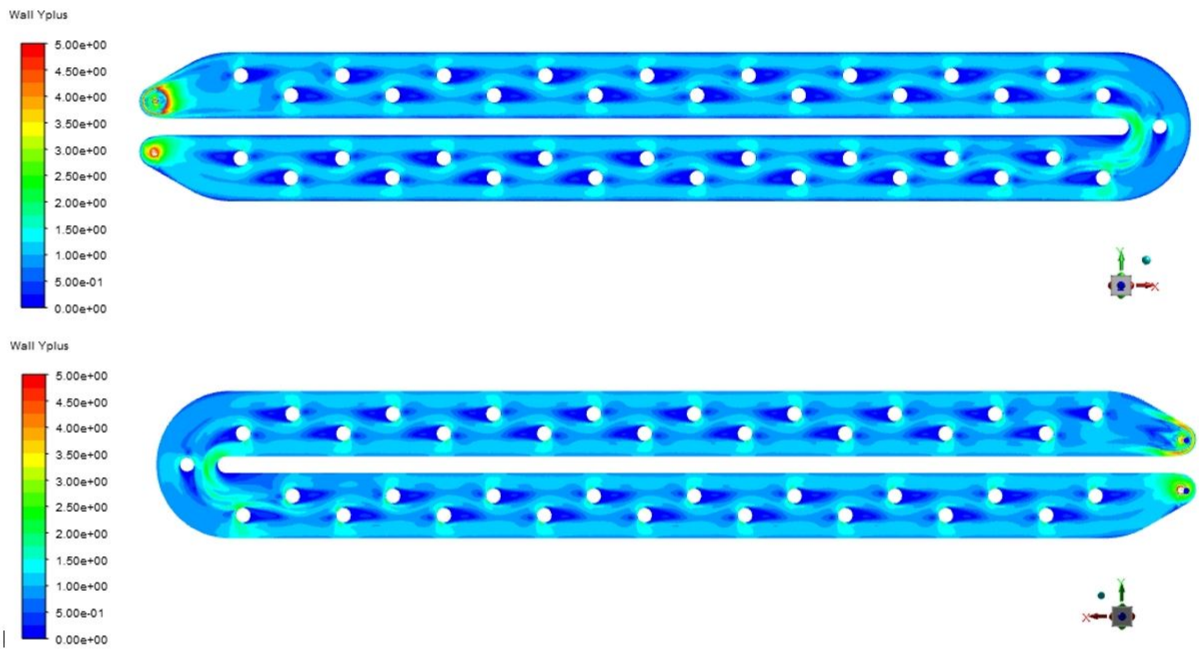

Figure C.2: Wall y^+ from above and from below for the new case with different pattern, with a scale from zero to five

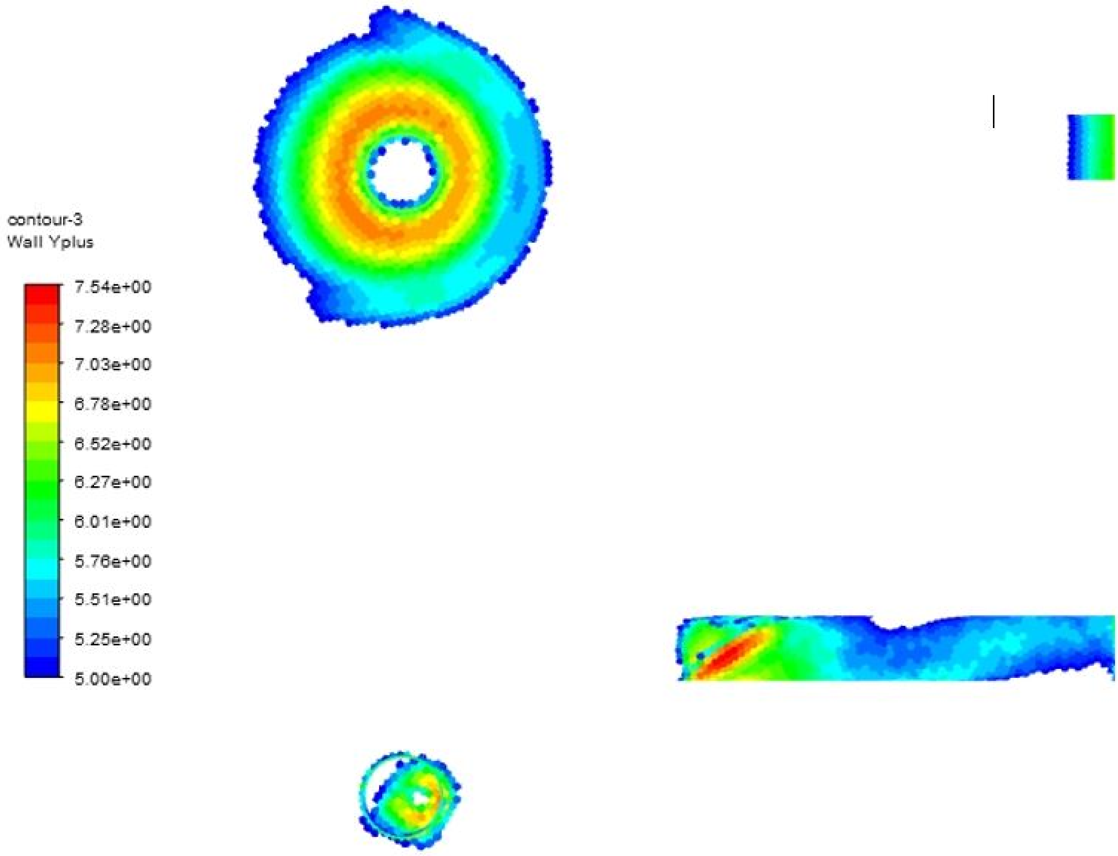

Figure C.3: y^+ above five which is outside the given limit. To the right from the side, and to the left from above

Three levels of refinements was done similar to the base case with a global refinement of 10% per step, see Table C.1.

Table C.1: How the mesh was globally refined in three steps with 10% refinement per step for the new case with a different pattern.

	Maximum Cell Size	Maximum Fluid Face Size	Total Number of Cells
Refinement 1	3 mm	0,75 mm	5493100
Refinement 2	2,7 mm	0,675 mm	5835454
Refinement 3	2,43 mm	0,6075 mm	6296917

In Figure C.4 and Figure C.5 the how the mesh was refined in areas of interests for the three steps are illustrated.

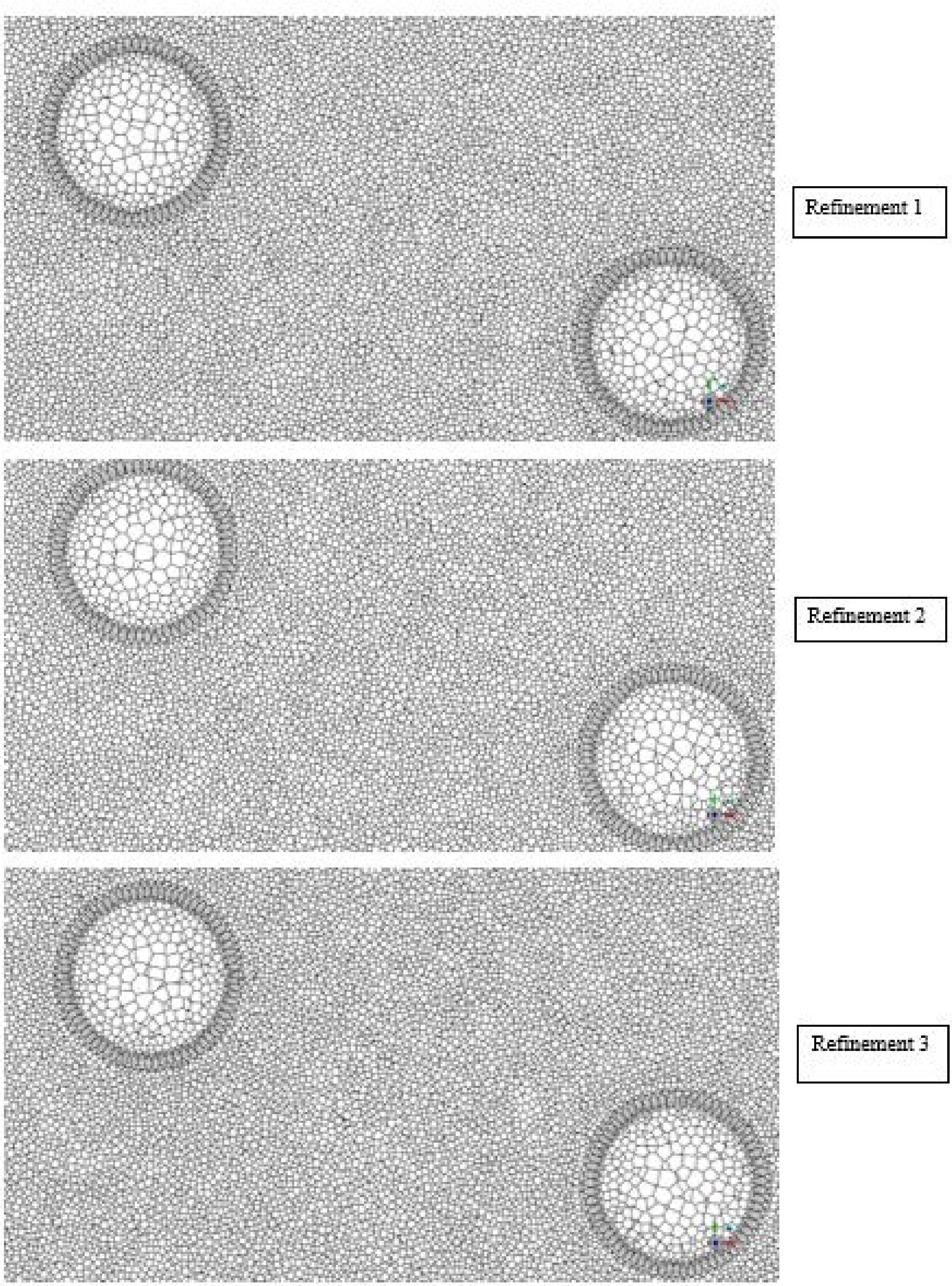

Figure C.4: Three steps of refinement of the New case with a different pattern. The picture is taken in the middle of the flow in z-led and just after the U-turn which was assigned an area of interest.

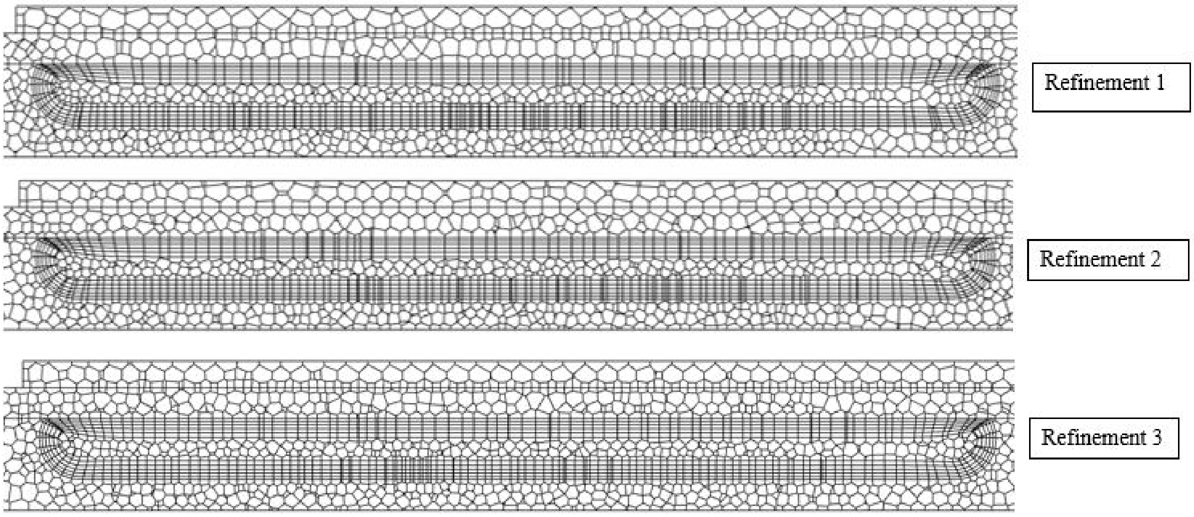

Figure C.5: Picture showing the three steps of refinement of the New Case with a different pattern. Taken in a cross section just after the U-turn which was assigned an area of interest.

Result of the mesh study for the new case with the different pattern is shown presented in Table C.2. It was conducted from the study that the second refinement was independent and therefore used in the analysis.

Table C.2: Result of the mesh study of the the new case with a different pattern. Deviation from previous mesh.

	Total Heat Transfer Rate	Deviation	$dT = T_{out} - T_{in}$	Deviation
Refinement 1	337.72 W	-	1,91 K	-
Refinement 2	337.76 W	1,02e-4	1,91 K	1,36e-4
Refinement 3	337.76 W	4,17e-5	1,91 K	1,54e-5

D
Comparison between Base Case and Pattern 1

In this Appendix a comparison between the temperature of the base case and the case with the moved structures are done. The contour plot taking in the middle of the flow in z-direction can be seen in Figure D.1 and D.2.

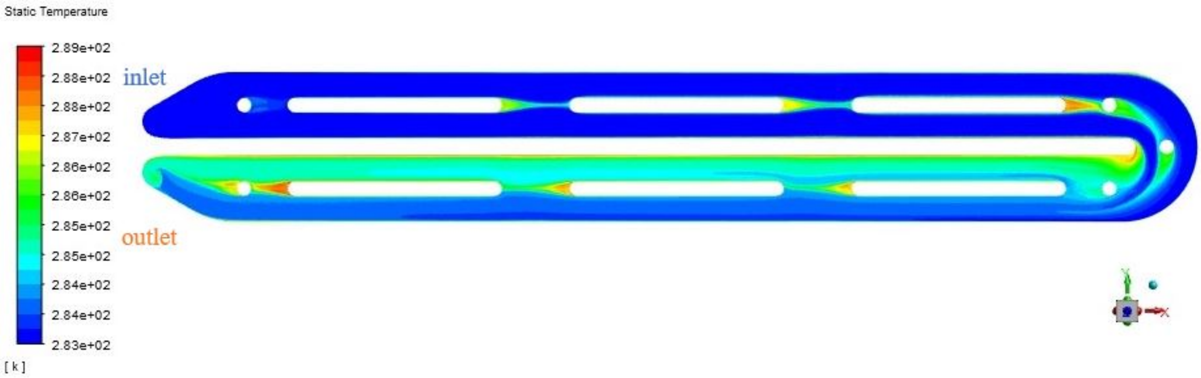

Figure D.1: A contour of the temperature of the fluid in a plan in the middle of the flow in z-direction for the base case. Side of inlet respectively outlet is marked.

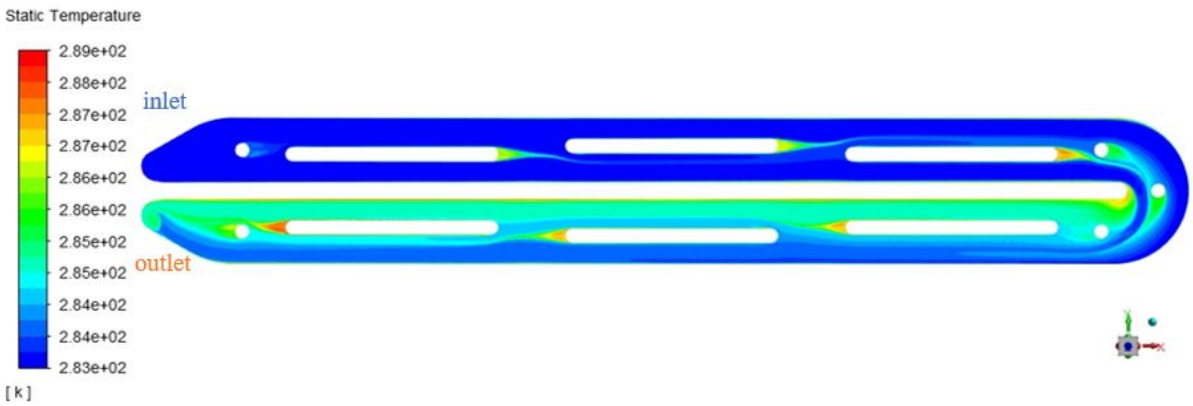

Figure D.2: A contour of the temperature of the fluid in a plan in the middle of the flow in z-direction for pattern 1. Side of inlet respectively outlet is marked.